

# Kernel learning approaches for summarising and combining posterior similarity matrices

Alessandra Cabassi<sup>1</sup>, Sylvia Richardson<sup>1</sup>, and Paul D. W. Kirk<sup>1,2</sup>

<sup>1</sup>*MRC Biostatistics Unit*

<sup>2</sup>*Cambridge Institute of Therapeutic Immunology & Infectious Disease  
University of Cambridge, U.K.*

Preprint, December 14, 2021

## Abstract.

**Summary:** When using Markov chain Monte Carlo (MCMC) algorithms to perform inference for Bayesian clustering models, such as mixture models, the output is typically a sample of clusterings (partitions) drawn from the posterior distribution. In practice, a key challenge is how to summarise this output. Here we build upon the notion of the *posterior similarity matrix* (PSM) in order to suggest new approaches for summarising the output of MCMC algorithms for Bayesian clustering models. A key contribution of our work is the observation that PSMs are positive semi-definite, and hence can be used to define probabilistically-motivated kernel matrices that capture the clustering structure present in the data. This observation enables us to employ a range of kernel methods to obtain summary clusterings, and otherwise exploit the information summarised by PSMs. For example, if we have multiple PSMs, each corresponding to a different dataset on a common set of statistical units, we may use standard methods for combining kernels in order to perform *integrative clustering*. We may moreover embed PSMs within predictive kernel models in order to perform *outcome-guided* data integration. We demonstrate the performances of the proposed methods through a range of simulation studies as well as two real data applications.

**Availability:** R code is available at <https://github.com/acabassi/combine-psms>.

**Contact:** [alessandra.cabassi@mrc-bsu.cam.ac.uk](mailto:alessandra.cabassi@mrc-bsu.cam.ac.uk), [paul.kirk@mrc-bsu.cam.ac.uk](mailto:paul.kirk@mrc-bsu.cam.ac.uk)

## 1 Introduction

Clustering techniques aim to partition a set of statistical units in such a way that items in the same group are similar and items in different groups are dissimilar. The definition of similarity between observations varies according to the application at hand. In biomedical applications, for example, clustering can be used to define groups of patients who have similar genotypes or phenotypes and therefore are more likely to respond similarly to a certain treatment and/or have similar prognoses. Statistical methods for clustering can be divided into two main categories: heuristic approaches as, for instance, *k*-means (Hartigan and Wong, 1979) and hierarchical clustering (Kaufman and Rousseeuw, 1990), and model-based techniques such as mixture models (McLachlan and Peel, 2004). Here we are interested in particular in Bayesian mixture models. Inference on the parameters of

these models can be performed either via deterministic approximate inference methods based on variational inference (Bishop, 2006, Blei et al., 2006) or using Markov chain Monte Carlo (MCMC) schemes to sample from the posterior distribution (Gelfand and Smith, 1990). One of the advantages of Bayesian model-based clustering is that, if infinite mixtures are used, one does not need to specify the number of clusters a priori (Rasmussen, 2000). On the other hand, summarising the output of MCMC algorithms can be challenging, as it includes a large number of partitions of the data sampled from the posterior distribution. The labels of each mixture component can change at each iteration of the MCMC, because the model likelihood is invariant under permutations of the indices. This phenomenon is known as *label switching* (Celeux et al., 2000). One way of summarising the cluster allocations that circumvents this problem is to compute a posterior similarity matrix (PSM) containing the probabilities of each pair of observations of belonging to the same cluster (more details about Bayesian mixture models and PSMs can be found in Section 2). In addition to that, however, one is often interested in finding one clustering of the data that best matches the information contained in the PSM (Fritsch and Ickstadt, 2009).

We propose a new method to summarise the PSMs derived from the MCMC output of Bayesian model-based clustering, showing that they are valid kernel matrices. Consequently, we are able to use kernel methods such as kernel  $k$ -means to find a summary clustering, and can make use of machine learning algorithms developed for pattern analysis (see e.g. Shawe-Taylor and Cristianini, 2004) to combine the PSMs obtained from different datasets. We assume that we have a similarity matrix for each dataset, from initial clustering analyses performed for each dataset independently. We show how these multiple kernel learning (MKL) techniques allow us to find a global clustering structure and assign different weights to each PSM, depending on how much information each provides about the clustering structure. We also show how we may include a response variable, if it is available, in order to perform outcome-guided integrative clustering. In particular, we show that, in the unsupervised framework, we can use the localised multiple kernel  $k$ -means approach of Gönen and Margolin (2014). We further demonstrate that, if a response variable is available for each data point, it is possible to incorporate this information using the *simpleMKL* algorithm of Rakotomamonjy et al. (2008) in order to perform outcome-guided integrative clustering. Both algorithms assign a weight to each PSM, that is output together with the global cluster assignment.

This work therefore contributes to the many ways of summarising the clusterings sampled from the posterior distribution that have already been proposed (Fritsch and Ickstadt, 2009, Wade and Ghahramani, 2018). Our approach performs equally well in the case of one dataset and has the advantage of being easily extended to the case of multiple data sources.

From a different perspective, this work also suggests a new rational way to define kernels that are appropriate when the data are believed to possess a clustering structure. Lanckriet et al. (2004) applied MKL methods to the problem of genomic data fusion, trying different kernels for each data source. However, how to define a kernel in general remained an open problem. Cabassi and Kirk (2020) suggested the use of methods based on multiple kernel learning to summarise the output of multiple similarity matrices, each resulting from applying consensus clustering (Monti et al., 2003) to a different dataset. Similarly, using PSMs as kernels ensures that the similarities between data points that we consider correctly reflect the clustering structure present in the data.

The manuscript is organised as follows. In Section 2 we introduce the problem of summarising PSMs. In Section 3 we recall the theory of kernel methods, prove that PSMs are valid kernel matrices and explain how this allows us to apply kernel methods to the problems mentioned above. We also present the method that we use to choose the best number of clusters in the final summary. In Section 4 we present some simulation studies demonstrating the performances of kernel methods to summarise PSMs and to integrate multiple datasets in an unsupervised and outcome-guided fashion. Finally, in Section 5 we introduce our motivating examples and illustrate how our methodology can

be applied to it.

## 2 Background

In this section we briefly recall the concept of Bayesian mixture models (Section 2.1) and we expose the problem of summarising the posterior distribution on the cluster allocations (Section 2.2).

### 2.1 Bayesian mixture models

Mixture models assume that the data are drawn from a mixture of distributions:

$$p(\mathbf{x}) = \sum_{k=1}^K \pi_k f_{\mathbf{x}}(\mathbf{x}|\phi_k). \quad (1)$$

where  $f_{\mathbf{x}}$  is a parametric density that depends on the parameter(s)  $\phi_k$ , and  $\pi_k$  are the mixture weights, which must satisfy  $0 \leq \pi_k \leq 1$  and  $\sum_{k=1}^K \pi_k = 1$ . In the Bayesian framework, we assign a prior distribution to the set of all parameters,  $\Pi = [\pi_1, \dots, \pi_K]$  and  $\Phi = [\phi_1, \dots, \phi_K]$ . In the finite mixtures case, methods to estimate the posterior distributions when the true number of mixture components is unknown include the MCMC-based algorithms proposed by [Ferguson \(1973\)](#) and [Richardson and Green \(1997\)](#). MCMC approaches also exist for so-called infinite mixture models ([Rasmussen, 2000](#)), such as Dirichlet process mixtures and their generalisations ([Antoniak, 1974](#)).

### 2.2 Posterior similarity matrices

When using MCMC methods in order to perform Bayesian clustering on a dataset  $X = [\mathbf{x}_1, \dots, \mathbf{x}_N]$ , one obtains a vector of cluster assignments  $\mathbf{c}^{(b)} = [c_1^{(b)}, \dots, c_N^{(b)}]$  from the posterior distribution for each iteration  $b = 1, \dots, B$  of the algorithm (see, for example, [Neal, 2000](#)). From this, it is possible to obtain a Monte Carlo estimate of the probability that observations  $i$  and  $j$  belong to the same cluster as follows:

$$P(c_i = c_j | X) \approx \frac{1}{B} \sum_{b=1}^B \mathbb{I}_{\{c_i^{(b)} = c_j^{(b)}\}} =: \Delta_{ij}. \quad (2)$$

We denote by  $\Delta$  the posterior similarity matrix that is the matrix that has  $ij$ th entry  $\Delta_{ij}$  equal to the right hand side of Equation (2).

Many ways to find a final clustering using the PSM  $\Delta$  have been proposed ([Binder, 1978](#), [Dahl, 2006](#), [Fritsch and Ickstadt, 2009](#), [Medvedovic and Sivaganesan, 2002](#), [Wade and Ghahramani, 2018](#)). A simple solution is to choose, among the  $\mathbf{c}^{(b)}$ , the one that maximises the posterior density. The problem with this approach is that many clusterings are associated with very similar posterior densities ([Fritsch and Ickstadt, 2009](#)). A more principled approach is to define a loss function  $L(\mathbf{c}, \hat{\mathbf{c}})$  measuring the loss of information that occurs when estimating the true clustering  $\mathbf{c}$  with  $\hat{\mathbf{c}}$  ([Binder, 1978](#)). The optimal clustering  $\mathbf{c}^*$  is then defined as the one minimising the posterior expected loss:

$$\mathbf{c}^* = \arg \min_{\hat{\mathbf{c}}} \mathbb{E} [L(\mathbf{c}, \hat{\mathbf{c}}) | X] = \arg \min_{\hat{\mathbf{c}}} \sum_{\mathbf{c}} L(\mathbf{c}, \hat{\mathbf{c}}) p(\mathbf{c} | X). \quad (3)$$

[Binder \(1978\)](#), for instance, suggested choosing the clustering  $\hat{\mathbf{c}}$  that minimises the loss function

$$L_{\text{Binder}}(\mathbf{c}, \hat{\mathbf{c}}) = \sum_{i < j} [l_1 \mathbb{I}(c_i = c_j) \mathbb{I}(\hat{c}_i \neq \hat{c}_j) + l_2 \mathbb{I}(c_i \neq c_j) \mathbb{I}(\hat{c}_i = \hat{c}_j)], \quad (4)$$

where  $l_1$  and  $l_2$  are positive constants determining whether assigning observations that belong to the same clusters to different clusters is penalised more highly than assigning observations that belong to different clusters to the same cluster ( $l_1/l_2 > 1$ ) or vice versa ( $l_1/l_2 < 1$ ) and  $\mathbb{I}$  is the indicator function. If  $l_1 = l_2$ , then

$$\mathbf{c}_{\text{Binder}}^* = \arg \min_{\hat{\mathbf{c}}} \sum_{i < j} |\mathbb{I}_{\{\hat{c}_i = \hat{c}_j\}} - \Delta_{ij}|. \quad (5)$$

More recently, [Wade and Ghahramani \(2018\)](#) proposed an alternative to Binder’s loss function based on the *variation of information* of [Meilă \(2007\)](#):

$$L_{\text{VI}}(\mathbf{c}, \hat{\mathbf{c}}) = H(\mathbf{c}) + H(\hat{\mathbf{c}}) - 2I(\mathbf{c}, \hat{\mathbf{c}}), \quad (6)$$

where  $H(\mathbf{c})$  and  $H(\hat{\mathbf{c}})$  represent the entropy of clusterings  $\mathbf{c}$  and  $\hat{\mathbf{c}}$  respectively,  $I(\mathbf{c}, \hat{\mathbf{c}})$  is the mutual information between clusterings  $\mathbf{c}$  and  $\hat{\mathbf{c}}$ . Defining by  $C_i$  the set of elements that belong to cluster  $i$  in clustering  $\mathbf{c}$ ,  $\hat{C}_j$  the set of elements that belong to cluster  $j$  in clustering  $\hat{\mathbf{c}}$ ,  $n_{ij} = |C_i \cap \hat{C}_j|$ ,  $n_{i+} = \sum_j n_{ij}$ ,  $n_{+j} = \sum_i n_{ij}$ , this is

$$L_{\text{VI}} = - \sum_{i=1}^{K_N} \frac{n_{i+}}{N} \log_2 \left( \frac{n_{i+}}{N} \right) - \sum_{j=1}^{\hat{K}_N} \frac{n_{+j}}{N} \log_2 \left( \frac{n_{+j}}{N} \right) - 2 \sum_{i=1}^{K_N} \sum_{j=1}^{\hat{K}_N} \frac{n_{ij}}{N} \log_2 \left( \frac{n_{ij}N}{n_{i+}n_{+j}} \right), \quad (7)$$

where  $K_N$  and  $\hat{K}_N$  represent the number of clusters in  $\mathbf{c}$  and  $\hat{\mathbf{c}}$  respectively.

[Dahl \(2006\)](#) advanced the idea to choose, among all the clustering vectors  $\mathbf{c}^{(b)}$ , the one that minimises the least-squared distance to the PSM:

$$\mathbf{c}_{\text{Dahl}}^* = \arg \min_{\hat{\mathbf{c}}} \sum_{i < j} \left( \mathbb{I}_{\{\hat{c}_i = \hat{c}_j\}} - \Delta_{ij} \right)^2. \quad (8)$$

This turned out to be equivalent to minimising Binder’s loss function (Equation 5). [Fritsch and Ickstadt \(2009\)](#) improved on the methods of Binder and Dahl by maximising the posterior expected adjusted Rand index of [Hubert and Arabie \(1985\)](#).

Moreover, [Medvedovic and Sivaganesan \(2002\)](#) applied the complete linkage approach of [Everitt \(1993\)](#) to the matrix of pseudo-distances  $1 - \Delta$ , while [Molitor et al. \(2010\)](#) used the partitioning around medoids algorithm of [Kaufman and Rousseeuw \(1990\)](#).

All of these methods are only applicable with one PSM. In what follows we describe a new way to find a clustering using posterior similarity matrices that also allows us to summarise multiple similarity matrices  $\Delta_m$  and find a global clustering.

### 3 Methods

In this section we explain how the output of the MCMC algorithms for Bayesian mixture models can be modified in order to obtain valid kernel matrices (Section 3.1). After that, in Section 3.2, we show that this allows us to (i) use the kernel  $k$ -means algorithm to summarise a PSM and find a summary clustering of the data; (ii) combine multiple PSMs to perform integrative clustering of multiple datasets using an extension of kernel  $k$ -means; (iii) use an external response variable to determine the weight of each dataset in the integrative setting, by using predictive kernel methods such as Support Vector Machines (SVMs). In the last part of the section we explain how we choose the number of clusters in the final clustering.



### 3.1 Kernels

Kernel methods allow non-linear relationships between data points with low computational complexity to be modelled, thanks to the so-called *kernel trick* (Shawe-Taylor and Cristianini, 2004). For this reason, kernel methods have been widely used to extend many traditional algorithms to the non-linear framework, such as the PCA (Schölkopf et al., 1998), linear discriminant analysis (Baudat and Anouar, 2000, Mika et al., 1999, Roth and Steinhage, 2000) and ridge regression (Friedman et al., 2001, Shawe-Taylor and Cristianini, 2004).

Kernel methods proceed by embedding the observations into a higher-dimensional feature space  $\mathcal{X}$  endowed with an inner product  $\langle \cdot, \cdot \rangle_{\mathcal{X}}$  and induced norm  $\|\cdot\|_{\mathcal{X}}$ , making use of a map  $\phi : \mathbb{R}^P \rightarrow \mathcal{X}$ .

**Definition 3.1.** A positive definite kernel or, more simply, a kernel  $\delta$  is a symmetric map  $\delta : \mathbb{R}^P \times \mathbb{R}^P \rightarrow \mathbb{R}$  for which for all  $\mathbf{x}_1, \mathbf{x}_2, \dots, \mathbf{x}_N \in \mathbb{R}^P$ , the matrix  $\Delta$  with entries  $\Delta_{ij} = \delta(\mathbf{x}_i, \mathbf{x}_j)$  is positive semi-definite. The matrix  $\Delta$  is called the kernel matrix or Gram matrix.

(The domain of the map  $\phi$  is set to be  $\mathbb{R}^P$  for simplicity, but the definition also holds for more general sets of departure for  $\phi$ .) Using this definition, it is possible to prove that any inner product of feature maps gives rise to a kernel:

**Proposition 3.1.** The map  $\delta : \mathbb{R}^P \times \mathbb{R}^P \rightarrow \mathbb{R}$  defined by  $\delta(\mathbf{x}, \mathbf{x}') = \langle \phi(\mathbf{x}), \phi(\mathbf{x}') \rangle_{\mathcal{X}}$  is a kernel.

Moreover, using Mercer’s theorem, it can be shown that for any positive semi-definite kernel function,  $\delta$ , there exists a corresponding feature map,  $\phi$  (see e.g. Vapnik, 1998). That is,

**Theorem 3.1.** For each kernel  $\delta$ , there exists a feature map  $\phi$  taking value in some inner product space  $\mathcal{X}$  such that  $\delta(\mathbf{x}, \mathbf{x}') = \langle \phi(\mathbf{x}), \phi(\mathbf{x}') \rangle_{\mathcal{X}}$ .

In practice, it is therefore often sufficient to specify a positive semi-definite kernel matrix,  $\Delta$ , in order to allow us to apply kernel methods such as those presented in the following sections. For a more detailed discussion of kernel methods, see e.g. Shawe-Taylor and Cristianini (2004).

### 3.2 Identifying PSMs as kernel matrices

It has been shown elsewhere that co-clustering matrices are valid kernel matrices (Cabassi and Kirk, 2020). We show here that this result also holds for PSMs, and hence they can be used as input for any kernel-based model. PSMs are convex combinations of co-clustering matrices  $C^{(b)}$ , where each matrix  $C^{(b)}$  is defined as follows:

$$C_{ij}^{(b)} = \begin{cases} 1 & \text{if } c_i^{(b)} = c_j^{(b)}, \\ 0 & \text{otherwise,} \end{cases}$$

where  $C_{ij}^{(b)}$  indicates whether the statistical units  $i$  and  $j$  are assigned to the same cluster at iteration  $b$  of the MCMC chain. Indicating by  $K$  the total number of clusters and reordering the rows and column, each  $C_{ij}^{(b)}$  can be written as a block-diagonal matrix where every block is a matrix of ones:

$$C^{(b)} = \begin{bmatrix} J_1 & 0 & 0 & \dots & 0 \\ 0 & J_2 & 0 & \dots & 0 \\ \vdots & & & \ddots & \vdots \\ 0 & 0 & 0 & \dots & J_K \end{bmatrix} \quad (9)$$

where  $J_k$  is an  $n_k \times n_k$  matrix of ones, with  $n_k$  being the number of items in cluster  $k$ . The eigenvalues of a block diagonal matrix are simply the eigenvalues of its blocks, which, in this case, are nonnegative. Therefore all  $C^{(b)}$ , with  $b = 1, \dots, B$ , are positive semidefinite. Now, if  $\lambda$  is a nonnegative scalar, and  $C$  is positive semidefinite, then  $\lambda C$  is also positive semidefinite. Moreover, the sum of positive semidefinite matrices is a positive semidefinite matrix. Therefore, given any set of nonnegative  $\lambda_b$ ,  $b = 1, \dots, B$ ,  $\sum_{b=1}^B \lambda_b C^{(b)}$  is positive semidefinite. We can conclude that any PSM is positive definite.

### 3.3 Summarising and combining PSMs using kernel methods

Here we show that the fact that all posterior similarity matrices are valid kernels allows us to use kernel methods to find a clustering of the data that summarises a sample of clusterings  $\mathbf{c}^{(1)}, \dots, \mathbf{c}^{(B)}$  from the posterior distribution of an MCMC algorithm for Bayesian clustering. To do this we suggest to use an extension of the well-known  $k$ -means algorithm that only needs as input a kernel matrix.

Moreover, this method can be easily extended to allow us to combine multiple PSMs. This can be a useful feature under many circumstances. For instance, as it is the case in our motivating examples, one could have different types of information relative to the same statistical observations. In this situation, it may be appropriate to define and fit different mixture models on each data type, and then summarise the two posterior samples of clusterings at a later stage. This can be achieved by using multiple kernel  $k$ -means algorithms, that allow us to combine multiple kernels to find a global clustering. On top of that, these techniques also assign different weights to each kernel. These can be used to assess how much each dataset contributed to the final clustering and therefore to get an idea of how much information is present in each data type about the clustering structure.

The problem with combining multiple kernels is, however, that it is not always clear whether they all have the same clustering structure. To overcome this issue, we also propose an *outcome-guided* algorithm to summarise multiple PSMs. The idea is that, instead of choosing the weight of each kernel in an unsupervised way, if we have a variable available which is closely related to the outcome of interest, we should weight more highly the kernels in which statistical units that have similar outcomes are closer to each other. In mathematical terms, this corresponds to using support vector machines to find the kernel weights, where the response variable is our proxy for the outcome.

#### 3.3.1 Summarising PSMs

In order to illustrate our method for summarising PSMs, first we recall the main ideas behind  $k$ -means clustering and then we present its extension to the kernel framework.

**$k$ -means clustering**  $k$ -means clustering is a widely used clustering algorithm, first introduced by [Steinhaus \(1956\)](#). Let  $\mathbf{x}_1, \dots, \mathbf{x}_N$  indicate the observed dataset, with  $\mathbf{x}_n \in \mathbb{R}^p$  and  $z_{nk}$  be the corresponding cluster labels, where  $\sum_k z_{nk} = 1$  and

$$z_{nk} = \begin{cases} 1, & \text{if } \mathbf{x}_n \text{ belongs to cluster } k, \\ 0, & \text{otherwise.} \end{cases} \quad (10)$$

We denote by  $\mathbf{Z}$  the  $N \times K$  matrix with  $ij$ th element equal to  $z_{ij}$ . The goal of the  $k$ -means algorithm is to minimise the sum of all squared distances between the data points  $\mathbf{x}_n$  and the corresponding

cluster centroid  $\mathbf{m}_k$ . The optimisation problem is

$$\underset{Z}{\text{minimise}} \quad \sum_n \sum_k z_{nk} \|\mathbf{x}_n - \mathbf{m}_k\|_2^2 \quad (11a)$$

$$\text{subject to} \quad \sum_k z_{nk} = 1, \forall n, \quad (11b)$$

$$N_k = \sum_n z_{nk}, \forall k, \quad (11c)$$

$$\mathbf{m}_k = \frac{1}{N_k} \sum_n z_{nk} \mathbf{x}_n, \forall k. \quad (11d)$$

where  $\|\cdot\|_2$  indicates the Euclidean norm.

**Kernel  $k$ -means clustering** Now we can show how the kernel trick works in the case of the  $k$ -means clustering algorithm (Girolami, 2002). Redefining the objective function of Equation (11a) based on the distances between observations and cluster centres in the feature space  $\mathcal{X}$ , the optimisation problem becomes:

$$\underset{Z}{\text{minimise}} \quad \sum_n \sum_k z_{nk} \|\phi(\mathbf{x}_n) - \tilde{\mathbf{m}}_k\|_{\mathcal{X}}^2 \quad (12a)$$

$$\text{subject to} \quad \sum_k z_{nk} = 1, \forall n, \quad (12b)$$

$$N_k = \sum_n z_{nk}, \forall k, \quad (12c)$$

$$\tilde{\mathbf{m}}_k = \frac{1}{N_k} \sum_n z_{nk} \phi(\mathbf{x}_n), \forall k. \quad (12d)$$

where we indicated by  $\tilde{\mathbf{m}}_k$  the cluster centroids in the feature space  $\mathcal{X}$ . Using this kernel, each term of the sum in Equation (12a) can be written as

$$\|\phi(\mathbf{x}_n) - \tilde{\mathbf{m}}_k\|_{\mathcal{X}}^2 = \langle \phi(\mathbf{x}_n) - \tilde{\mathbf{m}}_k, \phi(\mathbf{x}_n) - \tilde{\mathbf{m}}_k \rangle_{\mathcal{X}} \quad (13)$$

$$= \langle \phi(\mathbf{x}_n), \phi(\mathbf{x}_n) \rangle_{\mathcal{X}} - \frac{2}{N_k} \sum_{i=1}^N z_{ik} \langle \phi(\mathbf{x}_n), \phi(\mathbf{x}_i) \rangle_{\mathcal{X}} \quad (14)$$

$$+ \frac{1}{N_k^2} \sum_{i=1}^N \sum_{j=1}^N z_{ik} z_{jk} \langle \phi(\mathbf{x}_i), \phi(\mathbf{x}_j) \rangle_{\mathcal{X}} \quad (15)$$

$$= \delta(\mathbf{x}_n, \mathbf{x}_n) - \frac{2}{N_k} \sum_{i=1}^N z_{ik} \delta(\mathbf{x}_n, \mathbf{x}_i) + \frac{1}{N_k^2} \sum_{i=1}^N \sum_{j=1}^N z_{ik} z_{jk} \delta(\mathbf{x}_i, \mathbf{x}_j). \quad (16)$$

Therefore, we do not need to evaluate the map  $\phi$  at every point  $\mathbf{x}_i$  to compute the objective function of Equation (12a). Instead, we just need to know the values of the kernel evaluated at each pair of data points  $\delta(\mathbf{x}_i, \mathbf{x}_j)$ ,  $i, j = 1, \dots, N$ . This is what is commonly referred to as the kernel trick.

We have seen how kernels can be used to perform  $k$ -means clustering. Now, if we have a sample of clusterings from the posterior, we can easily exploit this technique to find a summary clustering. Once we compute our PSM  $\Delta$ , this will be our kernel matrix. The clustering of interest will then be the one given by kernel  $k$ -means in the form of  $z_{nk}$ ,  $n = 1, \dots, N$ ,  $k = 1, \dots, K$ . The number of clusters  $K$  is chosen as explained in Section 3.4.

### 3.3.2 Combining PSMs to perform integrative clustering

To combine multiple PSMs relative to the same statistical units, all we need to do is to use the extension of kernel  $k$ -means to the case of multiple kernels.

**Multiple kernel  $k$ -means clustering** [Gönen and Margolin \(2014\)](#) extended the kernel  $k$ -means approach to the case of multiple kernels. We consider multiple datasets  $X_1, \dots, X_M$  each with a different mapping function  $\phi_m : \mathbb{R}^P \rightarrow \mathcal{X}_m$  and corresponding kernel  $\delta_m(\mathbf{x}_i, \mathbf{x}_j) = \langle \phi_m(\mathbf{x}_i), \phi_m(\mathbf{x}_j) \rangle_{\mathcal{X}_m}$  and kernel matrix  $\Delta_m$ . Then, if we define

$$\phi_{\Theta}(\mathbf{x}_i) = [\theta_{i1}\phi_1(\mathbf{x}_i)', \theta_{i2}\phi_2(\mathbf{x}_i)', \dots, \theta_{iM}\phi_M(\mathbf{x}_i)']', \quad (17)$$

where  $\Theta \in \mathbb{R}_+^{N \times M}$  is a vector of kernel weights such that  $\theta_{im}$  is the weight of observation  $\mathbf{x}_i$  in dataset  $m$  and  $\sum_m \theta_{im} = 1$  for all  $i = 1, \dots, N$  and  $\theta_{im} \geq 0$ , the kernel function of this multiple feature problem is a convex sum of the single kernels:

$$\delta_{\Theta}(\mathbf{x}_i, \mathbf{x}_j) = \langle \phi_{\Theta}(\mathbf{x}_i), \phi_{\Theta}(\mathbf{x}_j) \rangle_{\mathcal{X}_m} \quad (18)$$

$$= \sum_{m=1}^M \theta_{im}\theta_{jm} \langle \phi_m(\mathbf{x}_i), \phi_m(\mathbf{x}_j) \rangle_{\mathcal{X}_m} \quad (19)$$

$$= \sum_{m=1}^M \theta_{im}\theta_{jm} \delta_m(\mathbf{x}_i, \mathbf{x}_j). \quad (20)$$

We denote the corresponding kernel matrix by  $\Delta_{\Theta}$ . The optimisation strategy proposed by [Gönen and Margolin \(2014\)](#) is based on the idea that, for some fixed vector of weights  $\theta$ , the problem is equivalent to the one of Equation (12a), where we had only one kernel. Therefore, they develop a two-step optimisation strategy: (1) given a fixed matrix of weights  $\Theta$ , solve the optimisation problem as in the case of one kernel, with kernel matrix  $\delta_{\Theta}$  and then (2) minimise the objective function with respect to the kernel weights, keeping the assignment variables fixed. This is a convex quadratic programming (QP) problem that can be solved with any standard QP solver up to a moderate number of kernels  $M$ .

Similarly to before, once we have defined the kernels  $\Delta_m$  to be equal to each of our PSMs, the labels found through multiple kernel  $k$ -means constitute the clustering that we are looking for. Moreover, the kernel weights give us an indication of how each PSM contributed to the final clustering.

### 3.3.3 Embedding PSMs within predictive kernel machines to perform outcome-guided integration

Suppose now that, in addition to the posterior similarity matrices  $\Delta_1, \dots, \Delta_M$ , we also have a categorical response variable  $y_n$  associated with each observation  $\mathbf{x}_n$ . As we explained above, we would like to use this information to guide our clustering algorithm. We can use the *simpleMKL* algorithm described in the remainder of this section to find the kernel weights  $\theta_1, \dots, \theta_M$  and then use kernel  $k$ -means on the weighted kernel  $\Delta = \sum_m \theta_m \Delta_m$  to find the final clustering (Figure 2).

**Support vector machines** We briefly recall here the concept of the support vector machine ([Boser et al., 1992](#)) that is widely used for solving problems in classification and regression ([Bishop, 2006](#), [Schölkopf and Smola, 2001](#)).

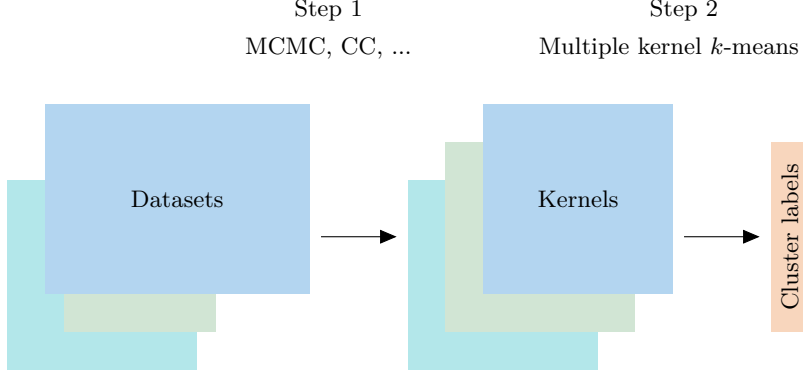


**Figure 1.** Schematic representation of the MKL-based integrative clustering approach. Each colour indicates a different dataset/kernel. First, a mixture model is fit using MCMC on each dataset separately. The resulting PSMs are valid kernels that can be used as input to kernel  $k$ -means to find a global clustering of the data. Note that, as shown elsewhere (Cabassi and Kirk, 2020), other similarity matrices, such as the similarity matrices given by consensus clustering (CC), define valid kernels. For this reason, they can be combined with PSMs via MKL.

In its simplest form, this method is applied to a binary classification problem, in which the data points  $\mathbf{x}_1, \dots, \mathbf{x}_N \in \mathbb{R}^P$  in the training set are assigned to two classes indicated by the target values  $y_n \in \{-1, 1\}, n = 1, \dots, N$ . We consider a feature map  $\phi : \mathbb{R}^P \rightarrow \mathcal{X}$  and the associated kernel  $\delta(\cdot, \cdot) : \mathcal{X} \times \mathcal{X} \rightarrow \mathbb{R}$  such that  $\delta(\mathbf{x}_i, \mathbf{x}_j) = \langle \phi(\mathbf{x}_i), \phi(\mathbf{x}_j) \rangle_{\mathcal{X}}$ . Suppose that there exist some values of  $\alpha_n$  and  $b$  such that

$$f(\mathbf{x}) = \sum_{n=1}^N \alpha_n \delta(\mathbf{x}, \mathbf{x}_n) \quad (21)$$

satisfies  $f(\mathbf{x}_n) + b > 0$  if  $y_n = 1$  and  $f(\mathbf{x}_n) + b < 0$  otherwise.  $f$  is a function that lives in a function space  $\mathcal{H}$  endowed with the norm  $\|\cdot\|_{\mathcal{H}}$ . Then, this function can be used to classify new data points  $\mathbf{x}$  according to the sign of  $f(\mathbf{x}) + b$ . For support vector machines, the parameters  $\alpha_n$  and  $b$  are chosen so as to maximise the *margin*, i.e. the distance between the decision boundary given by Equation (21) and the point  $\mathbf{x}_n$  that is closest to the boundary. It can be shown that this can be achieved by solving the quadratic programming problem (see e.g. Bishop, 2006, Rakotomamonjy et al., 2008)

$$\underset{f, b}{\text{minimise}} \quad \frac{1}{2} \|f\|_{\mathcal{H}}^2 \quad (22a)$$

$$\text{subject to} \quad y_n [f(\mathbf{x}_n) + b] \geq 1, \quad \forall n. \quad (22b)$$

However, in real applications, it is usually not possible to separate the two classes perfectly. Hence, in order to take into account misclassifications, it is necessary to introduce a penalty term that is linear with respect to the distance of the misclassified points to the classification boundary (Bennett and Mangasarian, 1992). To this end, we define a variable  $\xi_n$  (known as a *slack variable*) for each data point such that

$$\xi_n = \begin{cases} 0, & \text{if } \mathbf{x}_n \text{ is correctly classified,} \\ |y_n - f(\mathbf{x}_n)|, & \text{otherwise.} \end{cases} \quad (23)$$

The optimisation problem of Equation (22) then becomes

$$\underset{f, b, \{\xi_n\}}{\text{minimise}} \quad \frac{1}{2} \|f\|_{\mathcal{H}}^2 + \lambda \sum_n \xi_n \quad (24a)$$

$$\text{subject to} \quad y_n[f(\mathbf{x}_n) + b] \geq 1 - \xi_n, \quad \forall n, \quad (24b)$$

$$\xi_n \geq 0, \quad \forall n, \quad (24c)$$

where  $\lambda > 0$  is a parameter that controls the penalisation of misclassifications. The objective functions (22a) and (24a) are quadratic, so any local optimum is also a global optimum. One of the most popular approaches to solve this type of problems is *sequential minimal optimisation* (Platt, 1999). For more details about SVMs see e.g. Bishop (2006).

**Multiple kernel learning for SVMs** In the multiple kernel learning framework for SVMs, we consider  $M$  different feature representations, with mapping functions  $\phi_m$  and corresponding kernel functions  $\delta_m$  and feature spaces  $\mathcal{X}_m$ . We substitute the kernel  $\delta$  of Equation (21) with a convex combination of kernels  $\delta_m$  (Lanckriet et al., 2004):

$$f(\mathbf{x}) + b = \sum_{m=1}^M \theta_m f_m(\mathbf{x}) + b \quad (25)$$

where  $\theta_m \geq 0$ ,  $\sum_m \theta_m = 1$  and  $f_m = \sum_n \delta_m(\mathbf{x}, \mathbf{x}_n)$ . Rakotomamonjy and Bach (2007) proposed then to solve the optimisation problem

$$\underset{\{f_m\}, b, \{\xi_n\}, \{\theta_m\}}{\text{minimise}} \quad J(\boldsymbol{\theta}) := \frac{1}{2} \sum_m \frac{1}{\theta_m} \|f_m\|_{\mathcal{H}_m}^2 + \lambda \sum_n \xi_n \quad (26a)$$

$$\text{subject to} \quad y_n \left[ \sum_m f_m(\mathbf{x}_n) + b \right] \geq 1 - \xi_n, \quad \forall n, \quad (26b)$$

$$\xi_n \geq 0, \quad \forall n, \quad (26c)$$

$$\sum_m \theta_m = 1, \quad (26d)$$

$$\theta_m \geq 0, \quad \forall m \quad (26e)$$

using the convention that  $x/0 = 0$  if  $x = 0$  and  $\infty$  otherwise. The algorithm of Rakotomamonjy and Bach takes the name of *simpleMKL* and is based on the idea that one can iteratively solve a standard SVM problem (24a) for a fixed value of  $\boldsymbol{\theta}$  and then update the vector of weights  $\boldsymbol{\theta}$  using the gradient descent method on the objective function  $J(\boldsymbol{\theta})$ . Since the objective function is smooth and differentiable with Lipschitz gradient, it can be easily optimised with the reduced gradient algorithm (Luenberger and Ye, 1984, Chapter 11). If the standard SVM problem is solved exactly at each iteration, then convergence to the global optimum is guaranteed (Luenberger and Ye, 1984).

**Multiclass multiple kernel learning** SVMs can be used also when the target value  $y_n$  takes more than two different values. The most commonly used approaches are called *one-versus-one* (Knerr et al., 1990) and *one-versus-the-rest* (Vapnik, 1998). In the first one, we consider in turn each class as the “positive” case, and all the others as the “negative” cases. This way, we construct  $K$  different classifiers and then assign a new observation  $\mathbf{x}$  using

$$y(\mathbf{x}) = \max_{k \in \{1, \dots, K\}} y_k(\mathbf{x}) \quad (27)$$



The second approach is to train one SVM for each pair of classes and then assign a point  $\mathbf{x}$  to the class to which it is assigned more often.

Rakotomamonjy et al. (2008) extended the *simpleMKL* algorithm to the case of a response with  $K > 2$  classes. Both these approaches can be used with the simpleMKL algorithm, defining a new cost function  $J(\boldsymbol{\theta})$  as the sum of all the cost functions of the partial SVMs  $J_s(\boldsymbol{\theta})$ :

$$J(\boldsymbol{\theta}) = \sum_{s \in \mathcal{S}} J_s(\boldsymbol{\theta}) \quad (28)$$

where  $\mathcal{S}$  indicates the set of all partial SVMs and each  $J_s$  is defined as in Equation (26a).

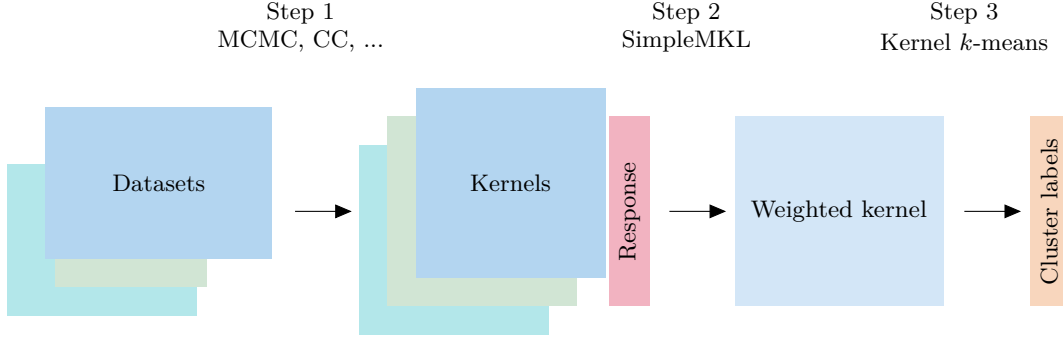


**Figure 2.** Schematic representation of the MKL-based outcome-guided integrative clustering approach. Each colour indicates a different dataset/kernel. First, a mixture model is fit on each dataset separately. The resulting PSMs are valid kernels that can be used as input to simpleMKL, if a response variable is available, to find a global clustering of the data.

It is important to note that none of these approaches explicitly rely on the fact that the  $\Delta_m$  are posterior similarity matrices. Hence, any other type of matrix  $\Delta_m$  can be used, as long as it is symmetric, positive semi-definite and the entries  $\Delta_{ij}^m$  can be interpreted as some measure of the similarity between  $\mathbf{x}_i$  and  $\mathbf{x}_j$ .

### 3.4 Choosing the number of clusters in the final summary

Many possible approaches have been proposed to choose the number of clusters (see e.g. Dudoit and Fridlyand, 2002, Milligan and Cooper, 1985, Tibshirani et al., 2001, Yeung et al., 2001). We focus on the so-called *silhouette*, a measure of compactness of the clustering structure, proposed by Rousseeuw (1987). There are two ways of defining the silhouette of a cluster, based respectively on the similarities and dissimilarities between the data. Here we briefly explain the former.

Given some cluster assignment labels  $\mathbf{c} = [c_1, \dots, c_N]$  and some measure of the dissimilarity between the data points  $\Delta_{ij}$  for all  $i, j = 1, \dots, N$ , we can define the following quantities:  $a_n$  is the average similarity of  $\mathbf{x}_n$  to all objects of cluster  $c_n$  and, for each  $c_i \neq c_n$ ,  $\Delta_{n,c_i}$  is the average similarity of  $n$  to all objects belonging to cluster  $c_i$ . Moreover, let us indicate by  $b_n$  the maximum  $\Delta_{n,c_i}$  over all  $i$  such that  $c_i \neq c_n$ . Then, for each observation  $n = 1, \dots, N$ , we can calculate

$$s_n = \begin{cases} 1 - a_n/b_n, & \text{if } a_n < b_n, \\ 0, & \text{if } a_n = b_n, \\ a_n/b_n - 1, & \text{if } a_n > b_n. \end{cases} \quad (29)$$

This takes values between  $-1$  and  $1$ , with higher values indicating that  $\mathbf{x}_i$  is *well-clustered* and negative values suggesting that  $\mathbf{x}_i$  has been misclassified.

Thus, we run our algorithms for combining the posterior similarity matrices with different number of clusters from  $K_{\min}$  to  $K_{\max}$ . We consider the overall average silhouette width  $\bar{s} = \frac{1}{N} \sum_{n=1}^N s_n$  as a measure of the compactness of clusters and we choose the value of  $K$  that gives the highest value of  $\bar{s}$ .

## 4 Simulation examples

Here we show how the methods presented above perform in practice. In Section 4.1 we explain how we generate the synthetic datasets for the simulation studies. In Section 4.2 we show that the kernel  $k$ -means approach applied to a posterior similarity matrix derived from a single dataset performs similarly to standard clustering methods. Additionally, to assess the MKL-based integrative clustering approaches described in Sections 3.3.2 and 3.3.3, we perform a range of simulation studies; the results are presented in Section 4.3.

### 4.1 Synthetic datasets

We generate four synthetic datasets, each composed of data belonging to six different clusters of equal size. Each observation  $\mathbf{x}_n^{(k)} \in \{0, 1, 2\}^{10}$  belonging to cluster  $k$  is drawn from a multivariate categorical distribution such that, for each covariate  $j = 1, \dots, 10$ ,

$$x_{nj}^{(k)} \sim \text{Categorical}(\pi_{1k}, \pi_{2k}, \pi_{3k}), \quad (30)$$

where  $\pi_{ik}$ ,  $i = 1, 2, 3$  are such that  $\pi_{ik} = w\rho_{ik} + (1-w)/3$ , with  $[\rho_{1k}, \rho_{2k}, \rho_{3k}] \sim \text{Dirichlet}(0.01)$ . Each dataset has a different value of  $w \in [0, 1]$ . Higher values of  $w$  give clearer clustering structures. The response variable is binary, with  $P(y_n = 1 | z_n = k) = \theta_k$ , where  $\theta_k \in \{0.01, 0.1, 0.15, 0.85, 0.9, 0.99\}$ . We repeat each experiment 100 times. For each synthetic dataset, we use the MCMC algorithm for Dirichlet process mixture models implemented in the R package `PreMiuM` of Liverani et al. (2015) to obtain the PSMs. We use discrete mixtures (Liverani et al., 2015, Section 3.2) except in one setting (detailed below) where the profile regression model of Molitor et al. (2010) is used, using a discrete mixture with categorical response. The idea of profile regression is that, if a response  $y_n$  is available for each  $n = 1, \dots, N$ , the observations  $d_n = (x_n, y_n)$  are jointly modelled as the product of the response model and a covariate model. In both cases we use the default hyperparameters, which we found to work well in practice.

We consider four different simulation settings:

- (A) The clustering structure in every dataset is the same and is related to the outcome of interest.
- (B) As in setting A, the clustering structure in each dataset is the same. In this case, however, each dataset contains some additional covariates that have no clustering structure.
- (C) The dataset with highest cluster separability has a clustering structure that is unrelated to the response variable, all the other datasets are the same as in setting A.
- (D) This is the same as setting C, but profile regression is used to derive the PSMs.

One set of PSMs used for setting A is shown in Figure 3.

In this case we know that higher values of  $w_d$  are associated with higher levels of cluster separability. However, in general, we do not know how dispersed the elements in each matrix are. So, we define another way to score how strong the signal is in each dataset. We use the *cophenetic correlation coefficient*, a measure of how faithfully hierarchical clustering would preserve the pairwise

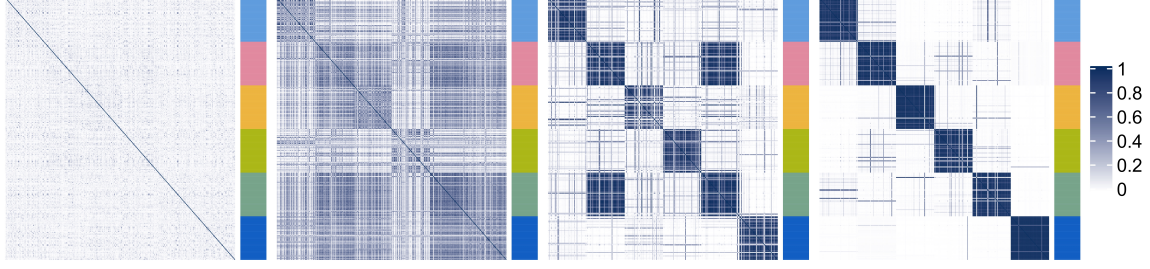


**Figure 3.** PSMs of the datasets used for setting A. The rows and columns correspond to the statistical units. The coloured bar on the right of each PSM represents the true clusters. Higher probabilities of belonging to the same cluster are indicated in blue. The values of  $w$  used to generate these matrices are, from left to right, 0.2, 0.4, 0.6, and 0.8.

distances between the original data points. Given a dataset  $X = [\mathbf{x}_1, \mathbf{x}_2, \dots, \mathbf{x}_N]$  and a similarity matrix  $\Delta \in \mathbb{R}^{N \times N}$ , we define the *dendrogrammatic distance* between  $\mathbf{x}_i$  and  $\mathbf{x}_j$  as the height of dendrogram at which these two points are first joined together by hierarchical clustering and we denote it by  $\eta_{ij}$ . The cophenetic correlation coefficient  $\rho$  is calculated as

$$\rho = \frac{\sum_{i < j} (\Delta_{ij} - \bar{\Delta})(\eta_{ij} - \bar{\eta})}{\sqrt{\sum_{i < j} (\Delta_{ij} - \bar{\Delta}) \sum_{i < j} (\eta_{ij} - \bar{\eta})}}, \quad (31)$$

where  $\bar{\Delta}$  and  $\bar{\eta}$  are the average values of  $\Delta_{ij}$  and  $\eta_{ij}$  respectively.

## 4.2 Summarising PSMs

Before using the PSMs with the MKL-based integrative clustering methods, we carry out some simulation studies to ensure that the kernel  $k$ -means algorithm performs equally well at summarising the MCMC output as other methods from the literature. The advantage is that the kernel  $k$ -means can be extended to combine multiple datasets.

We use the adjusted Rand index (ARI; Hubert and Arabie, 1985) as a measure of the similarity between the output of each clustering method and the true partition of the data.

To compute the ARI given two partitions  $U = \{U_1, \dots, U_K\}$  and  $V = \{V_1, \dots, V_L\}$ , we summarise the overlapping between each pair of subsets  $U_i$  and  $V_j$  by the values  $\nu_{ij} = |U_i \cap V_j|$ ,  $i = 1, \dots, K$ ,  $j = 1, \dots, L$ . The ARI is then calculated as

$$ARI = \frac{\sum_{k,l} (\nu_{kl} \binom{\nu_{k\cdot}}{2}) - \sum_k \binom{\nu_{k\cdot}}{2} \sum_l \binom{\nu_{\cdot l}}{2} / \binom{\nu}{2}}{\frac{1}{2} [\sum_k \binom{\nu_{k\cdot}}{2} + \sum_l \binom{\nu_{\cdot l}}{2}] - \sum_k \binom{\nu_{k\cdot}}{2} \sum_l \binom{\nu_{\cdot l}}{2} / \frac{\nu}{2}}. \quad (32)$$

This is the corrected-for-chance version of the Rand index (Rand, 1971) that is simply the number  $n_s$  of pairs of elements that are in the same subsets in both partitions  $U$  and  $V$ , plus the number  $n_d$  of pairs of elements that are in different subsets in both  $U$  and  $V$ , divided by the total number of pairs  $N^2$

$$RI = \frac{n_s + n_d}{N^2}. \quad (33)$$

We use the synthetic datasets described in setting A of Section 4.1 and compare the kernel  $k$ -means algorithm to the methods implemented in the R package `mcclust` (Fritsch and Ickstadt, 2009). All these methods take a PSM  $\Delta$  as input and find the clustering  $\mathbf{c}^*$  that maximises the

posterior expected adjusted Rand index (PEAR). This is achieved by choosing the clustering  $\mathbf{c}^*$  that maximises the following quantity:

$$\frac{\sum_{i < j} \mathbb{I}_{\{c_i^* = c_j^*\}} \Delta_{ij} - \sum_{i < j} \mathbb{I}_{\{c_i^* = c_j^*\}} \sum_{i < j} \Delta_{ij} / \binom{n}{2}}{\frac{1}{2} [\sum_{i < j} \mathbb{I}_{\{c_i^* = c_j^*\}} + \sum_{i < j} \Delta_{ij}] - \sum_{i < j} \mathbb{I}_{\{c_i^* = c_j^*\}} \sum_{i < j} \Delta_{ij} / \frac{n}{2}}. \quad (34)$$

The clusterings  $\mathbf{c}^*$  taken into consideration by these methods can be chosen in different ways. We use hierarchical clustering with  $1 - \Delta$  as distance matrix with average and complete linkage. The `maxpear` function tries all the possible number of clusters between one and a maximum number of cluster  $K_{\max}$  specified by the user. We consider both 6 and 20 as values for  $K_{\max}$ . We also use the `maxpear` function to try with all the clusterings in the MCMC output and take the one that maximises the quantity of Equation (34). We repeat this procedure using the `minVI` function of the R package `mcclust.ext` of [Wade and Ghahramani \(2018\)](#), where the selected  $\mathbf{c}^*$  is the one that minimises the lower bound to the posterior expected variation of information (Equation 6) from Jensen's inequality.

Figure 4 shows the boxplots of the adjusted Rand index obtained repeating the experiment with 100 different sets of synthetic data calculated for each of the considered clustering algorithms and for all values of  $w$ . We can see that the kernel  $k$ -means on average performs better than the other methods when the number of clusters is known and that it performs similarly to the others when the number of clusters is chosen to maximise the average silhouette.

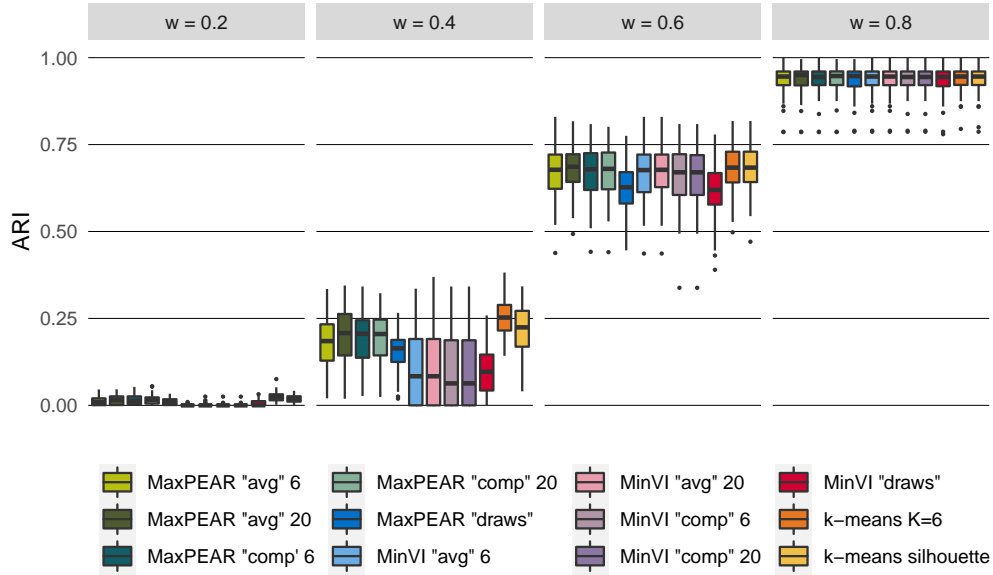


**Figure 4.** ARI for the kernel  $k$ -means applied to one dataset at a time, for different values of  $\rho$  compared to maximising the PEAR as suggested by [Fritsch and Ickstadt \(2009\)](#) and to minimising the VI as suggested by [Wade and Ghahramani \(2018\)](#). For both methods, we try different settings, namely: performing hierarchical clustering on the matrix  $1 - \Delta$  with average (avg) and complete (comp) linkage, with maximum number of clusters equal to either 6 or 20, as well as considering all the clusterings samples that are appear in the MCMC output (draws). For kernel  $k$ -means, the results obtained fixing the number of clusters to six and choosing it via the silhouette are presented.

### 4.3 Integrative clustering

We assess the MKL-based integrative clustering approaches described in Sections 3.3.2 and 3.3.3 in the four settings presented in Section 4.1. For each setting we consider four different subsets of data, each combining three out of our four synthetic datasets generated with  $w = 0.2, 0.4, 0.6, 0.8$ . In what follows, we refer to the dataset generated with  $w = 0.2$  as “dataset 0”, the one generated with  $w = 0.4$  as “dataset 1”, and so on, for ease of reference. Moreover, we indicate by “0+1+2” the integration of the datasets generated with values of  $w$  equal to 0.2, 0.4, and 0.6 respectively, and similarly for the other combinations of datasets. Here we show the ARI between the clusterings found via MKL integration and the true cluster labels, the weights assigned to each dataset in each setting are instead reported in the Supplementary Material.

**Setting A** The ARI obtained by combining the datasets in the unsupervised and outcome-guided frameworks is shown in the first row of Figure 5. The values of the ARI obtained in the previous section on each dataset separately are also reported. In all settings we set the number of clusters to the true value, six. The unsupervised integration performed using localised multiple kernel  $k$ -means allows us to reach values of the ARI that are close to those of the “best” dataset (i.e. the dataset that has the highest value of cluster separability) among the three datasets in each subset. This is because the unsupervised MKL approach considered here assign higher weights to the datasets that give rise to kernels with higher values of  $\rho$ , which in this case correspond to higher values of  $w$  (Cabassi and Kirk, 2020). Moreover, even higher values of the ARI are achieved via outcome-guided integration thanks to the smarter weighting of the datasets. In this case, the kernels that help separate the classes in the response have higher weights than the others.

**Setting B** In the second row of Figure 5 are shown the results obtained for setting B, where the PSMs are obtained exploiting (an adaptation of) the variable selection strategy of Chung and Dunson (2009) implemented in the R package PReMiuM. Despite the fact that the ARI of dataset 2 is lower than in the previous case, the integration results are better than in Setting A. Again, this is due to the fact that most informative kernels are weighted more highly than the other ones.

**Setting C** This simulation study helps us to show that the outcome-guided approach favours the clustering structures that agree with the structure in the response. For this reason we use a dataset with high cophenetic correlation coefficient whose clustering structure is not related to the response. The results are presented in the third row of Figure 5. Again, localised multiple kernel  $k$ -means assigns higher weights to the datasets that are more easily separable, i.e. datasets that give rise to kernels having higher cophenetic correlation coefficients. Note that here higher values of  $w$  correspond to higher cophenetic correlation. In this situation, this causes the ARI of the subsets of kernels that include dataset 4 to drop to zero. In the outcome-guided case, instead, the dataset that has the highest level of cluster separability but is not related to the outcome of interest has (almost) always weight equal to zero.

**Setting D** Lastly, we consider the case where the model used to generate the PSMs is profile regression (fourth row of Figure 5). We see that, as expected, the ARI is higher than in the previous cases for the clustering obtained with each dataset taken separately, except of course for dataset 4, that has a different clustering structure. This is reflected in an improvement of the ARI of the unsupervised and outcome-guided integration, for all considered subsets of data. In particular, the latter almost always allows us to retrieve the true clustering.

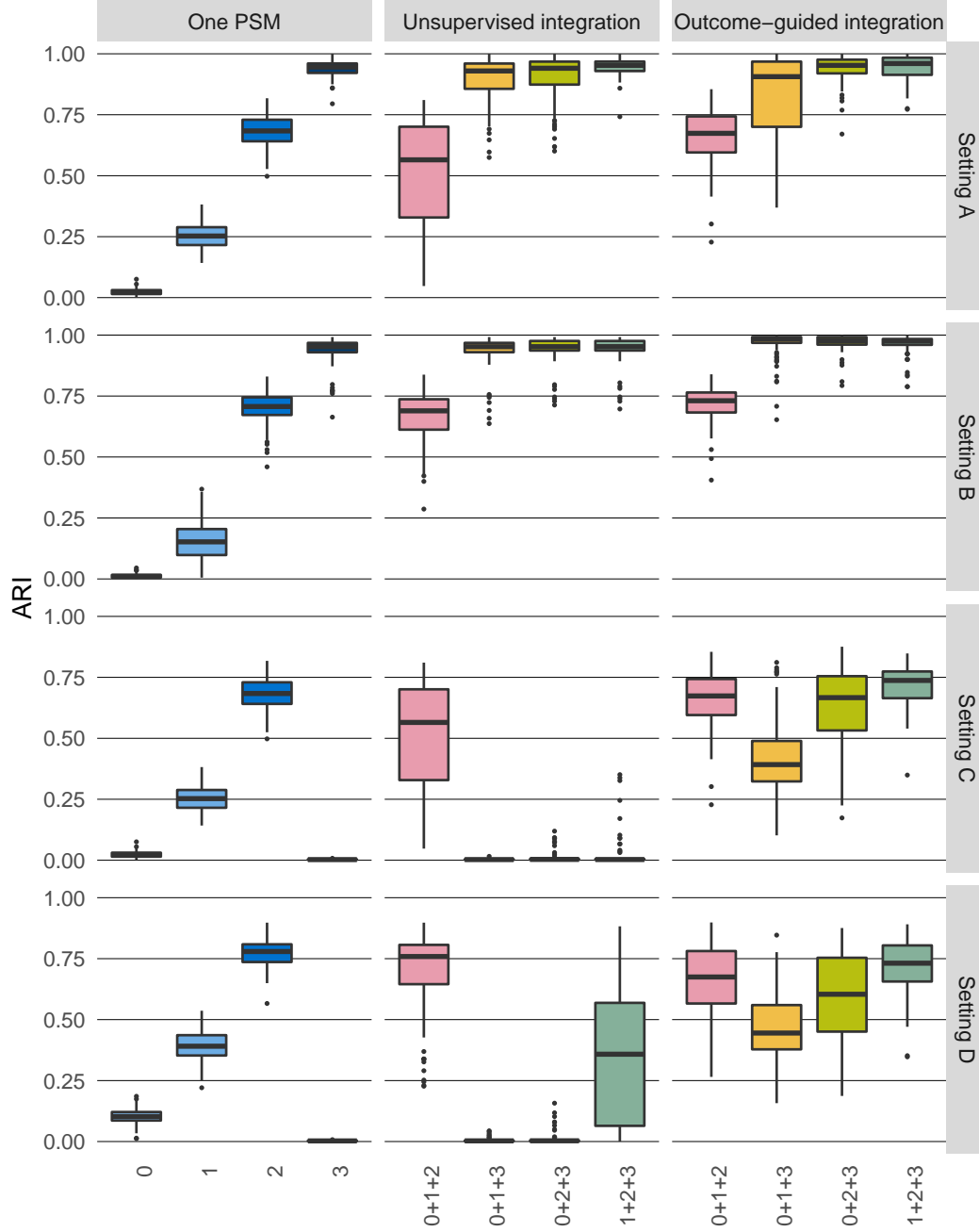


**Figure 5.** Simulation study, adjusted Rand index obtained by summarising the PSMs one at a time using kernel  $k$ -means (left), combining different subsets of three PSMs in an unsupervised fashion using localised multiple kernel  $k$ -means (centre), and combining the same subsets making use of a response variable and multi-class SVMs to determine each PSM's weight and using kernel  $k$ -means for the final clustering (right).



## 5 Integrative clustering: biological applications

We present results from applying our method to two exemplar integrative clustering problems from the literature. In Section 5.1 we perform integrative clustering on the dataset used for the analysis of 3,527 tumour samples from 12 different tumour types of Hoadley et al. (2014). In Section 5.2 we consider an example of *transcriptional module discovery*, to which a number of existing integrative clustering approaches have previously been applied (Cabassi and Kirk, 2020, Kirk et al., 2012, Savage et al., 2010).

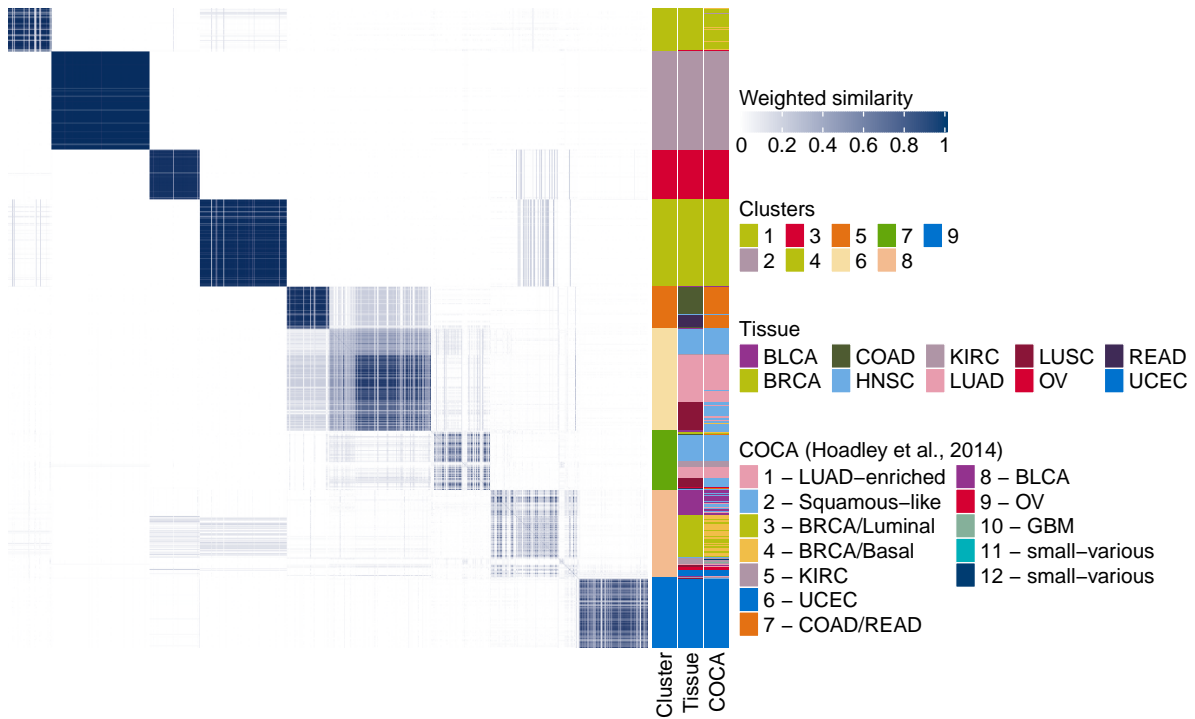
### 5.1 Multiplatform analysis of ten cancer types

We analyse the dataset of Hoadley et al. (2014), which contains data regarding 3,527 tumour samples spanning 12 different tumour types. This dataset is particularly suitable for two purposes: (i) determining whether 'omic signatures are shared across different tumour types and (ii) discovering tumour subtypes. The 'omic layers available are: DNA copy number, DNA methylation, mRNA expression, microRNA expression and protein expression. Hoadley et al. (2014) used *Cluster-Of-Clusters Analysis* (COCA; Cabassi and Kirk, 2020) to cluster the data and found that the clusters were highly correlated with the tissue of origin of each tumour sample and were shown to be of clinical interest.

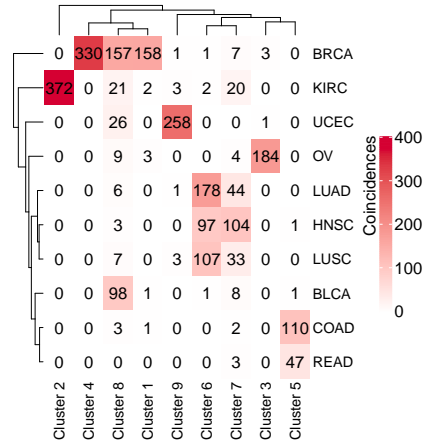
Here, we combine the data layers both in the unsupervised and outcome-guided frameworks. We make use of the C implementation (Mason et al., 2016) of the *multiple dataset integration* (MDI) method of Kirk et al. (2012) to produce PSMs for each data layer separately. In order to be able to do so, we only include in our analysis the tumour samples that have no missing values; this reduces the sample size to 2,421 and the number of tumour types available for the analysis to ten. A mixture of Gaussians is used for the continuous layers (DNA copy number, microRNA, and protein expression), while the multinomial model is used for the methylation data, which are categorical. Due to the high number of features, it is not possible to produce a PSM for the full mRNA dataset, so we exclude it from the analysis presented here. In the Supplementary Material, however, we show how the variable selection method developed specifically for multi-omic data by Cabassi et al. (2020) can be employed in this case to reduce the size of each data layer and integrate all five data types.

#### 5.1.1 Unsupervised integration

We combine the PSMs of the four data layers via multiple kernel  $k$ -means with number of clusters going from 2 to 50. We choose the number of clusters that maximises the silhouette, which is 9 (Supplementary Material). The resulting clusters are shown in Figure 6. Six out of the nine clusters contain almost exclusively samples from one tissue: most samples of renal cell carcinoma (KIRC) are in cluster 2, almost all statistical units in clusters 1 and 4 are breast cancer samples, most serous ovarian carcinoma (OV) samples are in cluster 3, bladder urothelial adenocarcinoma (BLCA) samples in cluster 8, and endometrial cancer (UCEC) samples in cluster 9. Cluster 5, instead, is formed by the colon and rectal adenocarcinoma samples together, and corresponds exactly to cluster 7 of Hoadley et al. (COAD/READ). Moreover, lung squamous cell carcinoma (LUSC), lung adenocarcinoma (LUAD), and head and neck squamous cell carcinoma (HNSC) are divided into two clusters (6 and 7). Cluster 8 contains the remaining samples. The average weights assigned to each data layer are: 6.9% to the copy number data, 7.5% to the methylation data, 7% to the microRNA expression data, and 78.7% to the protein expression data.



(a) Clusters and weighted kernel.



(b) Coincidence matrix.

**Figure 6.** Unsupervised multiplatform analysis of ten cancer types. (a) Left: weighted kernel. The rows and columns correspond to cancer samples. Higher values of similarity between samples are indicated in blue. Right: final clusters, tissues of origin, and COCA clusters. (b) Coincidence matrix comparing the tissue of origin of the tumour samples (rows) with the clusters (columns).

### 5.1.2 Outcome-guided integration

We obtain the weights for the outcome-guided integration via the SimpleMKL algorithm, which are as follows: DNA copy number 35.9%, methylation 13.5%, microRNA expression 33.8%, and protein expression 16.8%. We then cluster the data using kernel  $k$ -means with number of clusters going from 2 to 50. The silhouette is maximised at  $K = 27$  (Supplementary Material). The clusters obtained in this way are shown in Figure 7. It is interesting to note that, in this case, each cluster contains almost exclusively tumour samples from the same tissue. The only exceptions are clusters 4 and 22, which contain both lung and head/neck squamous cell carcinoma samples, and clusters 14 and 25 in which colon and rectal adenocarcinomas are clustered together, like in the unsupervised case. Each tumour type, except for ovarian and bladder cancers, is divided into multiple subclusters. Further analysis would be required to assess whether these clusters are clinically relevant. Interestingly, we observe a distinction between luminal (i.e. estrogen receptor-positive and HER2-positive) and basal breast cancer samples (the former are in clusters 8, 9, 17, 19, 23, 24, 27, while the latter are in cluster 13). This was also observed by Hoadley et al. (2014).

## 5.2 Transcriptional module discovery

For this example we consider transcriptional module discovery for yeast (*Saccharomyces cerevisiae*). The goal is to find clusters of genes that share a common biological function and are co-regulated by a common set of transcription factors. Previous studies have demonstrated that combining gene expression datasets with information about transcription factor binding can improve detection of meaningful transcriptional modules (Ihmels et al., 2002, Savage et al., 2010).

We combine the ChIP-chip dataset of Harbison et al. (2004), which provides binding information for 117 transcriptional regulators, with the expression dataset of Granovskaia et al. (2010). The ChIP-chip data are discretised as in Savage et al. (2010) and Kirk et al. (2012). The measurements in the dataset of Granovskaia et al. (2010) represent the expression profiles of 551 genes at 41 different time points of the cell cycle.

Since the goal is to find clusters of genes, here the statistical units correspond to the genes and the covariates to 41 experiments of gene expression measurement for the expression dataset and to the 117 considered transcriptional regulators in the ChIP-chip dataset. To produce the posterior similarity matrices for the two datasets, we use the DPMSysBio Matlab package of Žurauskienė et al. (2016). For each dataset, we run 10,000 iterations of the MCMC algorithm and summarise the output into a PSM. The PSMs obtained in this way are reported in the Supplementary Material.

We combine the PSMs using our unsupervised MKL approach. The average weights assigned by the localised multiple kernel  $k$ -means to each matrix and the values of the average silhouette for different numbers of clusters are reported in the Supplementary Material. We set the number of clusters to 25, which is the value that maximises the silhouette. The final clusters are shown in Figure 8 next to the two datasets and the combined PSM. In order to determine whether our clustering is biologically meaningful, we use the Gene Ontology Term Overlap (GOTO) scores defined by Mistry and Pavlidis (2008). Denoting by  $\text{annot}g_i$  the set of all direct annotations for each gene and all of their associated parent terms, the GOTO similarity between two genes  $g_i, g_j$  is the number of annotations that the two genes share:

$$\text{sim}_{\text{GOTO}}(g_i, g_j) = |\text{annot}g_i \cap \text{annot}g_j|. \quad (35)$$

Details on how to compute the average overall GOTO score of a clustering are given in the Supplementary Material of Kirk et al. (2012). The GOTO scores are reported in Table 1. The two datasets combined achieve higher GOTO scores than those of the clusters obtained using each



dataset separately. We also compare these GOTO scores to those obtained with the two methods used in Cabassi and Kirk (2020). The first one is COCA, a simple, unweighted algorithm for integrative clustering that is widely used in practice (Hoadley et al., 2014, The Cancer Genome Atlas Research Network, 2012). The other integrative method considered here is KLIC (*Kernel Learning Integrative Clustering*), by which we mean the integration of multiple kernels via multiple kernel  $k$ -means, where the kernels are generated via consensus clustering (Figure 1). The clusters obtained with these two alternative methods have lower GOTO scores than the integration of PSMs. For COCA, this is result not unexpected, since the method is unweighted and has previously been shown to perform less well than KLIC. The difference between what is referred to as KLIC here and the unsupervised integration of PSMs, however, only lies in how the kernels are constructed. These scores therefore suggest that kernels generated from probabilistic models can lead to more accurate results than those built using consensus clustering.

Dataset(s)	GOTO BP	GOTO MF	GOTO CC
ChIP data (Harbison <i>et al.</i> )	6.18	0.97	8.54
Expression data (Granovskaia <i>et al.</i> )	7.07	1.04	8.90
ChIP+Expression data: COCA	5.74	0.90	8.19
ChIP+Expression data: KLIC	6.60	0.96	8.66
ChIP+Expression data: integration of PSMs	<b>7.15</b>	<b>1.05</b>	<b>8.93</b>

**Table 1.** Gene Ontology Term Overlap scores. “BP” stands for Biological Process ontology, “MF” for Molecular Function, and “CC” for Cellular Component. The number of clusters used for every method is 25.

## 6 Conclusion

We have presented a novel method for summarising a sample of clusterings from the posterior distribution of an MCMC algorithm for Bayesian clustering, based on kernel methods. We have also extended this method to allow us to integrate multiple PSMs. This can be done either in an unsupervised or in an outcome-guided way. The former weights each PSM according to how well defined is the clustering structure that it shows, the latter gives more importance to the PSMs that better reflect the structure encountered in the response variable of choice.

We have used simulation examples to show that our method gives comparable performances in terms of proportion of correct co-clustering as the existing techniques. We have also demonstrated that the integration of multiple datasets gives better results than using one dataset at a time. Additionally, we proved that, if a variable related to the output of interest is available, our method can assign higher weights to the PSMs that are more closely related to that. The simulation examples prove that this feature can be extremely useful when not all the PSMs have the same clustering structure.

Finally, we have applied the novel methods to two real data applications. The pancancer data analysis shows that the outcome-guided integration of multiple PSMs can potentially be used in the context of tumour subtype discovery. The yeast example demonstrates that the proposed method is able to identify groups of genes that are co-expressed and co-regulated that are more biologically meaningful than those determined via state-of-the-art integrative algorithms.

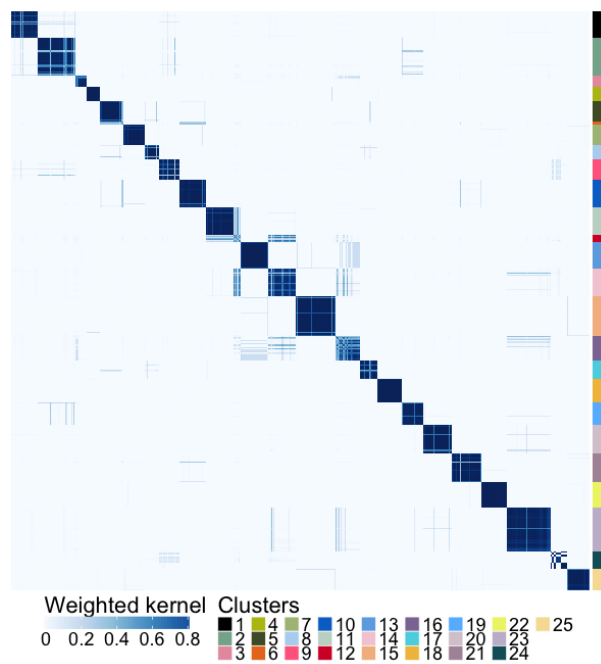
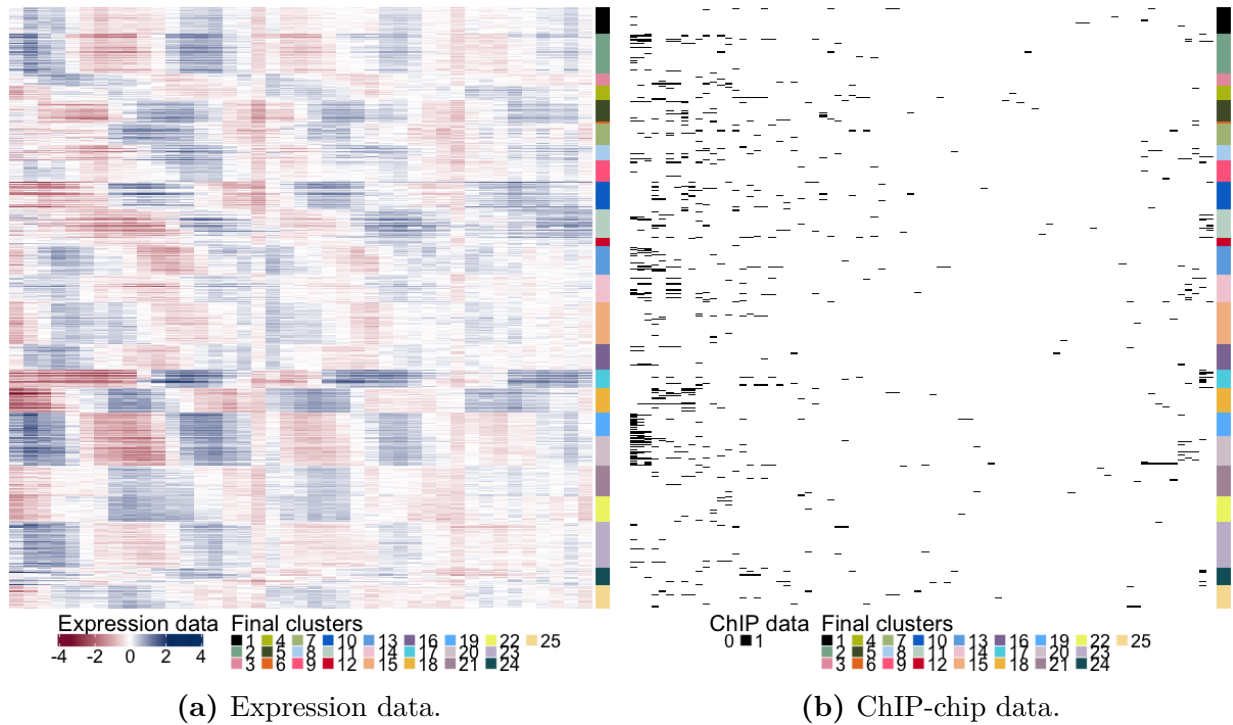


**Figure 8.** Transcriptional module discovery, integration of the [Harbison et al. \(2004\)](#) and [Granovskaia et al. \(2010\)](#) datasets. **(a)** Expression data. Each row corresponds to a gene and each column to a different time point. **(b)** ChIP-chip data. Each row corresponds to a gene and each column to a transcriptional regulator. **(c)** Weighted kernel. The rows and columns correspond to the genes. Higher values of similarity between genes are indicated in blue. To the left of each plot is shown the final clustering, obtained by integrating the PSMs of the expression and ChIP-chip data via multiple kernel  $k$ -means.



## Funding

A. Cabassi and P.D.W. Kirk are supported by the MRC [MC\_UU\_00002/13]. This work was supported by the National Institute for Health Research [Cambridge Biomedical Research Centre at the Cambridge University Hospitals NHS Foundation Trust]. The views expressed are those of the authors and not necessarily those of the NHS, the NIHR or the Department of Health and Social Care. Partly funded by the RESCUER project. RESCUER has received funding from the European Union’s Horizon 2020 research and innovation programme under grant agreement No. 847912.

## References

- Antoniak, C. E. (1974). Mixtures of dirichlet processes with applications to bayesian nonparametric problems. *The annals of statistics*, pages 1152–1174. *Referred to on page 3*.
- Baudat, G. and Anouar, F. (2000). Generalized discriminant analysis using a kernel approach. *Neural Computation*, 12(10):2385–2404. *Referred to on page 5*.
- Bennett, K. and Mangasarian, O. L. (1992). Robust linear programming discrimination of two linearly inseparable sets. *Optimization Methods and Software*, 1(1):23–34. *Referred to on page 9*.
- Binder, D. A. (1978). Bayesian cluster analysis. *Biometrika*, 1:31–38. *Referred to on page 3*.
- Bishop, C. M. (2006). *Pattern Recognition and Machine Learning*. Springer, 1st edition edition. *Referred to on pages 2, 8, 9, and 10*.
- Blei, D. M., Jordan, M. I., et al. (2006). Variational inference for dirichlet process mixtures. *Bayesian analysis*, 1(1):121–143. *Referred to on page 2*.
- Boser, B. E., Guyon, I. M., and Vapnik, V. N. (1992). A training algorithm for optimal margin classifiers. *Proceedings of the 5th annual workshop on Computational Learning Theory*. *Referred to on page 8*.
- Cabassi, A. and Kirk, P. D. W. (2020). Multiple kernel learning for integrative consensus clustering of ‘omic datasets. *Bioinformatics*. btaa593. *Referred to on pages 2, 5, 9, 15, 17, and 21*.
- Cabassi, A., Seyres, D., Frontini, M., and Kirk, P. D. W. (2020). Penalised logistic regression for multi-omic data with an application to cardiometabolic syndrome. *arXiv*. 2008.00235. *Referred to on page 17*.
- Celeux, G., Hurn, M., and Robert, C. P. (2000). Computational and inferential difficulties with mixture posterior distributions. *Journal of the American Statistical Association*, 95(451):957–970. *Referred to on page 2*.
- Chung, Y. and Dunson, D. B. (2009). Nonparametric bayes conditional distribution modeling with variable selection. *Journal of the American Statistical Association*, 104(488):1646–1660. *Referred to on page 15*.
- Dahl, D. B. (2006). Model-based clustering for expression data via a dirichlet process mixture model. *Bayesian inference for gene expression and proteomics*, 4:201–218. *Referred to on pages 3 and 4*.
- Dudoit, S. and Fridlyand, J. (2002). A prediction-based resampling method for estimating the number of clusters in a dataset. *Genome Biology*, 3(7). *Referred to on page 11*.

- Everitt, B. S. (1993). *Cluster analysis*. Hodder Education. *Referred to on page 4.*
- Ferguson, T. S. (1973). A bayesian analysis of some nonparametric problems. *The Annals of Statistics*, pages 209–230. *Referred to on page 3.*
- Friedman, J., Hastie, T., and Tibshirani, R. (2001). *The elements of statistical learning*, volume 1. Springer Series in Statistics. *Referred to on page 5.*
- Fritsch, A. and Ickstadt, K. (2009). Improved Criteria for Clustering Based on the Posterior Similarity Matrix. *Bayesian Analysis*, 4(2):367–392. *Referred to on pages 2, 3, 4, 13, and 14.*
- Gelfand, A. E. and Smith, A. F. (1990). Sampling-based approaches to calculating marginal densities. *Journal of the American statistical association*, 85(410):398–409. *Referred to on page 2.*
- Girolami, M. (2002). Mercer kernel-based clustering in feature space. *IEEE Transactions on Neural Networks*, 13(3):780–784. *Referred to on page 7.*
- Gönen, M. and Margolin, A. A. (2014). Localized data fusion for kernel k-means clustering with application to cancer biology. In *Advances in Neural Information Processing Systems*, pages 1305–1313. *Referred to on pages 2 and 8.*
- Granovskaia, M. V., Jensen, L. J., Ritchie, M. E., Toedling, J., Ning, Y., Bork, P., Huber, W., and Steinmetz, L. M. (2010). High-resolution transcription atlas of the mitotic cell cycle in budding yeast. *Genome Biology*, 11(3):R24. *Referred to on pages 19 and 22.*
- Harbison, C. T., Gordon, D. B., Lee, T. I., Rinaldi, N. J., Macisaac, K. D., Danford, T. W., Hannett, N. M., Tagne, J.-B., Reynolds, D. B., Yoo, J., et al. (2004). Transcriptional regulatory code of a eucaryotic genome. *Nature*, 431(7004):99–104. *Referred to on pages 19 and 22.*
- Hartigan, J. A. and Wong, M. A. (1979). Algorithm as 136: A k-means clustering algorithm. *Journal of the Royal Statistical Society. Series c (Applied Statistics)*, 28(1):100–108. *Referred to on page 1.*
- Hoadley, K. A., Yau, C., Wolf, D. M., Cherniack, A. D., Tamborero, D., Ng, S., Leiserson, M. D., Niu, B., McLellan, M. D., Uzunangelov, V., et al. (2014). Multiplatform analysis of 12 cancer types reveals molecular classification within and across tissues of origin. *Cell*, 158(4):929–944. *Referred to on pages 17, 19, and 21.*
- Hubert, L. and Arabie, P. (1985). Comparing partitions. *Journal of Classification*, 2(1):193–218. *Referred to on pages 4 and 13.*
- Ihmels, J., Friedlander, G., Bergmann, S., Sarig, O., Ziv, Y., and Barkai, N. (2002). Revealing modular organization in the yeast transcriptional network. *Nature Genetics*, 31(4):370. *Referred to on page 19.*
- Kaufman, L. and Rousseeuw, P. J. (1990). *Finding groups in data: an introduction to cluster analysis*, volume 344. John Wiley & Sons. *Referred to on pages 1 and 4.*
- Kirk, P. D., Griffin, J. E., Savage, R. S., Ghahramani, Z., and Wild, D. L. (2012). Bayesian correlated clustering to integrate multiple datasets. *Bioinformatics*, 28(24):3290–3297. *Referred to on pages 17 and 19.*

- Knerr, S., Personnaz, L., and Dreyfus, G. (1990). Single-layer learning revisited: a stepwise procedure for building and training a neural network. *Neurocomputing: Algorithms, Architectures and Applications*, 68(41-50):71. Referred to on page 10.
- Lanckriet, G. R., De Bie, T., Cristianini, N., Jordan, M. I., and Noble, W. S. (2004). A statistical framework for genomic data fusion. *Bioinformatics*, 20(16):2626–2635. Referred to on pages 2 and 10.
- Liverani, S., Hastie, D. I., Azizi, L., Papathomas, M., and Richardson, S. (2015). PReMiuM: An R package for Profile Regression Mixture Models Using Dirichlet Processes. *Journal of Statistical Software*, 31(2). Referred to on page 12.
- Luenberger, D. G. and Ye, Y. (1984). *Linear and nonlinear programming*, volume 2. Springer. Referred to on page 10.
- Mason, S. A., Sayyid, F., Kirk, P. D., Starr, C., and Wild, D. L. (2016). Mdi-gpu: accelerating integrative modelling for genomic-scale data using gp-gpu computing. *Statistical Applications in Genetics and Molecular Biology*, 15(1):83–86. Referred to on page 17.
- McLachlan, G. J. and Peel, D. (2004). *Finite mixture models*. John Wiley & Sons. Referred to on page 1.
- Medvedovic, M. and Sivaganesan, S. (2002). Bayesian infinite mixture model based clustering of gene expression profiles. *Bioinformatics*, 18(9):1194–1206. Referred to on pages 3 and 4.
- Meilă, M. (2007). Comparing clusterings—an information based distance. *Journal of multivariate analysis*, 98(5):873–895. Referred to on page 4.
- Mika, S., Rätsch, G., Weston, J., Schölkopf, B., and Müllers, K.-R. (1999). Fisher discriminant analysis with kernels. In *Proceedings of the 1999 IEEE Signal Processing Society Workshop.*, pages 41–48. IEEE. Referred to on page 5.
- Milligan, G. W. and Cooper, M. C. (1985). An examination of procedures for determining the number of clusters in a data set. *Psychometrika*, 50(2):159–179. Referred to on page 11.
- Mistry, M. and Pavlidis, P. (2008). Gene ontology term overlap as a measure of gene functional similarity. *BMC bioinformatics*, 9:327. Referred to on page 19.
- Molitor, J., Papathomas, M., Jerrett, M., and Richardson, S. (2010). Bayesian profile regression with an application to the national survey of children’s health. *Biostatistics*, 11(3):484–498. Referred to on pages 4 and 12.
- Monti, S., Tamayo, P., Mesirov, J., and Golub, T. (2003). Consensus clustering: a resampling-based method for class discovery and visualization of gene expression microarray data. *Machine Learning*, 52(1-2):91–118. Referred to on page 2.
- Neal, R. M. (2000). Markov Chain Sampling Methods for Dirichlet Process Mixture Models. *Journal of Computational and Graphical Statistics*, 9(2):249–265. Referred to on page 3.
- Platt, J. C. (1999). Fast training of support vector machines using sequential minimal optimization. In B. Schölkopf, C. J. C. Burges, A. J. S., editor, *Advances in Kernel Methods – Support Vector Learning*, chapter 12, pages 185–208. MIT Press. Referred to on page 10.

- Rakotomamonjy, A. and Bach, F. (2007). More efficiency in multiple kernel learning. In *Proceedings of the 24th International Conference on Machine Learning*, pages 775–782. Referred to on page [10](#).
- Rakotomamonjy, A., Bach, F. R., Canu, S., and Grandvalet, Y. (2008). SimpleMKL. *Journal of Machine Learning Research*, 9:2491–2521. Referred to on pages [2](#), [9](#), and [11](#).
- Rand, W. M. (1971). Objective Criteria for the Evaluation of Clustering Methods. *Journal of the American Statistical Association*, 66(336):846–850. Referred to on page [13](#).
- Rasmussen, C. E. (2000). The infinite gaussian mixture model. In *Advances in neural information processing systems*, pages 554–560. Referred to on pages [2](#) and [3](#).
- Richardson, S. and Green, P. (1997). On Bayesian Analysis of Mixtures with an Unknown Number of Components. *Journal of the Royal Statistical Society: Series B (Statistical Methodology)*, (59.4):731–792. Referred to on page [3](#).
- Roth, V. and Steinhage, V. (2000). Nonlinear discriminant analysis using kernel functions. In *Advances in neural information processing systems*, pages 568–574. Referred to on page [5](#).
- Rousseeuw, P. J. (1987). Silhouettes: a graphical aid to the interpretation and validation of cluster analysis. *Journal of computational and applied mathematics*, 20:53–65. Referred to on page [11](#).
- Savage, R. S., Ghahramani, Z., Griffin, J. E., De La Cruz, B. J., and Wild, D. L. (2010). Discovering transcriptional modules by bayesian data integration. *Bioinformatics*, 26(12):i158–i167. Referred to on pages [17](#) and [19](#).
- Schölkopf, B., Smola, A., and Müller, K.-R. (1998). Nonlinear component analysis as a kernel eigenvalue problem. *Neural Computation*, 10(5):1299–1319. Referred to on page [5](#).
- Schölkopf, B. and Smola, A. J. (2001). *Learning with kernels: support vector machines, regularization, optimization, and beyond*. MIT press. Referred to on page [8](#).
- Shawe-Taylor, J. and Cristianini, N. (2004). *Kernel methods for pattern analysis*. Cambridge University Press. Referred to on pages [2](#) and [5](#).
- Steinhaus, H. (1956). Sur la division des corps matériels en parties. *Bulletin de l’Académie Polonaise des Sciences*, IV(12):801–804. Referred to on page [6](#).
- The Cancer Genome Atlas Research Network (2012). Comprehensive molecular portraits of human breast tumours. *Nature*, 487(7407):61–70. Referred to on page [21](#).
- Tibshirani, R. et al. (2001). Estimating the number of clusters in a data set via the gap statistic. *Journal of the Royal Statistical Society: Series B (Statistical Methodology)*, 63(2):411–423. Referred to on page [11](#).
- Vapnik, V. N. (1998). *Statistical learning theory*. Wiley New York. Referred to on pages [5](#) and [10](#).
- Wade, S. and Ghahramani, Z. (2018). Bayesian cluster analysis: Point estimation and credible balls (with discussion). *Bayesian Analysis*, 13(2):559–626. Referred to on pages [2](#), [3](#), [4](#), and [14](#).
- Yeung, K. Y., Haynor, D. R., and Ruzzo, W. L. (2001). Validating clustering for gene expression data. *Bioinformatics*, 17(4):309–318. Referred to on page [11](#).

Žurauskienė, J., Kirk, P. D., and Stumpf, M. P. (2016). A graph theoretical approach to data fusion. *Statistical Applications in Genetics and Molecular Biology*, 15(2):107–122. Referred to on page [19](#).

# Kernel learning approaches for summarising and combining posterior similarity matrices

Alessandra Cabassi<sup>1</sup>, Sylvia Richardson<sup>1</sup>, and Paul D. W. Kirk<sup>1,2</sup>

<sup>1</sup>*MRC Biostatistics Unit*

<sup>2</sup>*Cambridge Institute of Therapeutic Immunology & Infectious Disease  
University of Cambridge, U.K.*

## Contents

<b>S1 Simulation study</b>	<b>S2</b>
S1.1 Data . . . . .	S2
S1.2 Integrative clustering . . . . .	S3
S1.3 Additional simulation settings . . . . .	S5
S1.3.1 Different number of covariates . . . . .	S5
S1.3.2 Using the true cluster labels as response variable . . . . .	S7
<b>S2 Integrative clustering: biological applications</b>	<b>S10</b>
S2.1 Multiplatform analysis of ten cancer types . . . . .	S10
S2.1.1 Variable selection . . . . .	S10
S2.1.2 MCMC convergence assessment . . . . .	S10
S2.1.3 Unsupervised integration: additional figures . . . . .	S33
S2.1.4 Unsupervised integration after variable selection, $\alpha = 0.1$ . . . . .	S39
S2.1.5 Unsupervised integration after variable selection, $\alpha = 0.5$ . . . . .	S42
S2.1.6 Unsupervised integration after variable selection, $\alpha = 1$ . . . . .	S44
S2.1.7 Outcome-guided integration: additional figures . . . . .	S46
S2.1.8 Outcome-guided integration after variable selection, $\alpha = 0.1$ . . . . .	S51
S2.1.9 Outcome-guided integration after variable selection, $\alpha = 0.5$ . . . . .	S53
S2.1.10 Outcome-guided integration after variable selection, $\alpha = 1$ . . . . .	S55
S2.2 Transcriptional module discovery . . . . .	S57
S2.2.1 Additional figures . . . . .	S57
S2.2.2 A different set of data . . . . .	S59
<b>Bibliography</b>	<b>S62</b>



## S1 Simulation study

### S1.1 Data

In Figure S1 is shown one of the datasets used for the simulation studies, with value of  $w$  set to 0.8 and number of covariates equal to 20. The first ten covariates determine six different clusters, the remaining covariates have no clustering structure. The response variable is generated as described in the main paper.

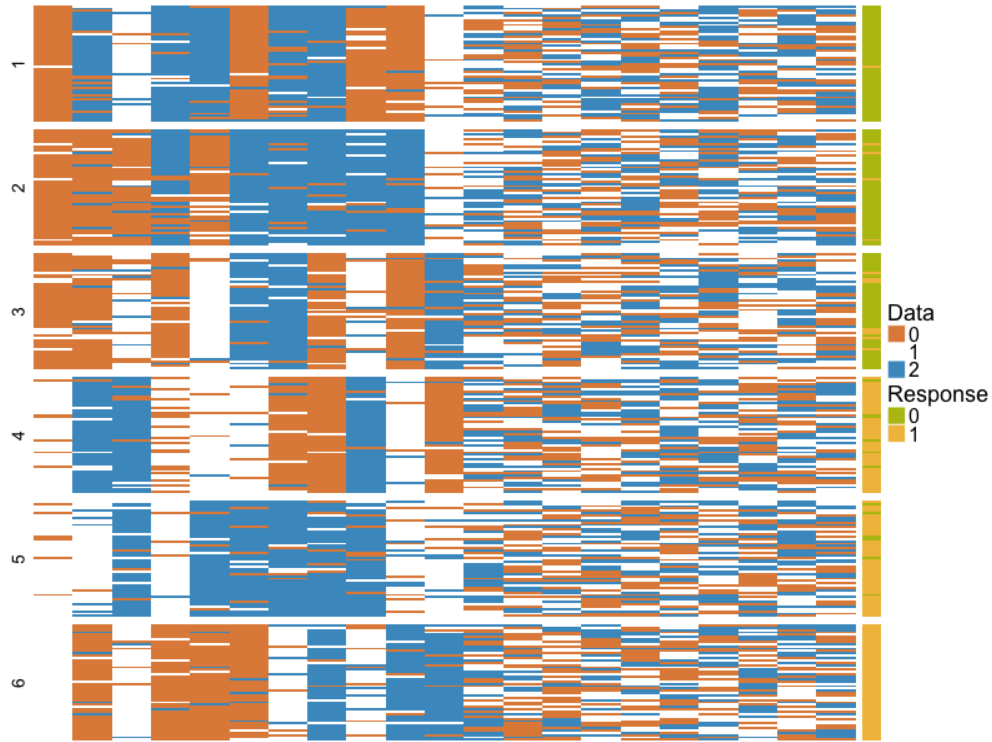


**Figure S1.** One of the datasets used for the simulation studies. The data are categorical, taking values 0, 1 or 2, the response is binary. The rows are separated by cluster, the cluster labels are indicated on the right of the data matrix.

## S1.2 Integrative clustering

Figures S2 and S3 show the weights assigned to each dataset by the unsupervised and outcome-guided methods for the integration of multiple PSMs presented in the main paper.

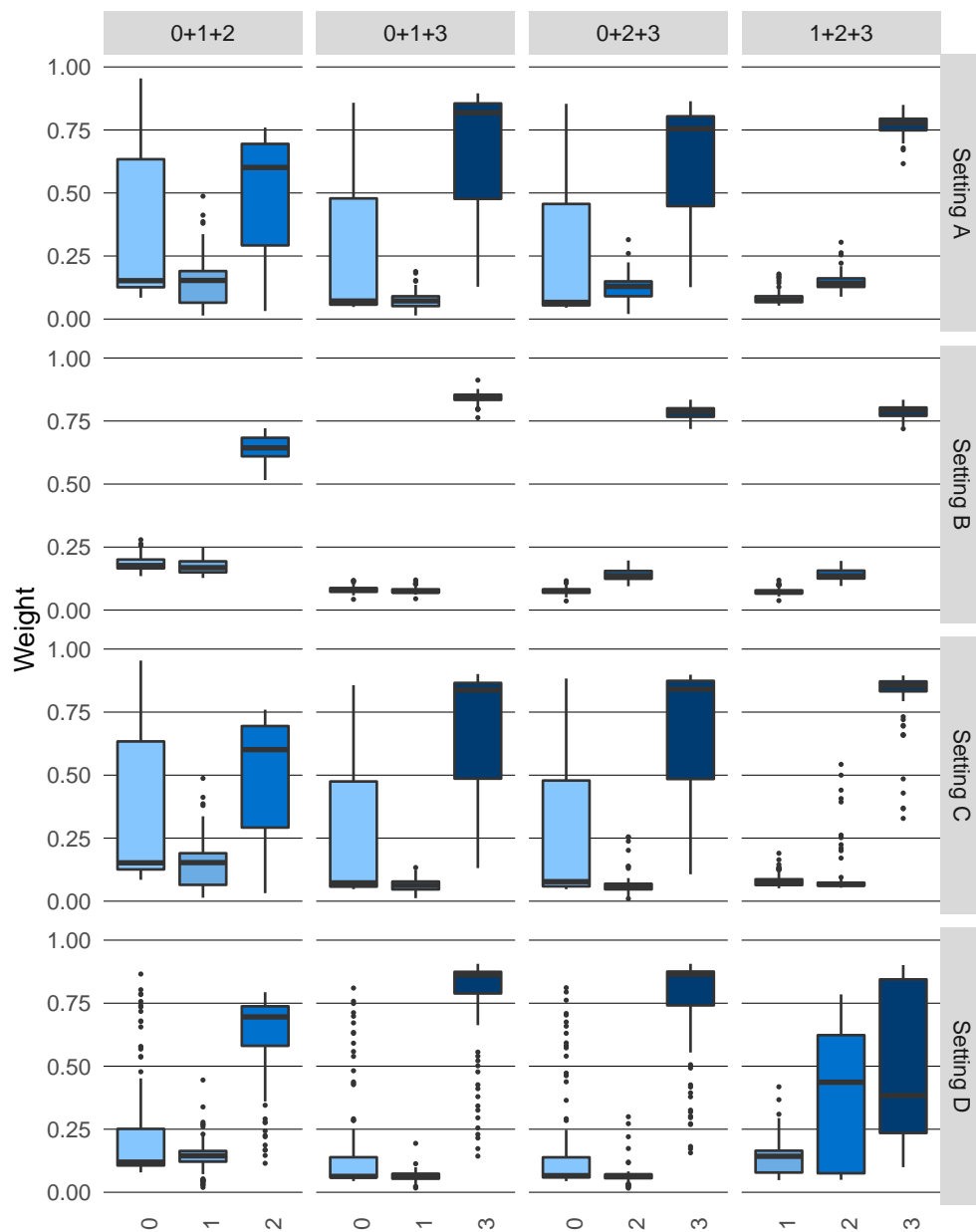


**Figure S2.** Weights assigned to each PSM for each subset of datasets by the unsupervised integration method.

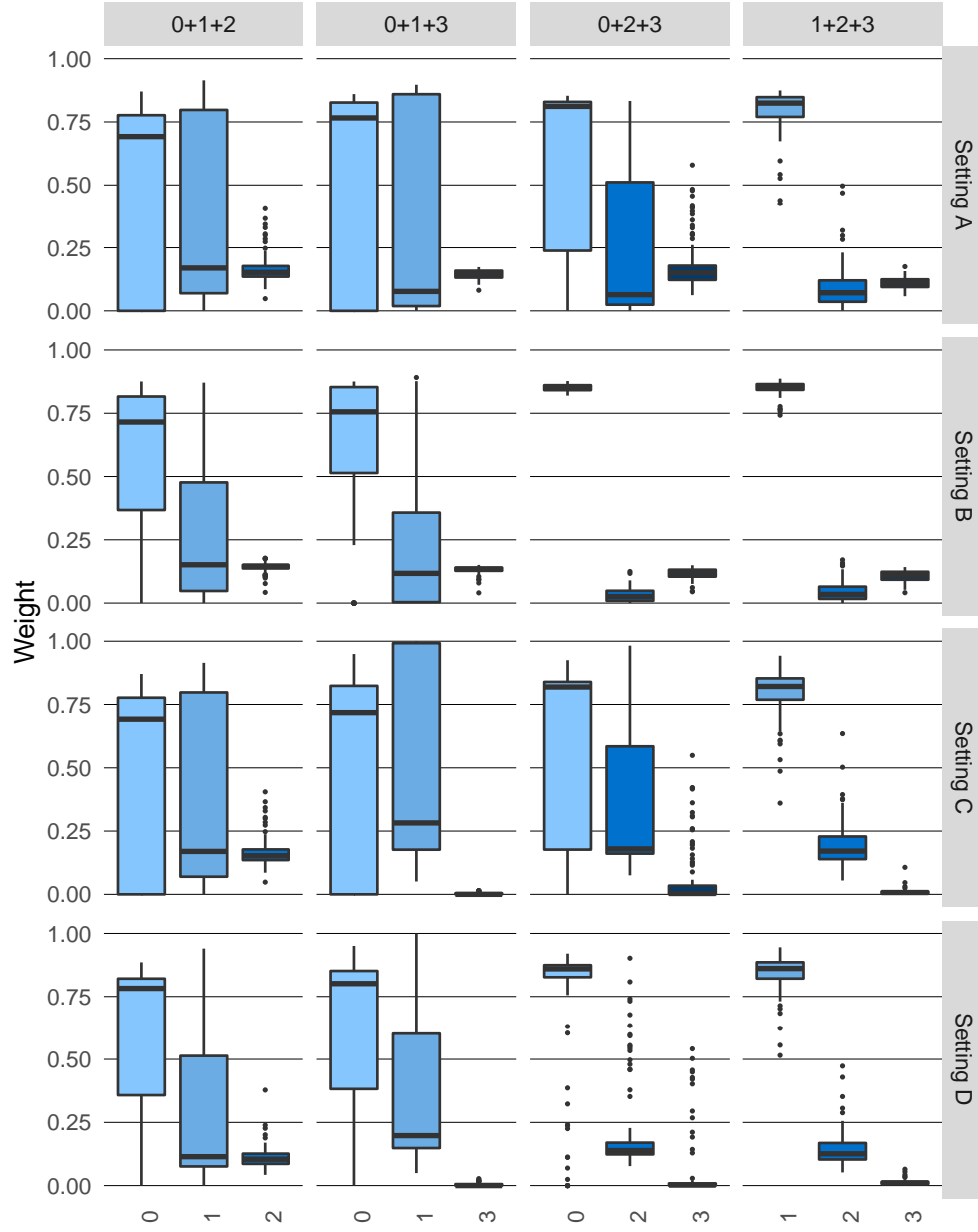
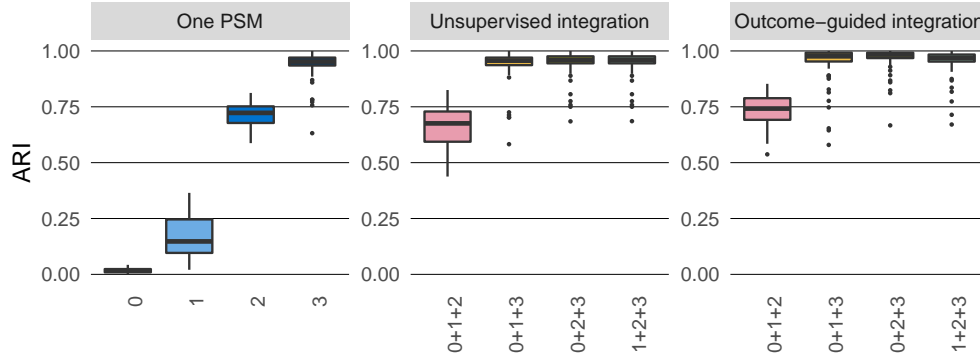


**Figure S3.** Weights assigned to each PSM for each subset of datasets by the outcome-guided integration methods.

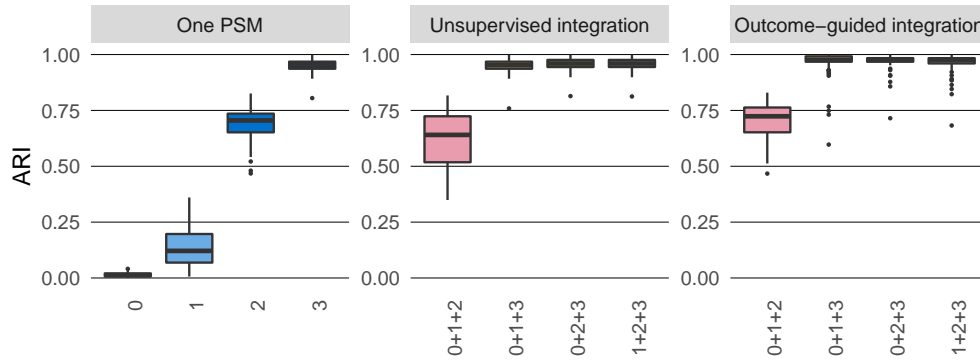
### S1.3 Additional simulation settings

#### S1.3.1 Different number of covariates

We present here the results obtained for simulation setting B, with different numbers of irrelevant covariates. Figure S4 shows the adjusted Rand index and Figure S5 the weights assigned to each kernel.

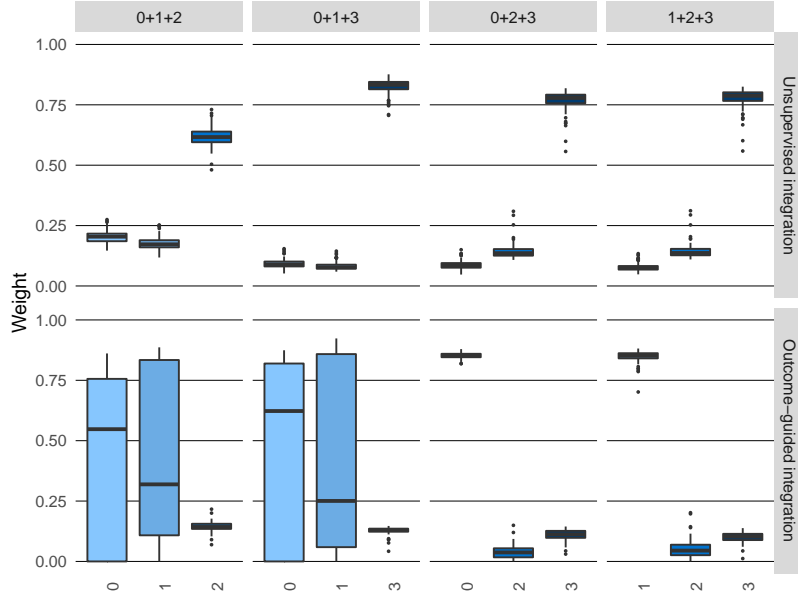


(a) Setting B, 2 covariates without clustering structure.

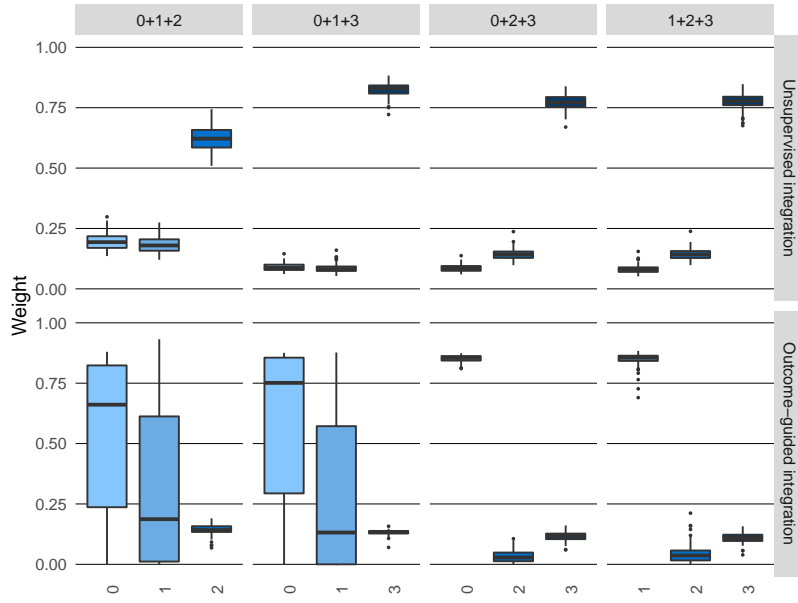


(b) Setting B, 5 covariates without clustering structure.

**Figure S4.** Adjusted Rand index obtained by summarising the PSMs one at a time using kernel  $k$ -means (left), combining different subsets of three PSMs in an unsupervised fashion using localised multiple kernel  $k$ -means (centre), and combining the same subsets making use of a response variable and multi-class SVMs to determine each PSM's weight and using kernel  $k$ -means for the final clustering (right).



(a) Setting B, 2 covariates without clustering structure.



(b) Setting B, 5 covariates without clustering structure.

**Figure S5.** Weights assigned to each PSM for each subset of datasets by the unsupervised (above) and outcome-guided (below) integration methods for PSMs.

### S1.3.2 Using the true cluster labels as response variable

We repeat the simulation study presented in the main paper, using the true cluster labels as the response variable, both for the outcome-guided integration (in all simulation settings) and to generate the PSMs with profile regression (in Setting D). Although the true cluster labels are not available in practice, this simulation study is used here to determine a putative upper bound on the performances of outcome-guided integration.

The ARI is reported in Figure S6. As expected, the outcome-guided integration has higher values of the ARI in all settings, compared to the case where the outcome is a binary variable. Moreover, in Setting D the ARI of each PSM taken individually is also higher here than in the other simulation study.

The weights assigned to each kernel matrix are shown in Figure S7. These are of easier interpretation compared to those presented above (Figure S3): on average, kernels originated from datasets with higher cluster separability have higher weights.

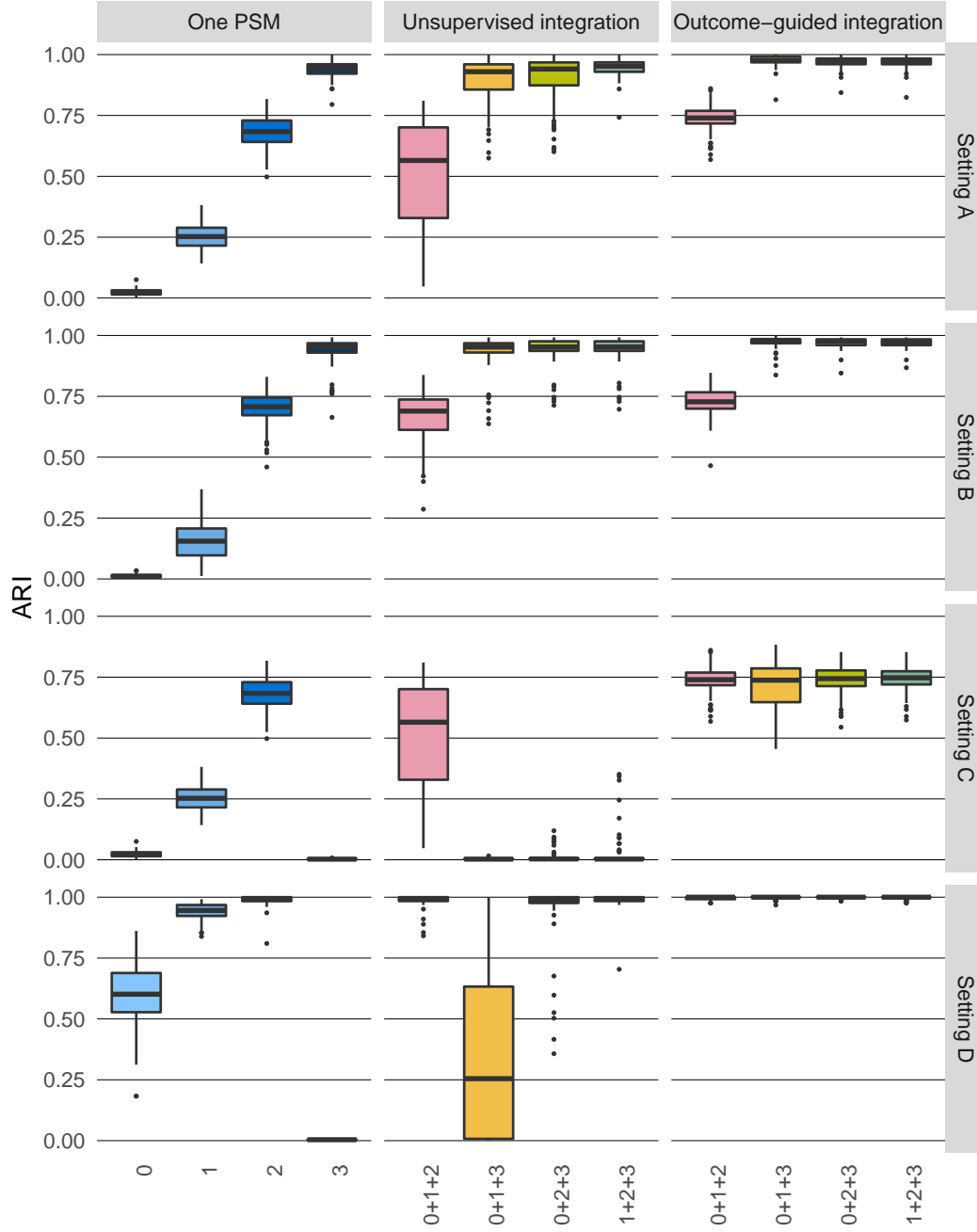


**Figure S6.** Simulation study where the response for each observation is given by its true cluster label. Adjusted Rand index obtained by summarising the PSMs one at a time using kernel  $k$ -means (left), combining different subsets of three PSMs in an unsupervised fashion using localised multiple kernel  $k$ -means (centre), and combining the same subsets making use of a response variable and multi-class SVMs to determine each PSM's weight and using kernel  $k$ -means for the final clustering (right).



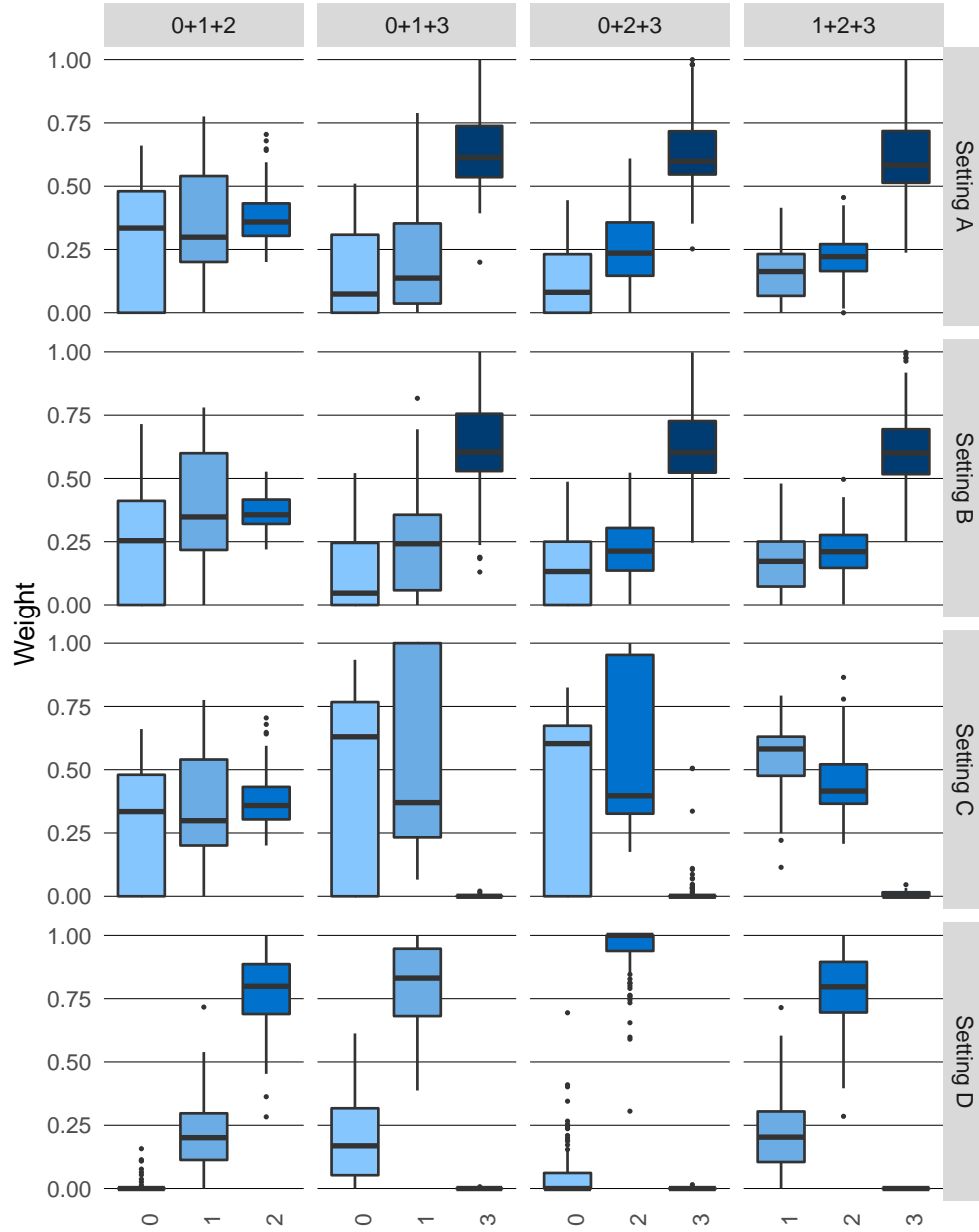


**Figure S7.** Weights assigned to each PSM for each subset of datasets by the unsupervised (above) and outcome-guided (below) integration methods for PSMs for the simulation study where the response for each observation is given by its true cluster label.

## S2 Integrative clustering: biological applications

### S2.1 Multiplatform analysis of ten cancer types

#### S2.1.1 Variable selection

In Table S1 are reported the number of variables measured in each layer and the number of selected variables using separate elastic-net (EN) on each layer as in Cabassi et al. (2020) and Seyres et al. (2020).

Dataset	Full dataset	$\alpha = 0.1$	$\alpha = 0.5$	$\alpha = 1$
Protein expression	131	131	131	124
mRNA expression	6000	1893	568	258
Methylation	2043	1439	623	322
DNA copy number	84	84	84	84
microRNA expression	51	51	51	50

**Table S1.** Number of selected variables in each dataset for different values of the EN parameter  $\alpha$ .

The full mRNA dataset is too large to be used as input to MDI and for this reason it is only used for the integration of the reduced datasets obtained via variable selection with values of  $\alpha$  of 0.5 and 1.

#### S2.1.2 MCMC convergence assessment

We run five MCMC chains for 50.000 iterations, with a burn-in period of 25.000 iterations and thinning of 5. For each set of five chains, we check the Vats-Knudson  $\hat{R}$  (Vats and Knudson, 2018) with parameters  $\epsilon = 0.1$  and  $\alpha = 0.1$  to assess the convergence of the mass parameter. The PSMs obtained for the five chains are summarised into one by taking the average.

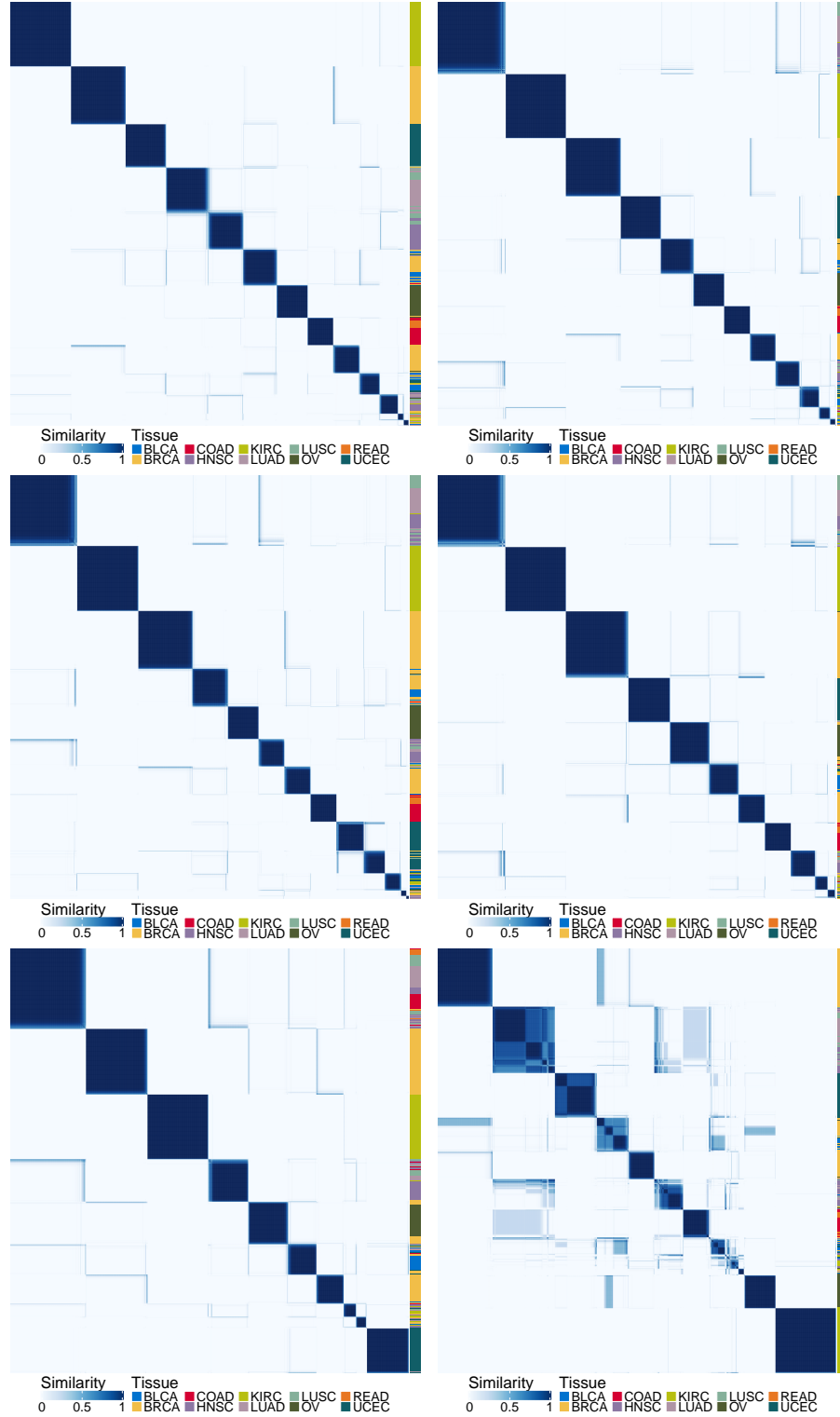


**Figure S8.** PSMs of the protein expression data.  $\lambda = 0$ ,  $\alpha = 0.1, 0.5$ .

	Chain 2	Chain 3	Chain 4	Chain 5
Chain 1	0.87	0.80	0.76	0.69
Chain 2	1	0.91	0.87	0.73
Chain 3		1	0.82	0.68
Chain 4			1	0.83

**Table S2.** ARI between the clusterings found on the PSMs of different chains with the number of clusters that maximises the silhouette.

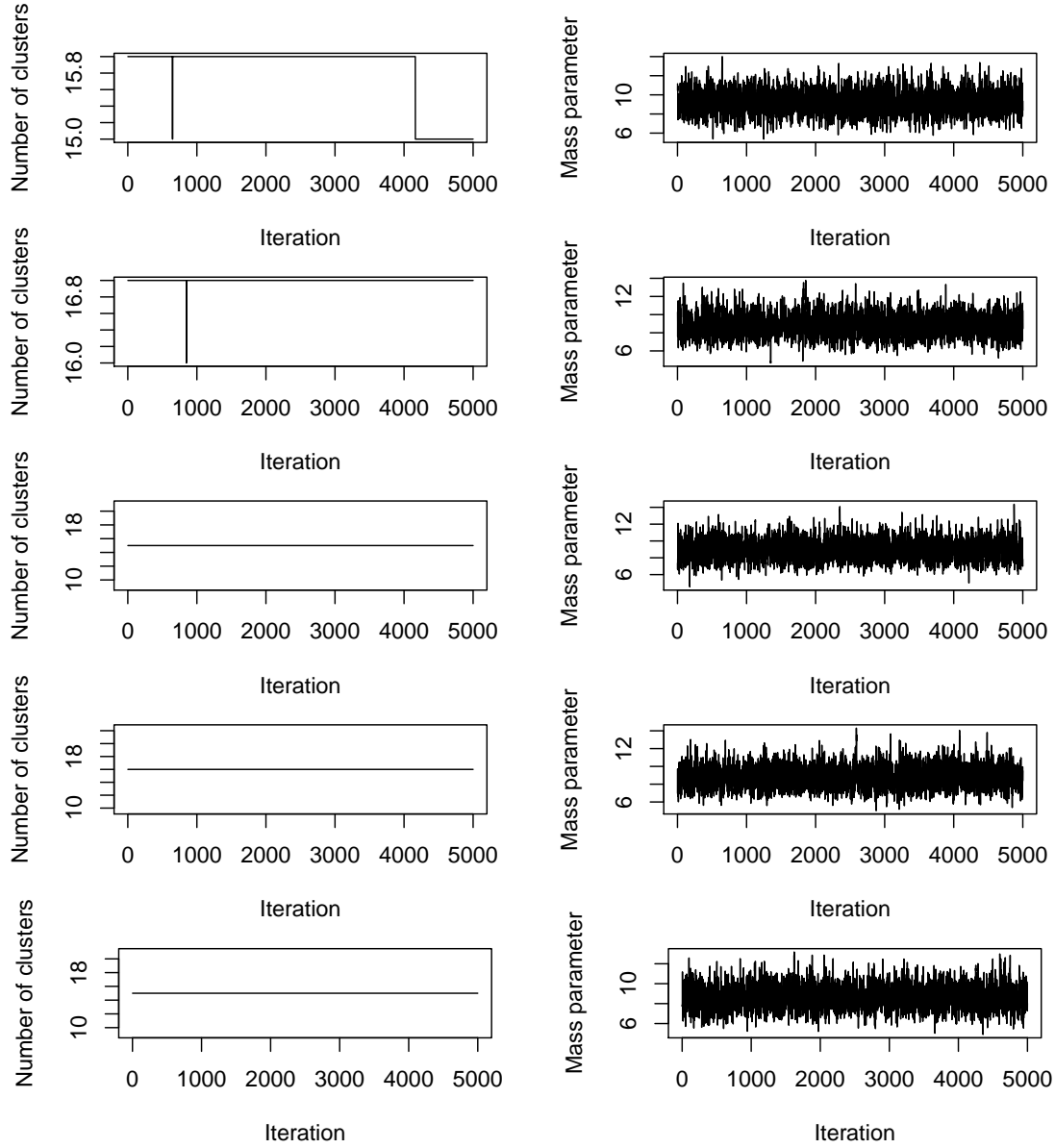


**Figure S9.** MCMC convergence assessment, protein expression data.  $\lambda = 0, \alpha = 0.1, 0.5$ .

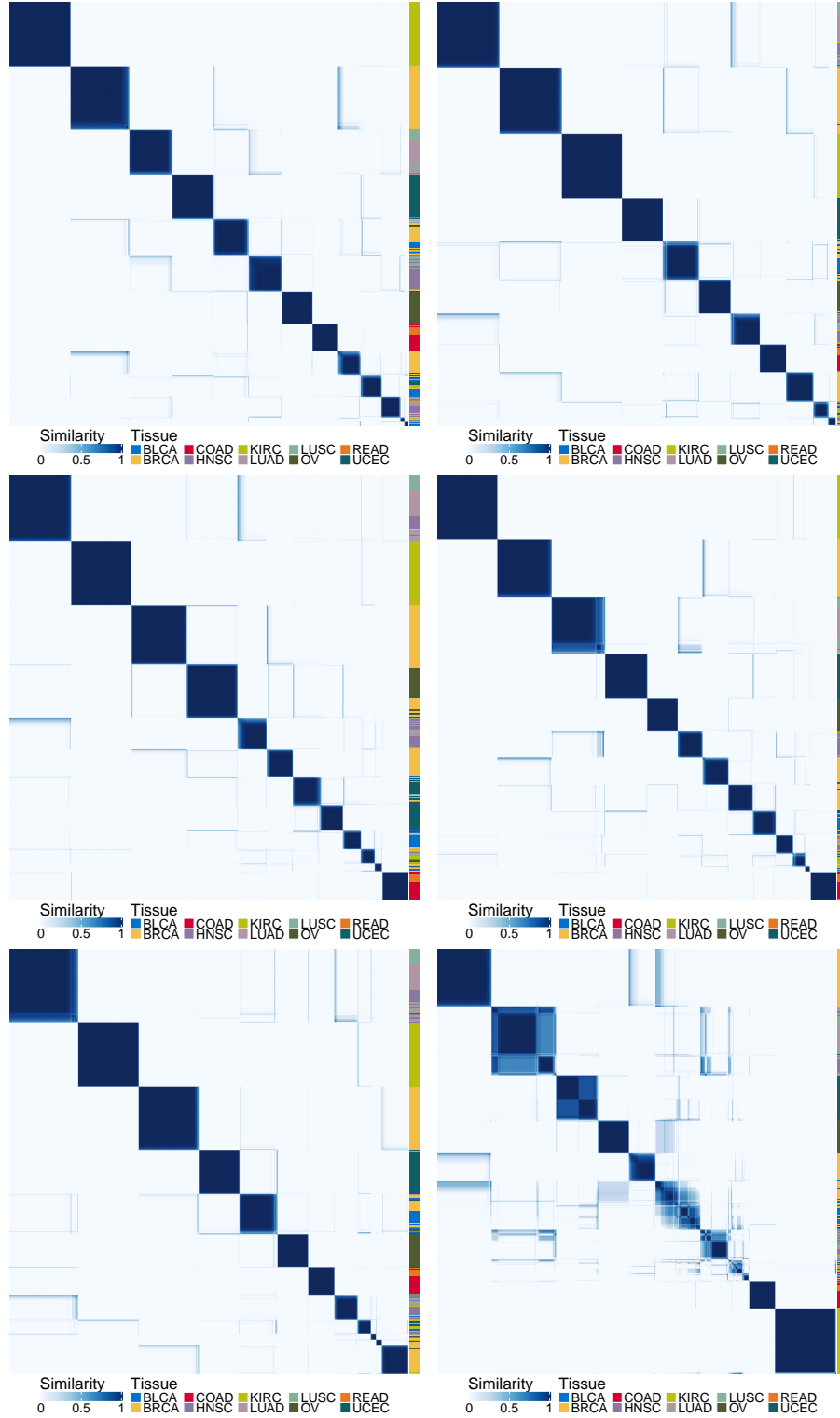


**Figure S10.** PSMs of the protein expression data.  $\alpha = 1$ .

	Chain 2	Chain 3	Chain 4	Chain 5
Chain 1	0.75	0.72	0.89	0.79
Chain 2	1	0.82	0.80	0.92
Chain 3		1	0.76	0.81
Chain 4			1	0.80

**Table S3.** ARI between the clusterings found on the PSMs of different chains with the number of clusters that maximises the silhouette.

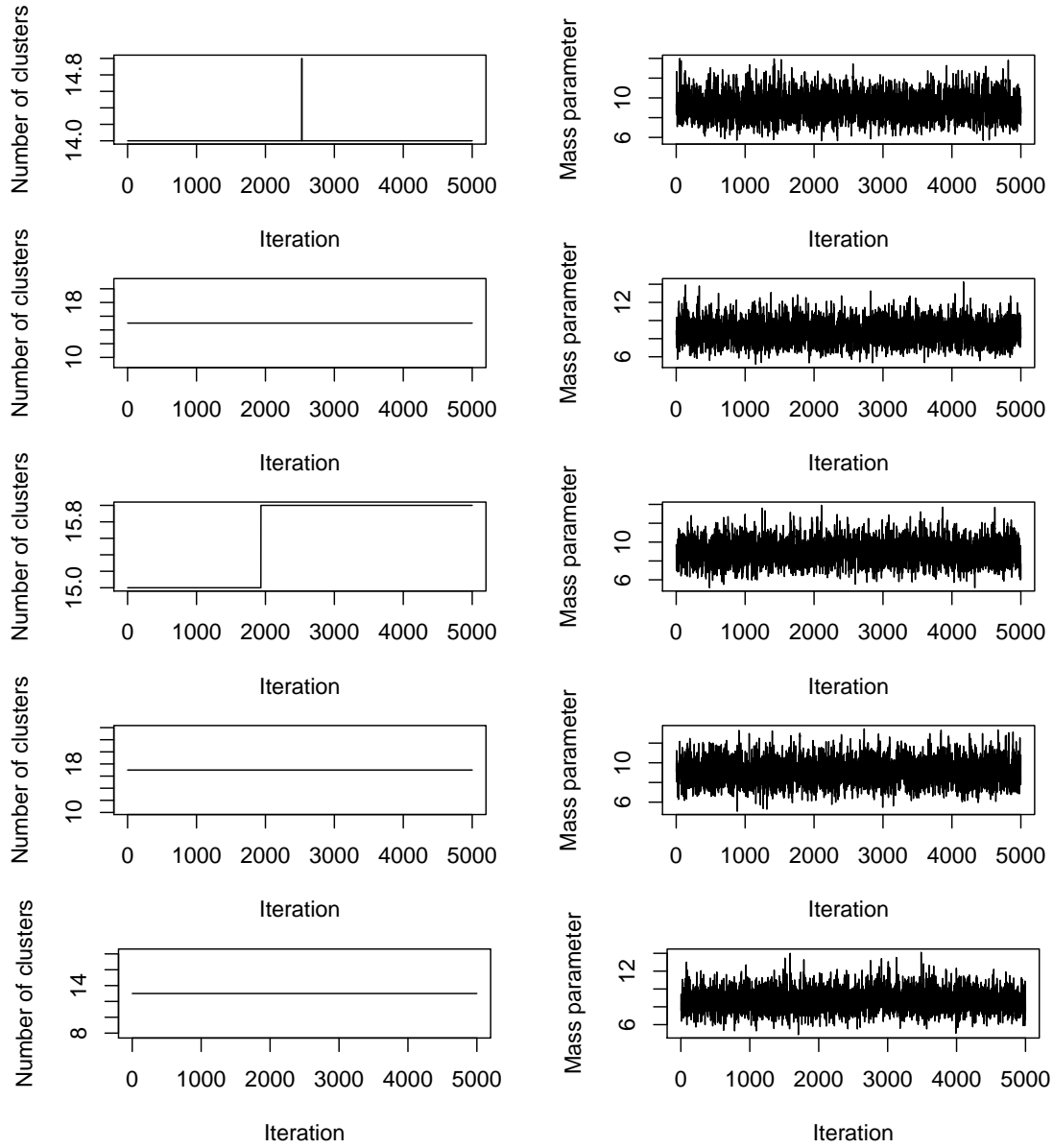


**Figure S11.** MCMC convergence assessment, protein expression data.  $\alpha = 1$ .

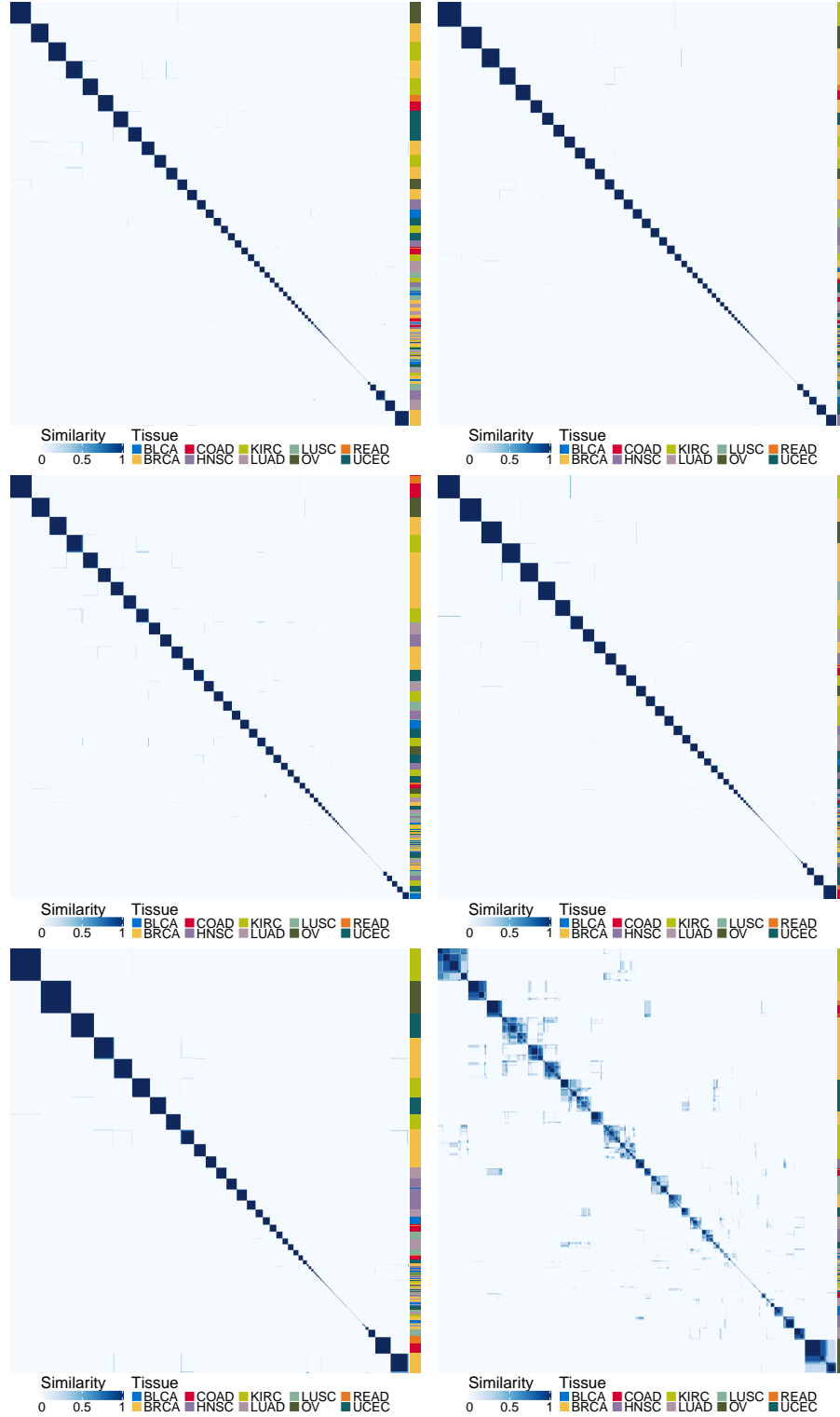


**Figure S12.** PSMs of the mRNA expression data.  $\alpha = 0.5$ .



	Chain 2	Chain 3	Chain 4	Chain 5
Chain 1	0.46	0.43	0.48	0.42
Chain 2	1	0.42	0.52	0.42
Chain 3		1	0.43	0.41
Chain 4			1	0.49

**Table S4.** ARI between the clusterings found on the PSMs of different chains with the number of clusters that maximises the silhouette.

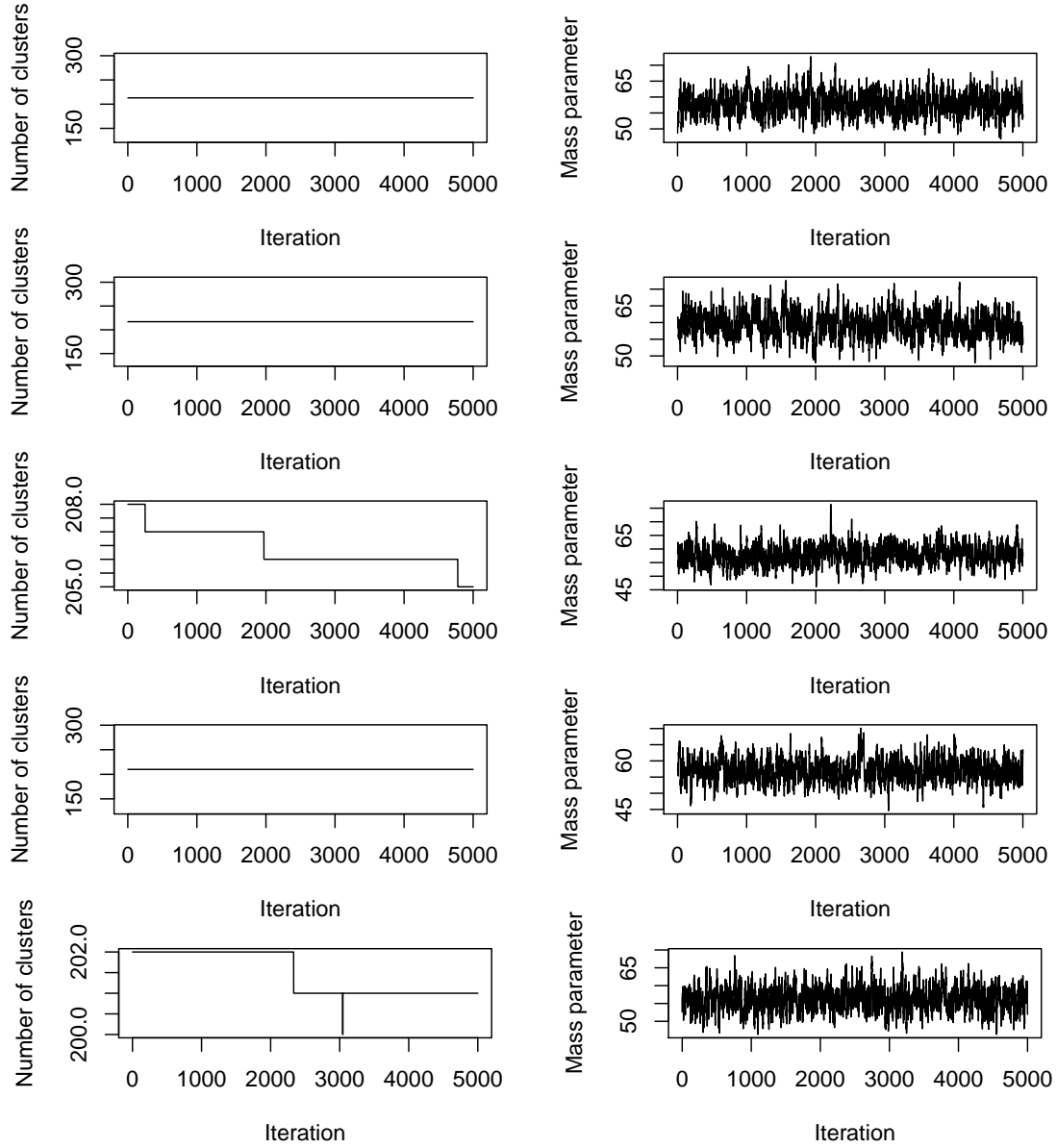


**Figure S13.** MCMC convergence assessment, mRNA expression data.  $\alpha = 0.5$ .

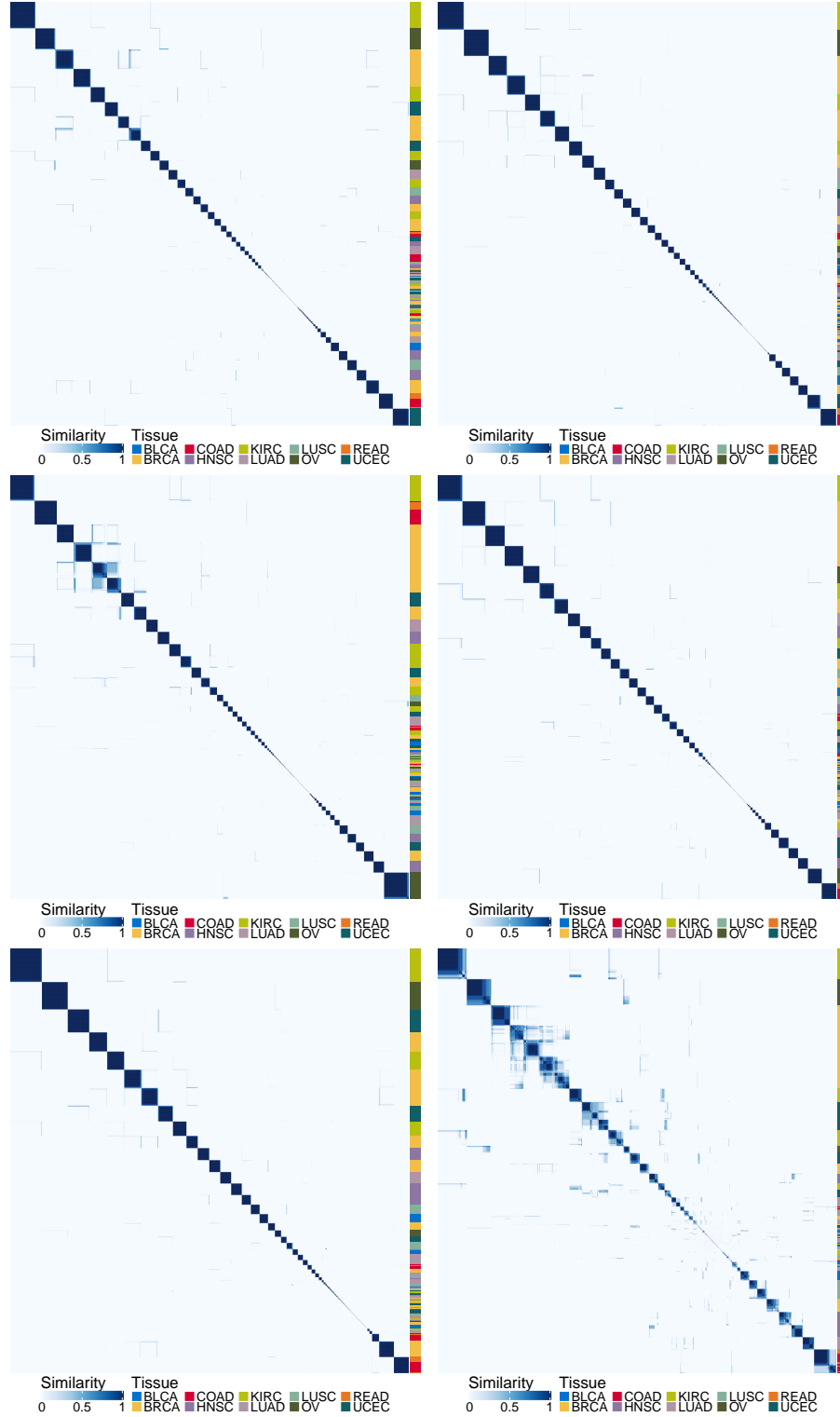


**Figure S14.** PSMs of the mRNA expression data.  $\alpha = 1$ .

	Chain 2	Chain 3	Chain 4	Chain 5
Chain 1	0.63	0.55	0.61	0.52
Chain 2	1	0.58	0.64	0.63
Chain 3		1	0.59	0.58
Chain 4			1	0.57

**Table S5.** ARI between the clusterings found on the PSMs of different chains with the number of clusters that maximises the silhouette.

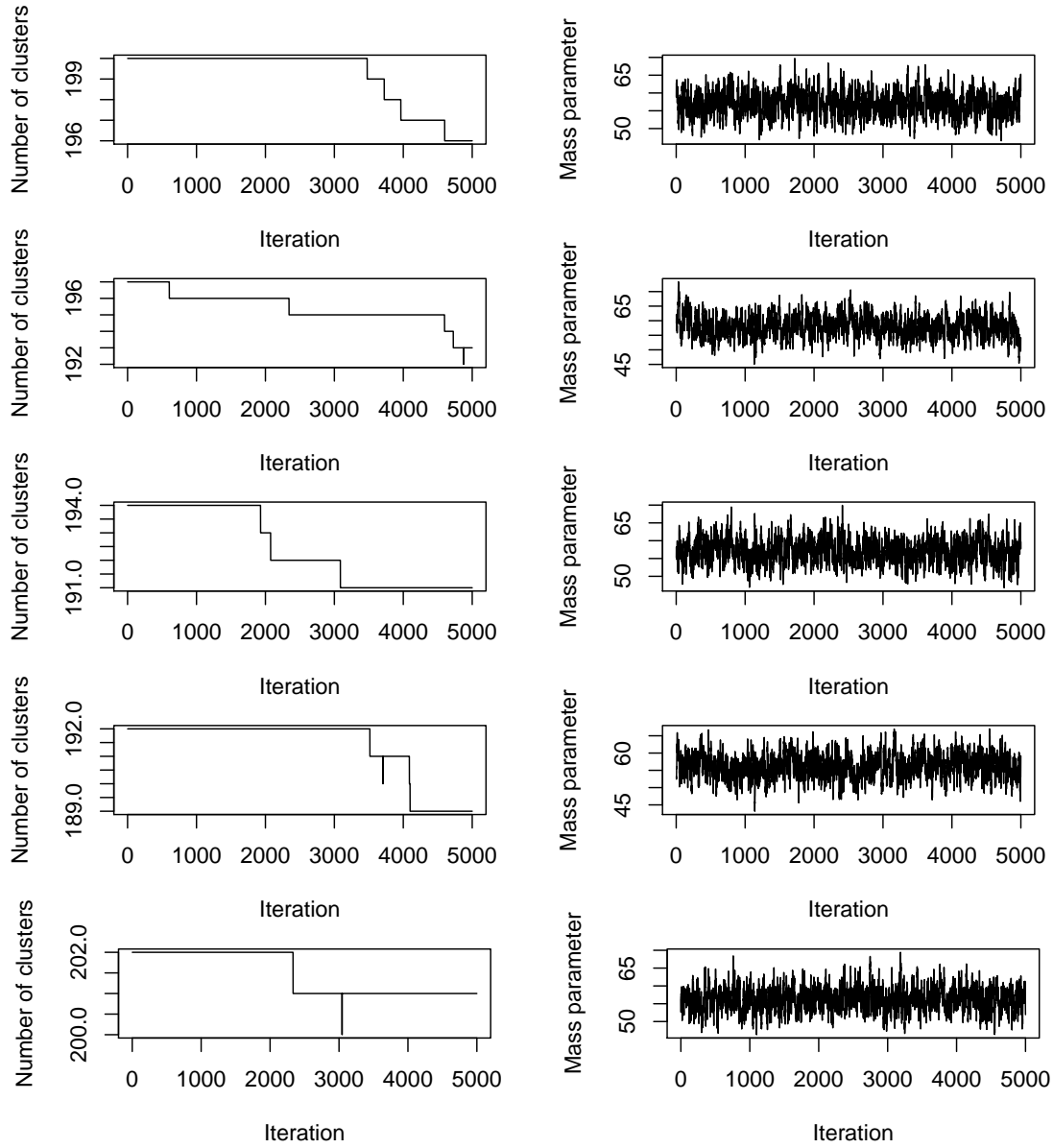


**Figure S15.** MCMC convergence assessment, mRNA expression data.  $\alpha = 1$ .

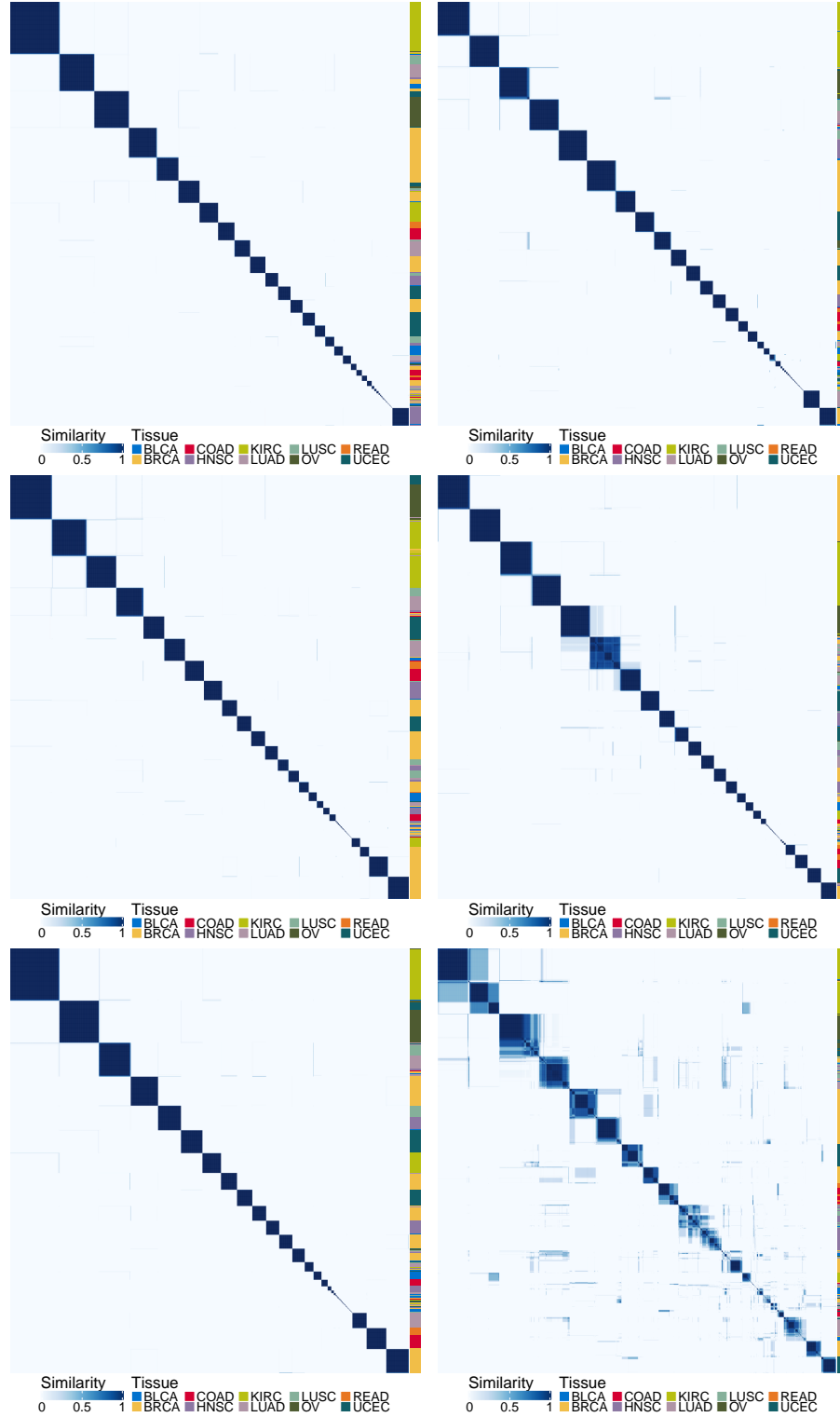


**Figure S16.** PSMs of the methylation data.  $\lambda = 0$ .

	Chain 2	Chain 3	Chain 4	Chain 5
Chain 1	0.60	0.57	0.53	0.79
Chain 2	1	0.67	0.63	0.64
Chain 3		1	0.59	0.66
Chain 4			1	0.54

**Table S6.** ARI between the clusterings found on the PSMs of different chains with the number of clusters that maximises the silhouette.

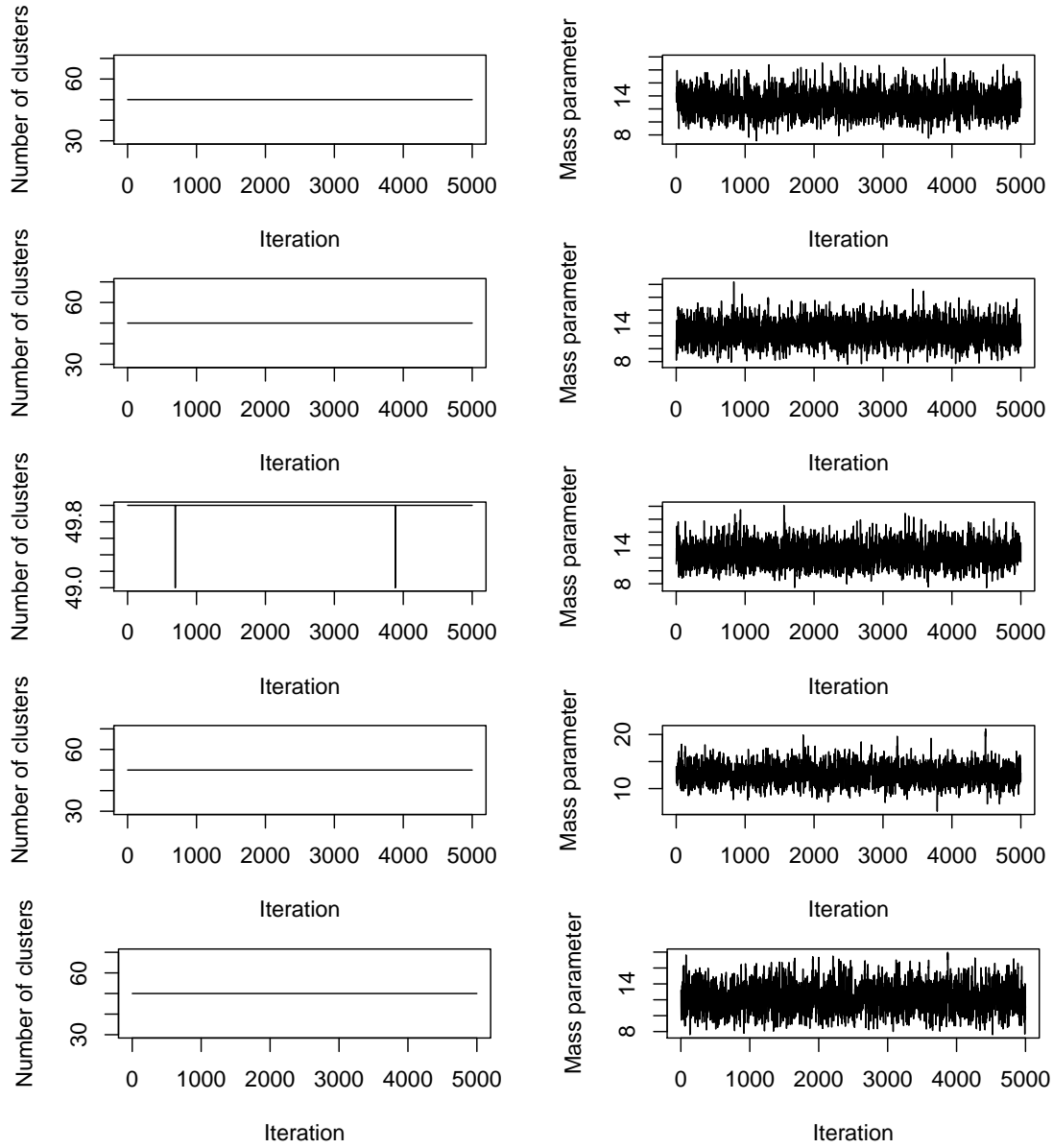


**Figure S17.** MCMC convergence assessment, methylation data.  $\lambda = 0$ .

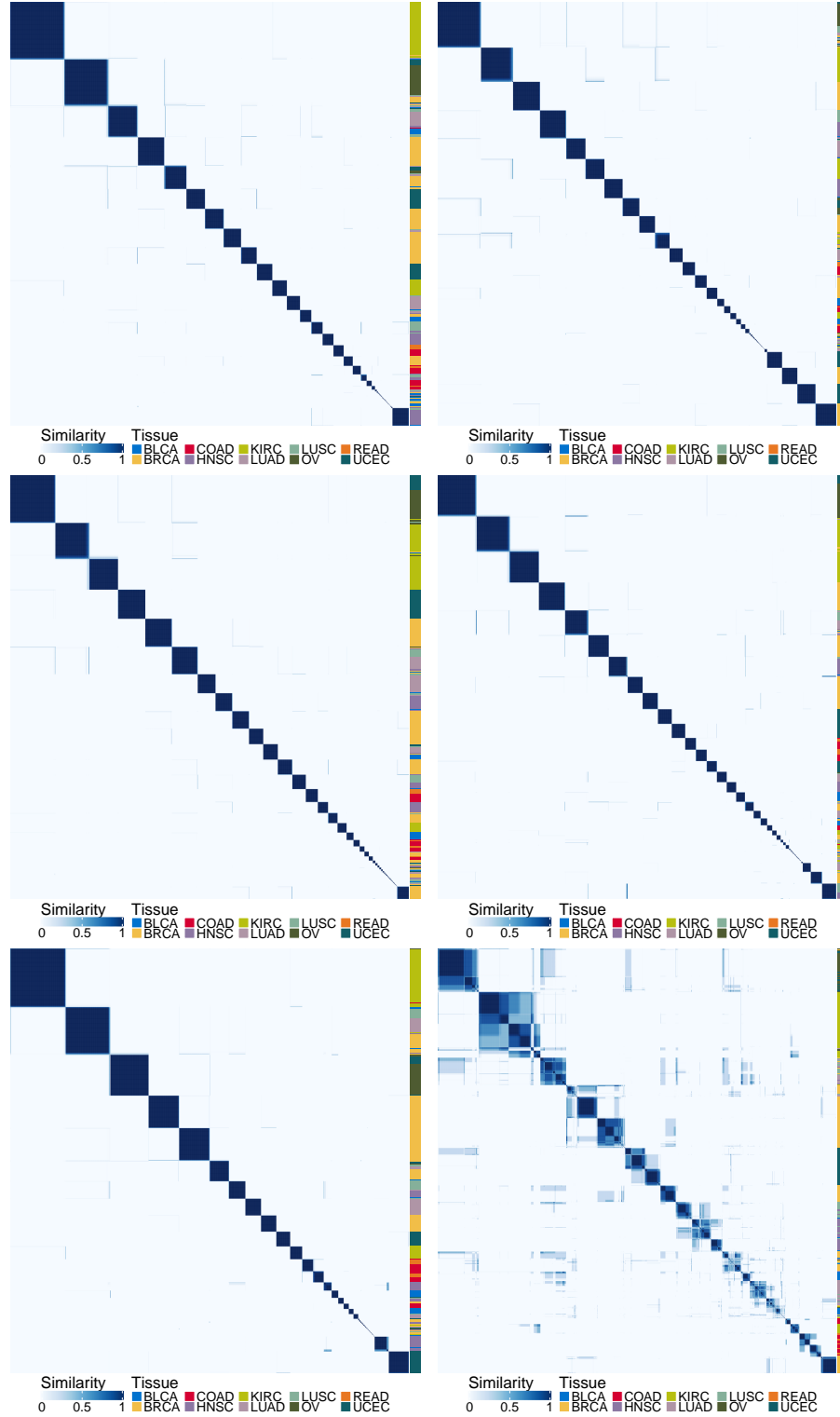


**Figure S18.** PSMs of the methylation data.  $\alpha = 0.1$ .

	Chain 2	Chain 3	Chain 4	Chain 5
Chain 1	0.55	0.53	0.61	0.64
Chain 2	1	0.48	0.57	0.49
Chain 3		1	0.71	0.55
Chain 4			1	0.57

**Table S7.** ARI between the clusterings found on the PSMs of different chains with the number of clusters that maximises the silhouette.

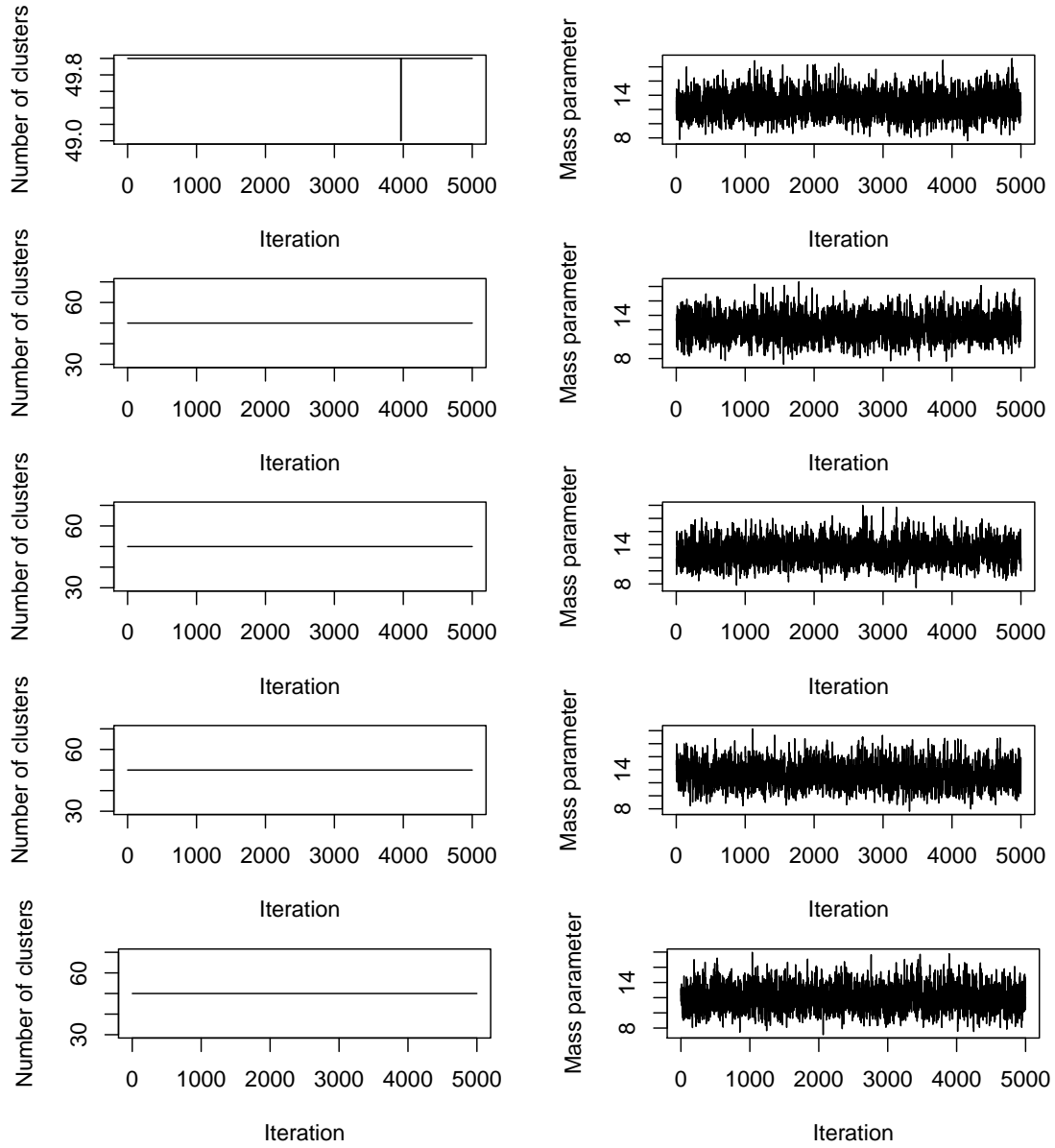


**Figure S19.** MCMC convergence assessment, methylation data.  $\alpha = 0.1$



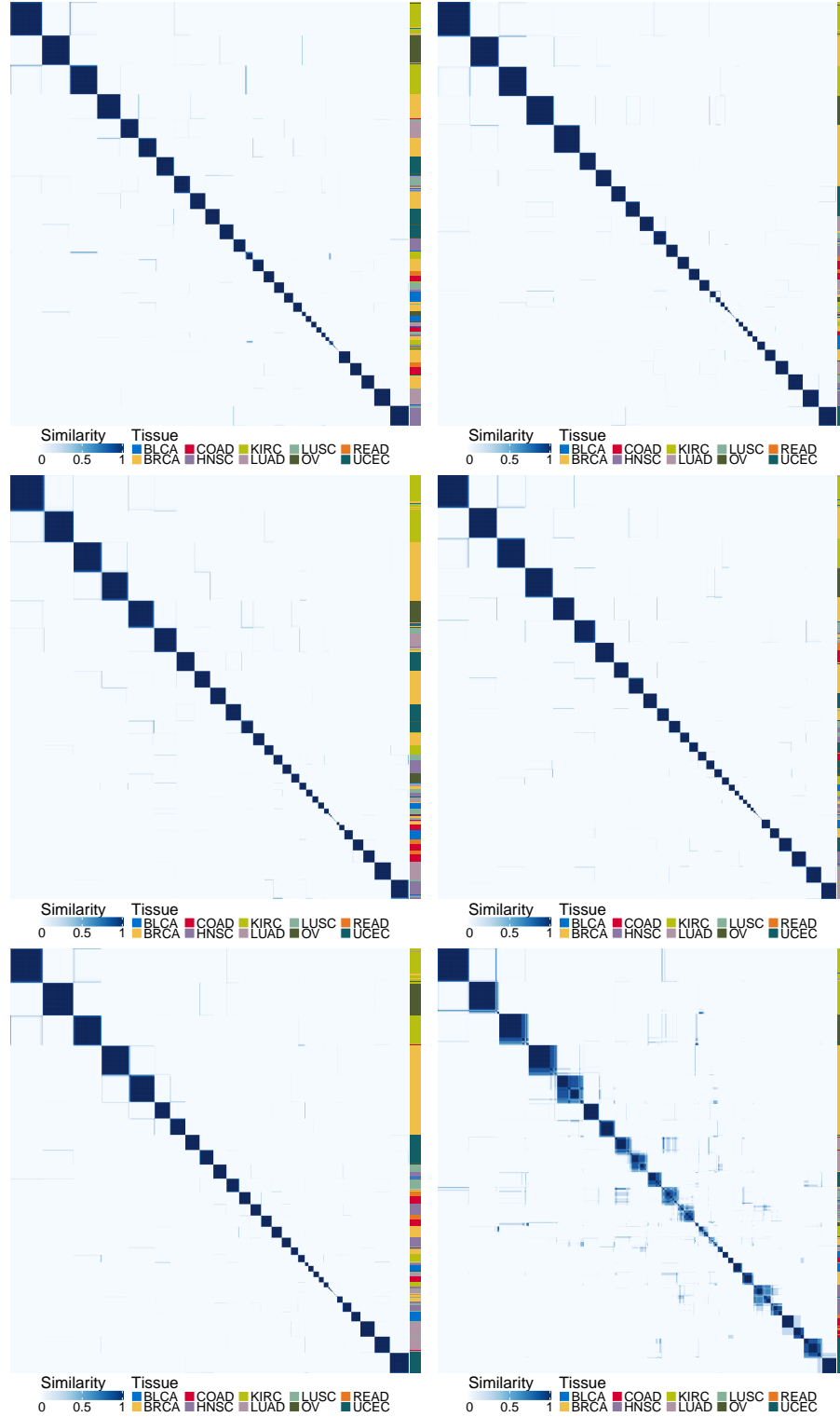


**Figure S20.** PSMs of the methylation data.  $\alpha = 0.5$ .

	Chain 2	Chain 3	Chain 4	Chain 5
Chain 1	0.79	0.74	0.74	0.78
Chain 2	1	0.81	0.73	0.82
Chain 3		1	0.70	0.77
Chain 4			1	0.75

**Table S8.** ARI between the clusterings found on the PSMs of different chains with the number of clusters that maximises the silhouette.

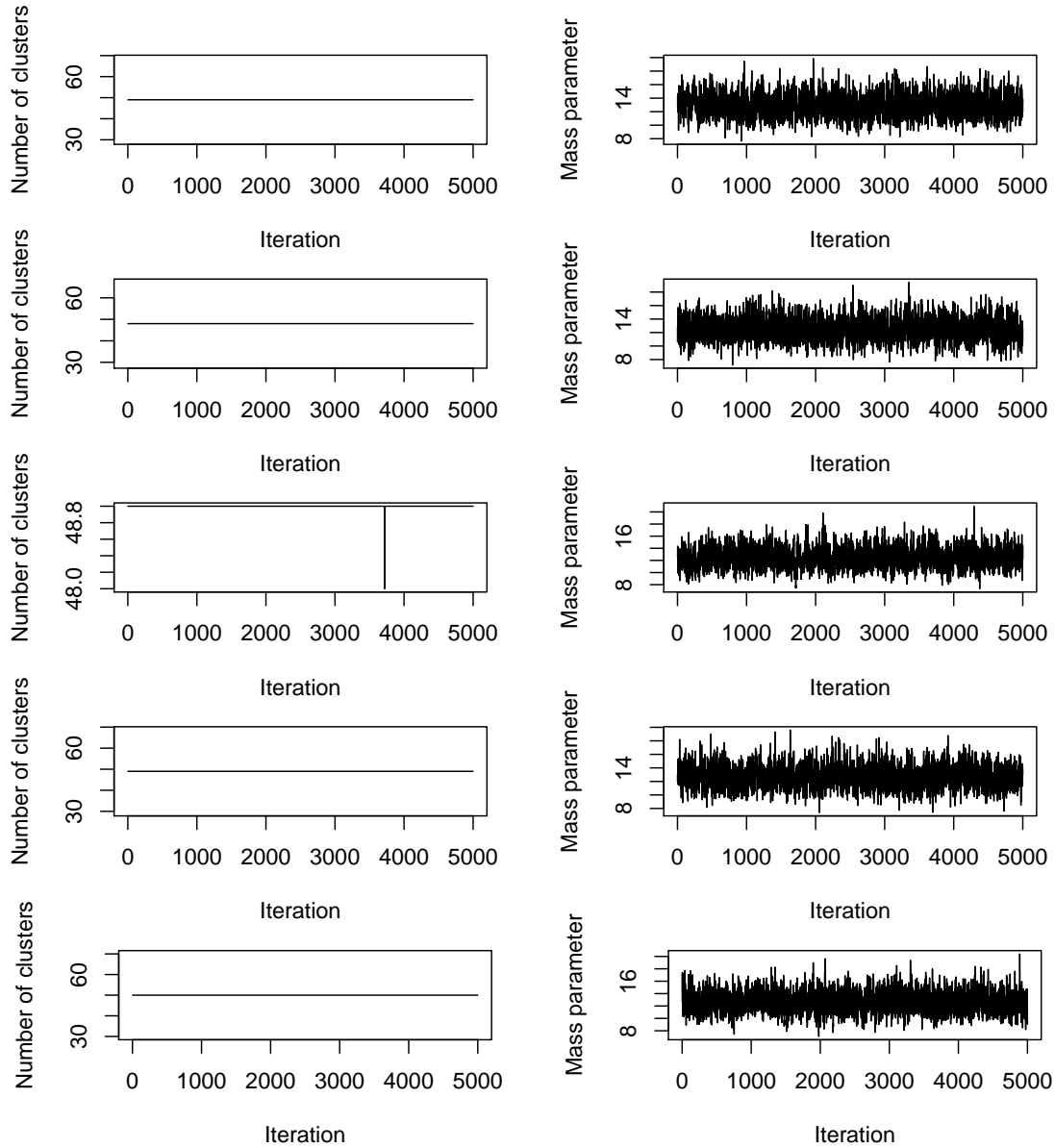


**Figure S21.** MCMC convergence assessment, methylation data.

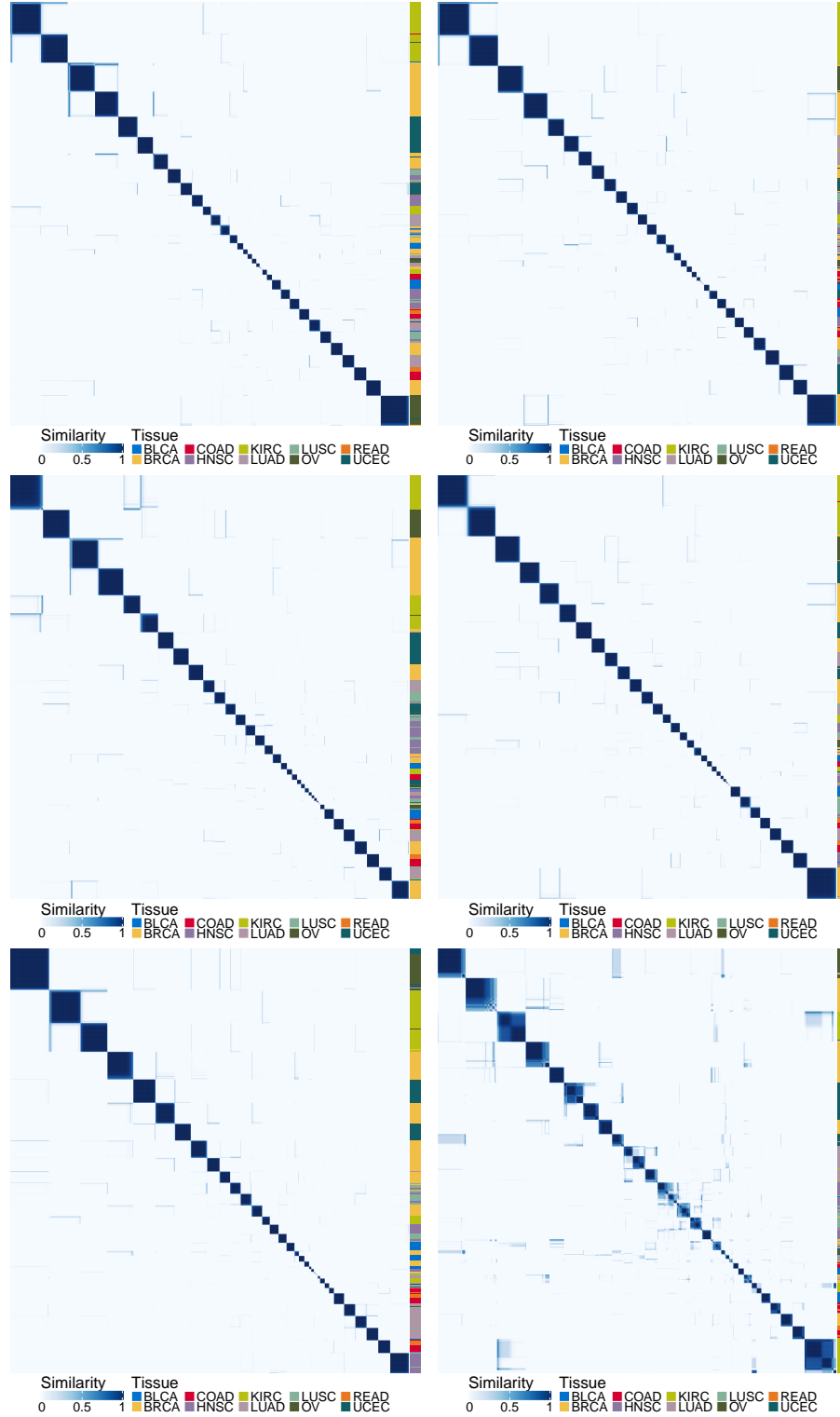


**Figure S22.** PSMs of the methylation data.  $\alpha = 1$ .

	Chain 2	Chain 3	Chain 4	Chain 5
Chain 1	0.81	0.70	0.83	0.78
Chain 2	1	0.61	0.76	0.67
Chain 3		1	0.67	0.60
Chain 4			1	0.76

**Table S9.** ARI between the clusterings found on the PSMs of different chains with the number of clusters that maximises the silhouette.

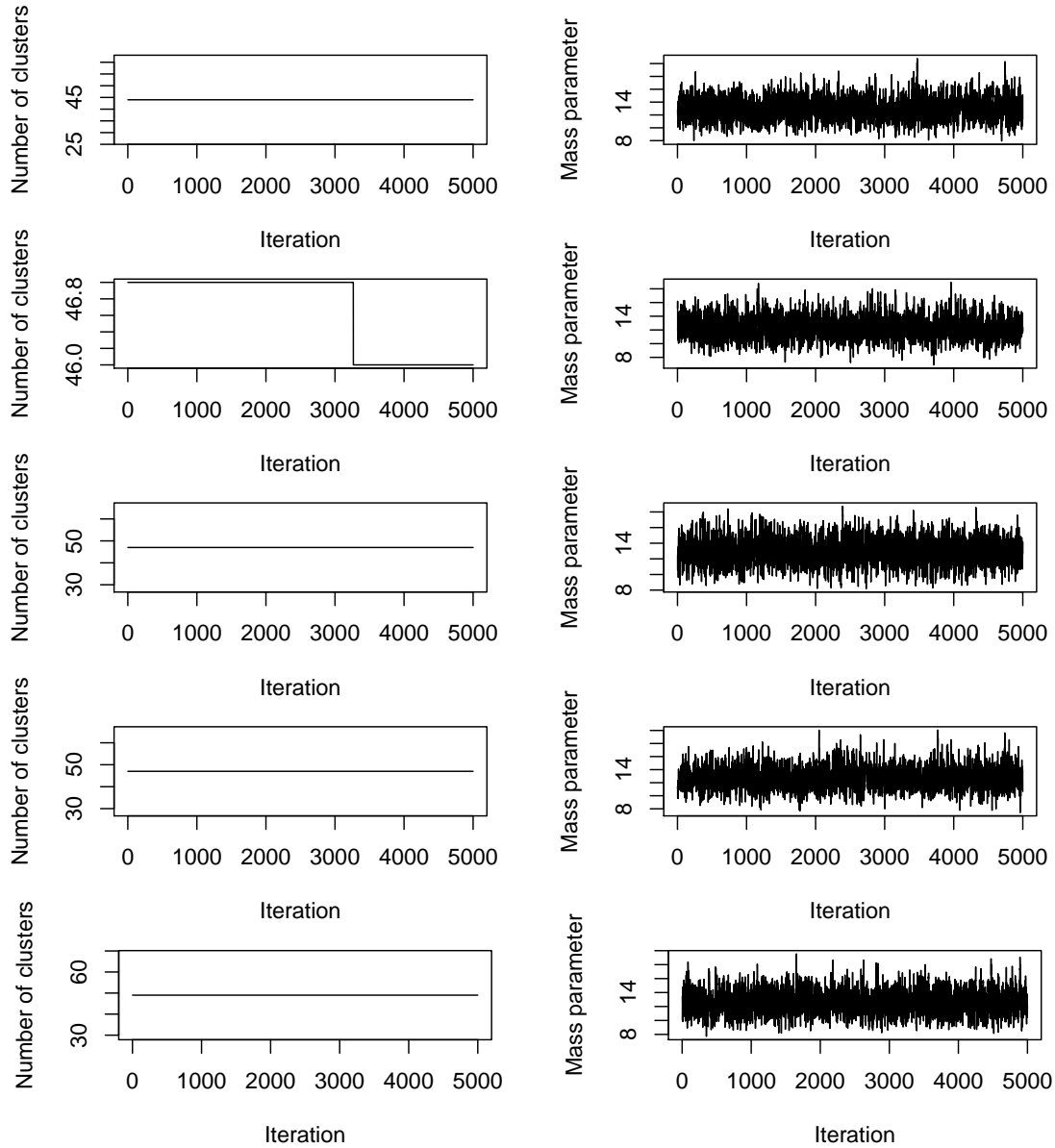


**Figure S23.** MCMC convergence assessment, methylation data.

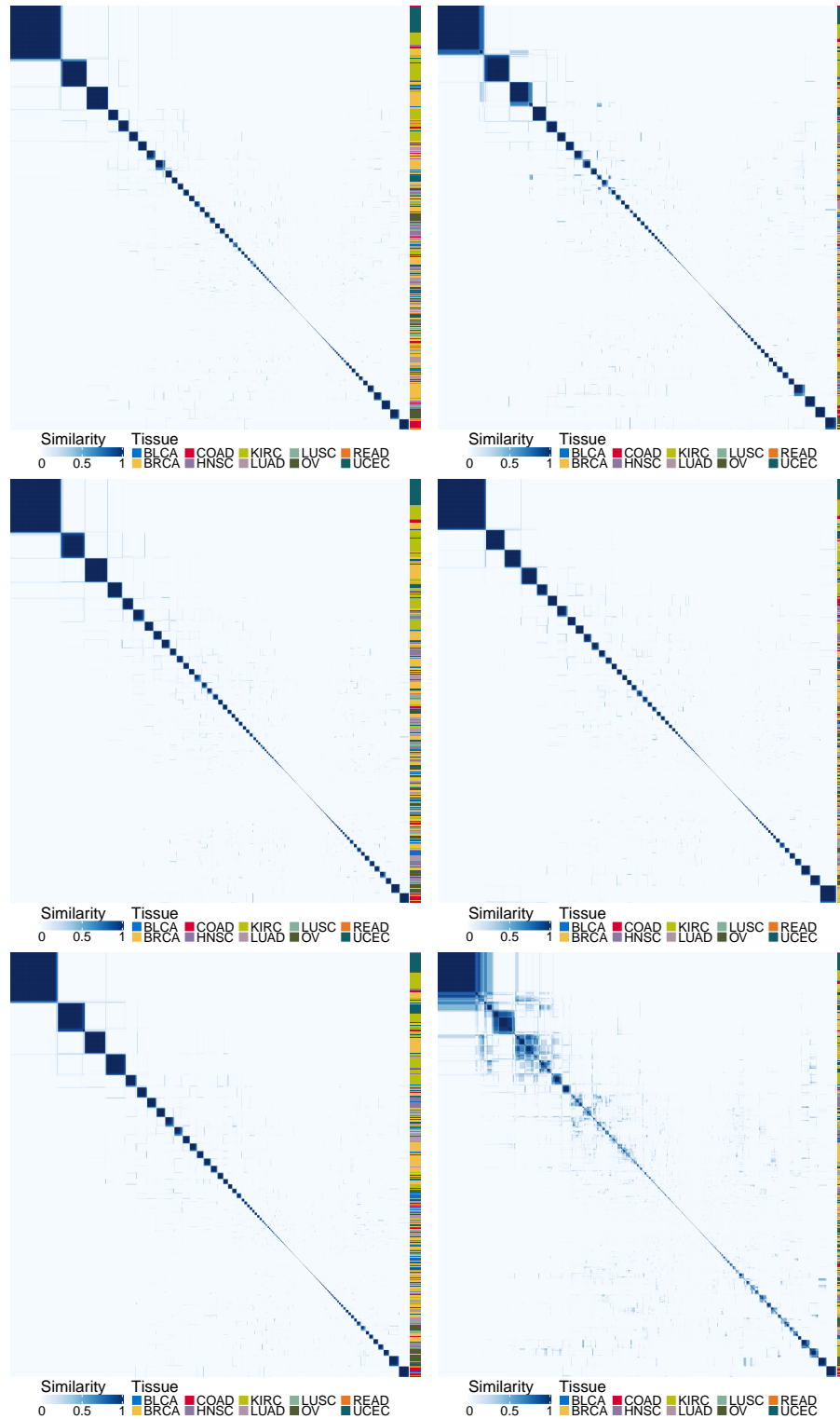


**Figure S24.** PSMs of the DNA copy number data.

	Chain 2	Chain 3	Chain 4	Chain 5
Chain 1	0.39	0.45	0.35	0.35
Chain 2	1	0.58	0.60	0.62
Chain 3		1	0.59	0.57
Chain 4			1	0.54

**Table S10.** ARI between the clusterings found on the PSMs of different chains with the number of clusters that maximises the silhouette.

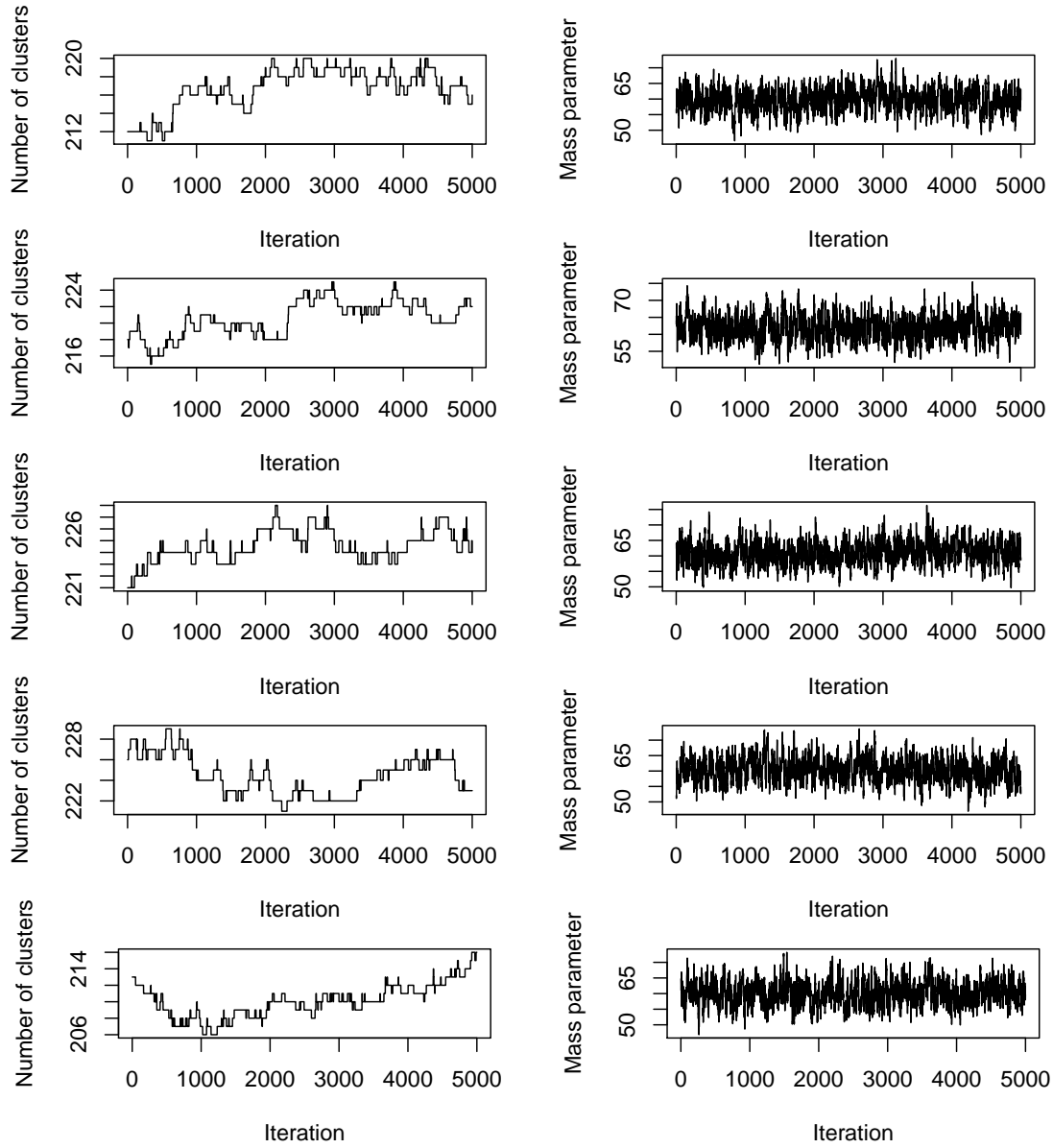


**Figure S25.** MCMC convergence assessment, DNA copy number data.

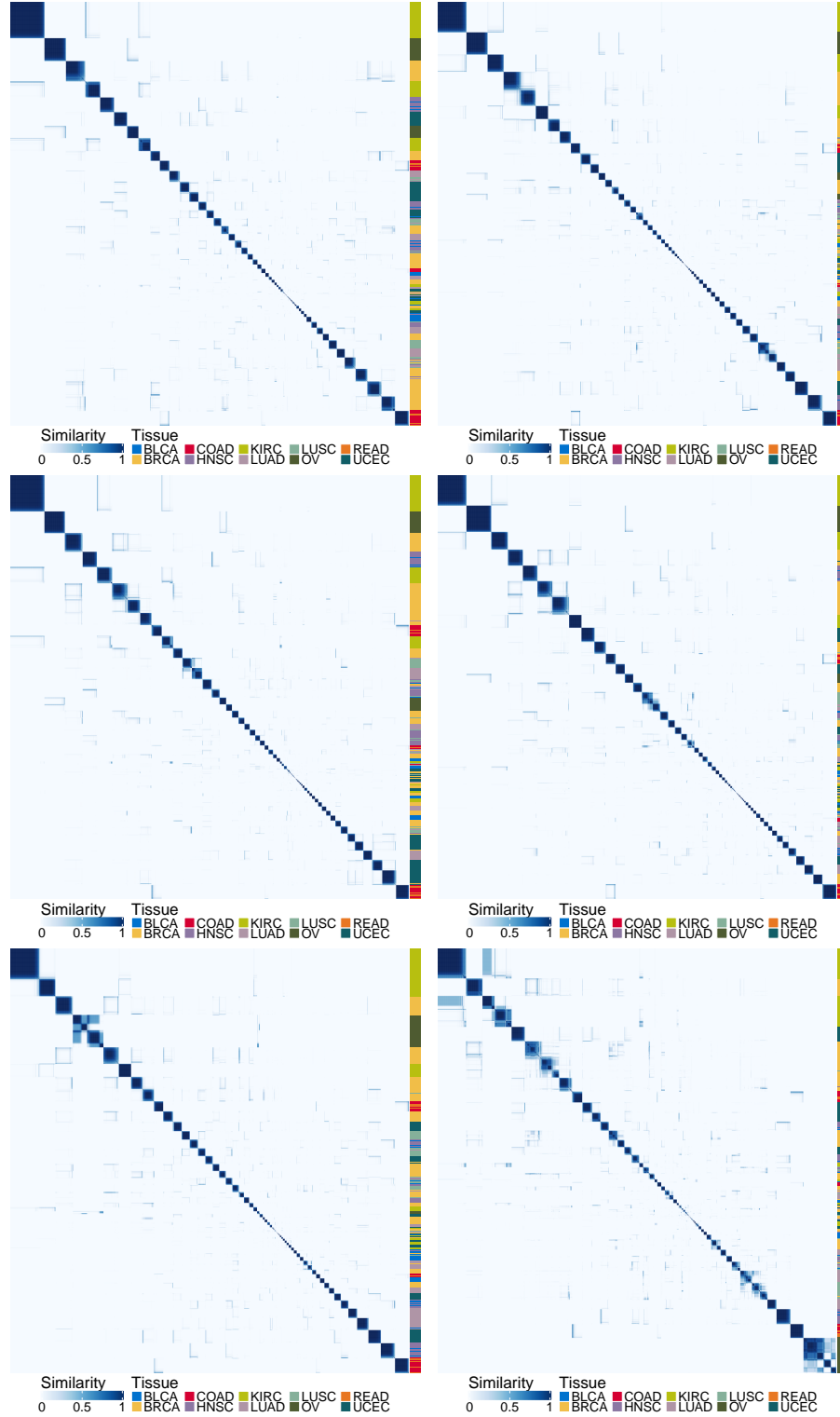


**Figure S26.** PSMs of the microRNA data.  $\lambda = 0$ ,  $\alpha = 0.1, 0.5$ .



	Chain 2	Chain 3	Chain 4	Chain 5
Chain 1	0.63	0.75	0.59	0.64
Chain 2	1	0.74	0.82	0.82
Chain 3		1	0.68	0.69
Chain 4			1	0.75

**Table S11.** ARI between the clusterings found on the PSMs of different chains with the number of clusters that maximises the silhouette.

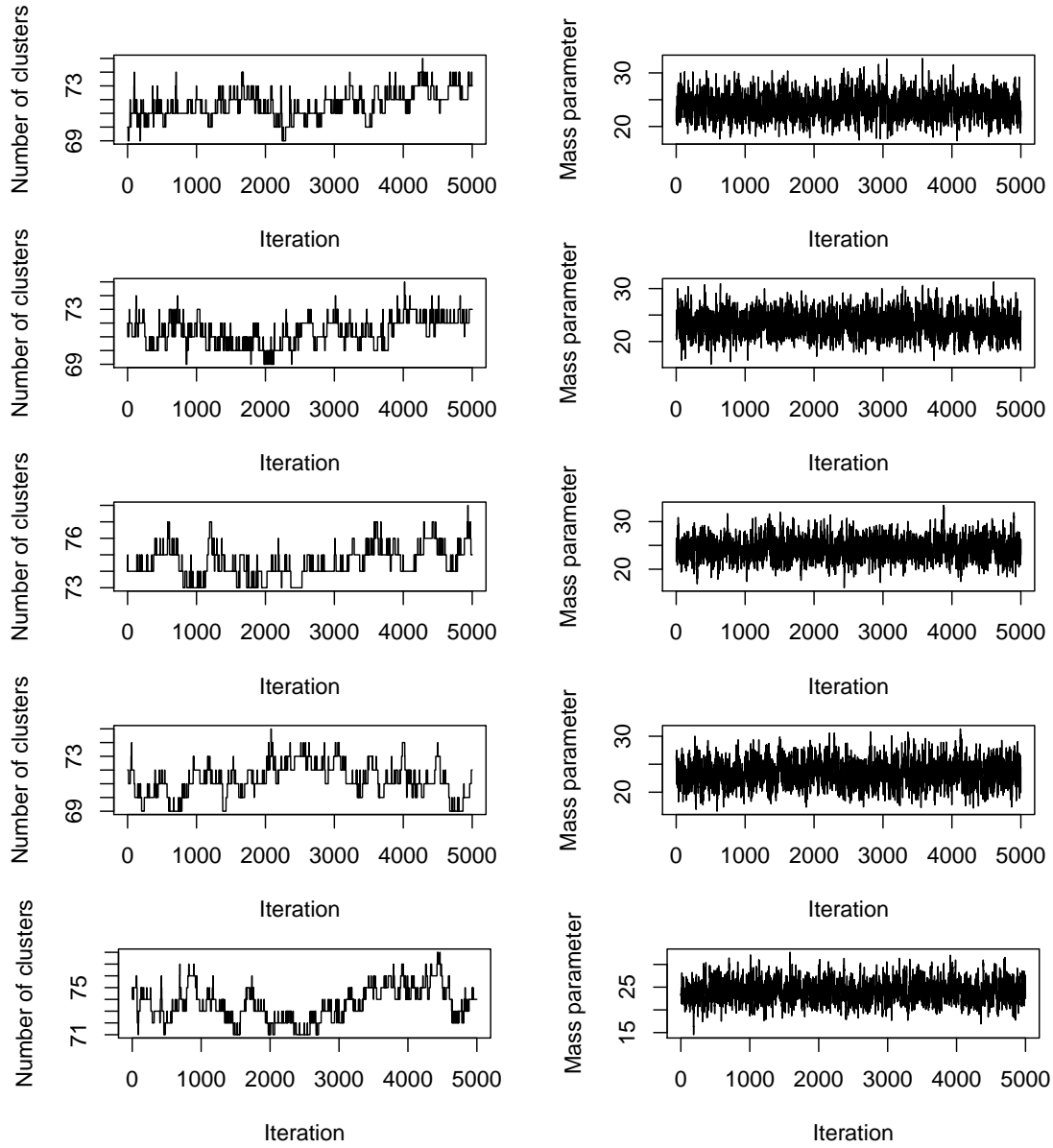


**Figure S27.** MCMC convergence assessment, microRNA data.  $\lambda = 0$ ,  $\alpha = 0.1, 0.5$ .

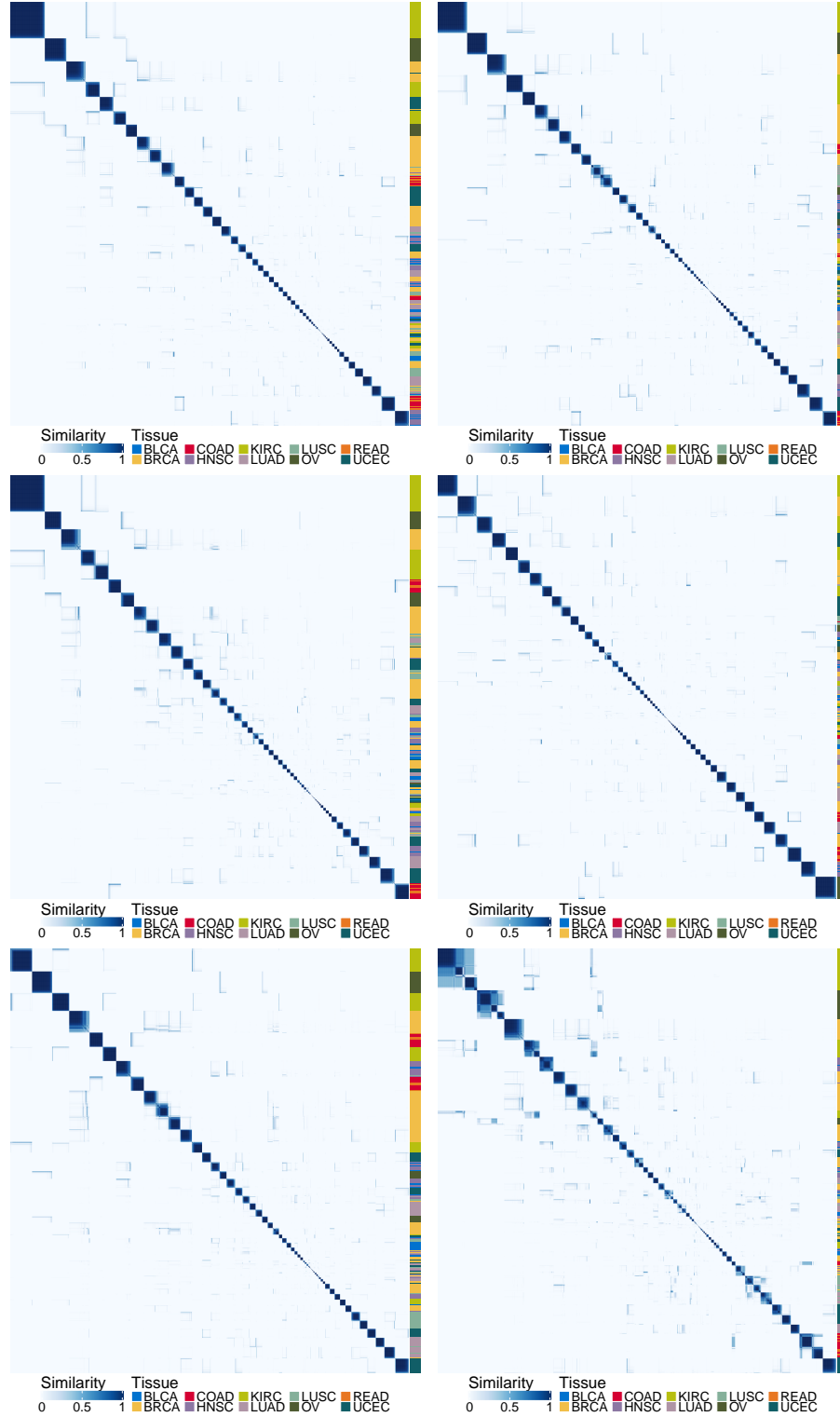


**Figure S28.** PSMs of the microRNA data.  $\alpha = 1$ .

	Chain 2	Chain 3	Chain 4	Chain 5
Chain 1	0.66	0.72	0.70	0.57
Chain 2	1	0.59	0.76	0.69
Chain 3		1	0.55	0.56
Chain 4			1	0.72

**Table S12.** ARI between the clusterings found on the PSMs of different chains with the number of clusters that maximises the silhouette.

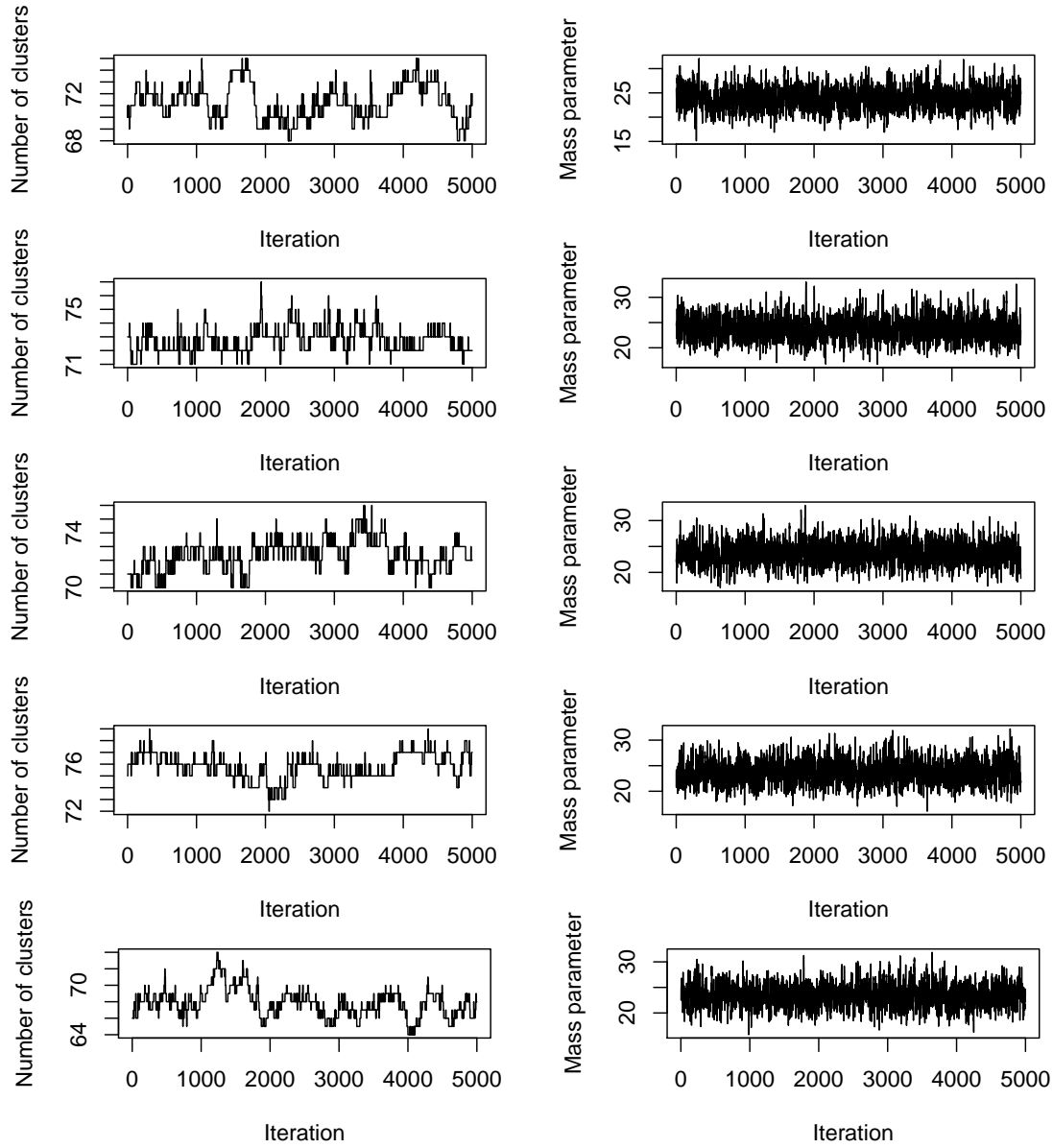


**Figure S29.** MCMC convergence assessment, microRNA data.  $\alpha = 1$ .

### S2.1.3 Unsupervised integration: additional figures

**Choice of the number of clusters** In Figure S30 are reported the average values of the silhouette when the number of clusters goes from 2 to 50. The maximum is at  $K = 15$ .

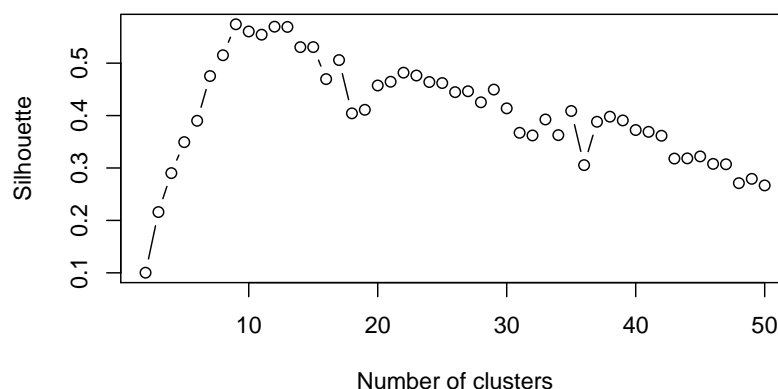


**Figure S30.** Average silhouette.

**Kernel weights** Figure S31 shows the weights assigned to each PSM by the multiple kernel  $k$ -means algorithm.

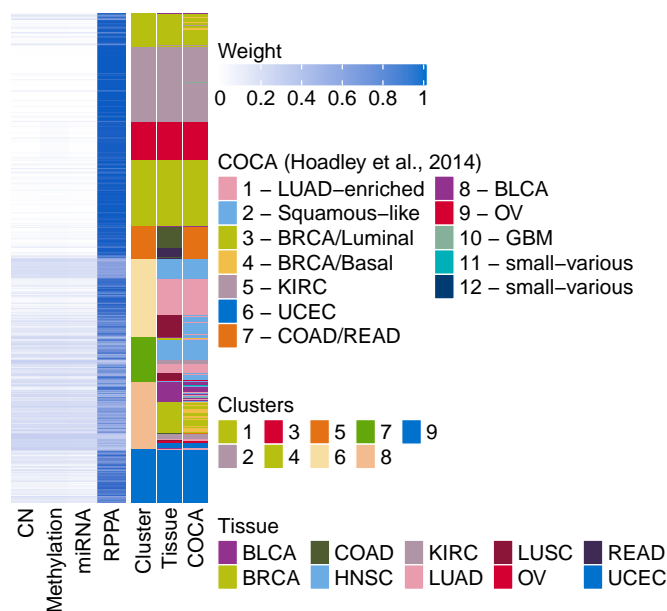


**Figure S31.** Weights assigned by the multiple kernel  $k$ -means algorithm to each observations in each layer, where “CN” stands for copy number and “RPPA” for reverse phase protein array.

**Comparison with the clusters identified by Hoadley et al. (2014)** In Figure S32 are shown the correspondences between the clusters found in the main paper and the clusters identified by Hoadley et al. (2014) using Cluster-Of-Clusters Analysis (COCA).

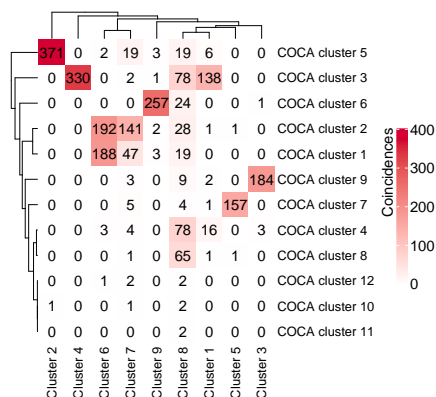


**Figure S32.** Comparison between the clusters found combining the PSMs of each layer using multiple kernel learning and those identified by Hoadley et al. (2014) using COCA.

**Clustering structure in the data** Figures S33, S34, S34, and S36 show the four data layers where the rows have been sorted by final cluster.

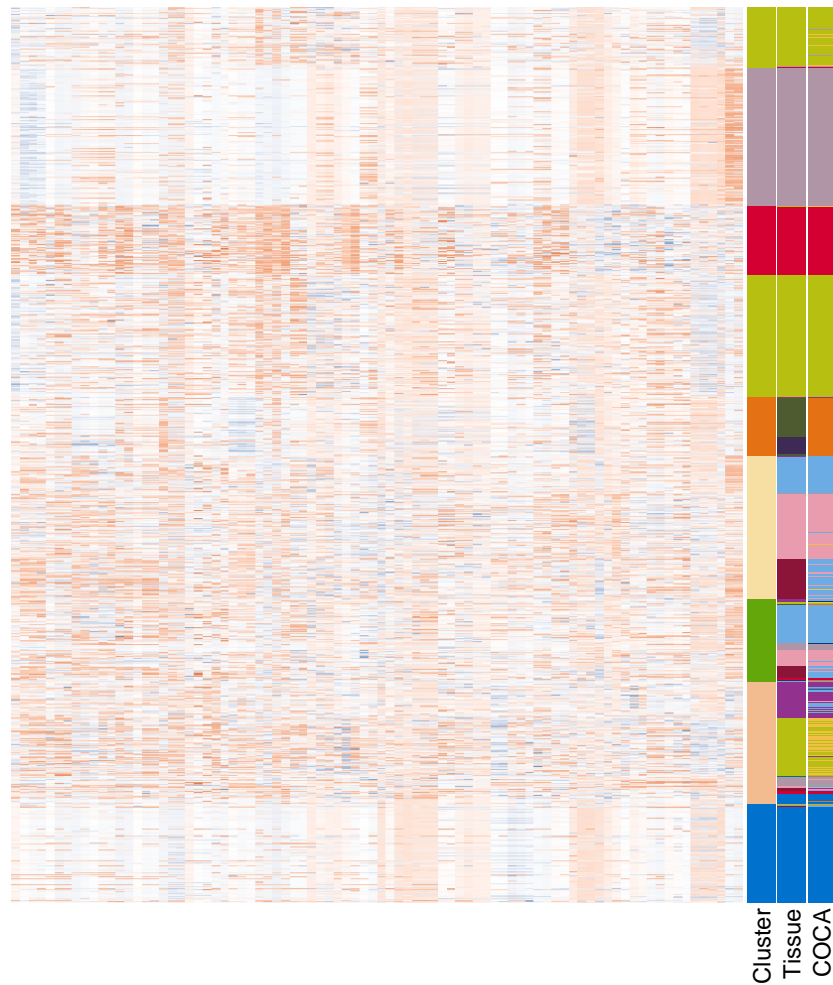


**Figure S33.** Copy number data and final clusters.

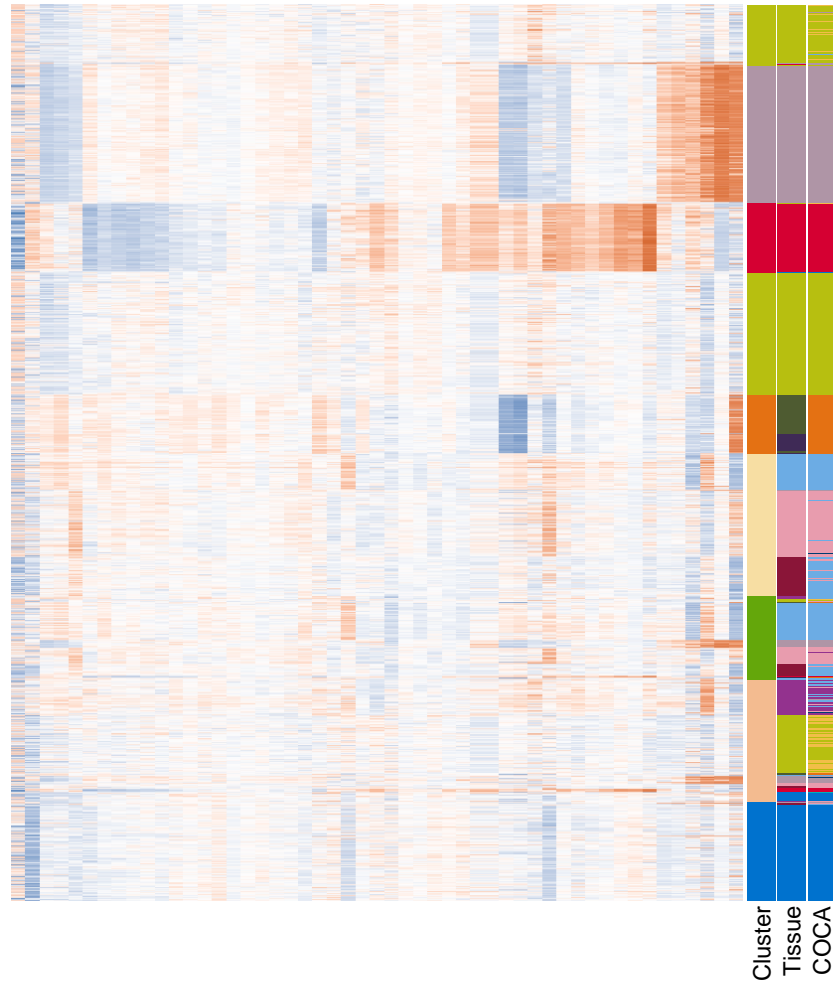


**Figure S34.** microRNA expression data and final clusters.

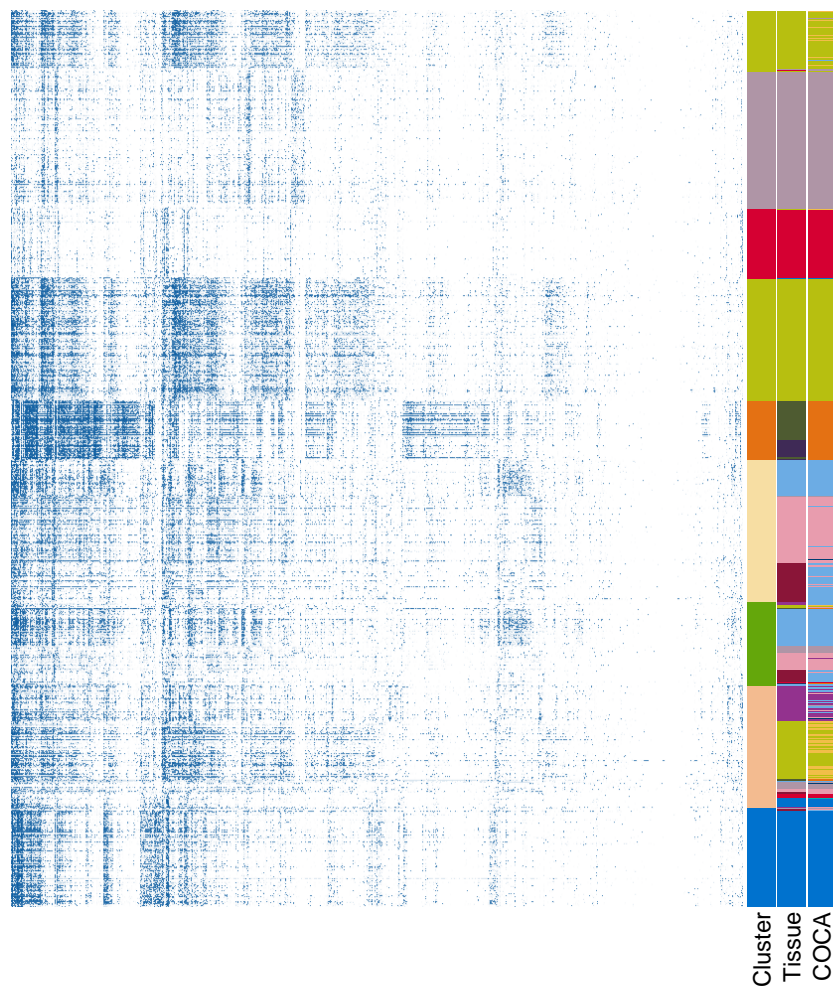


**Figure S35.** Methylation data and final clusters.



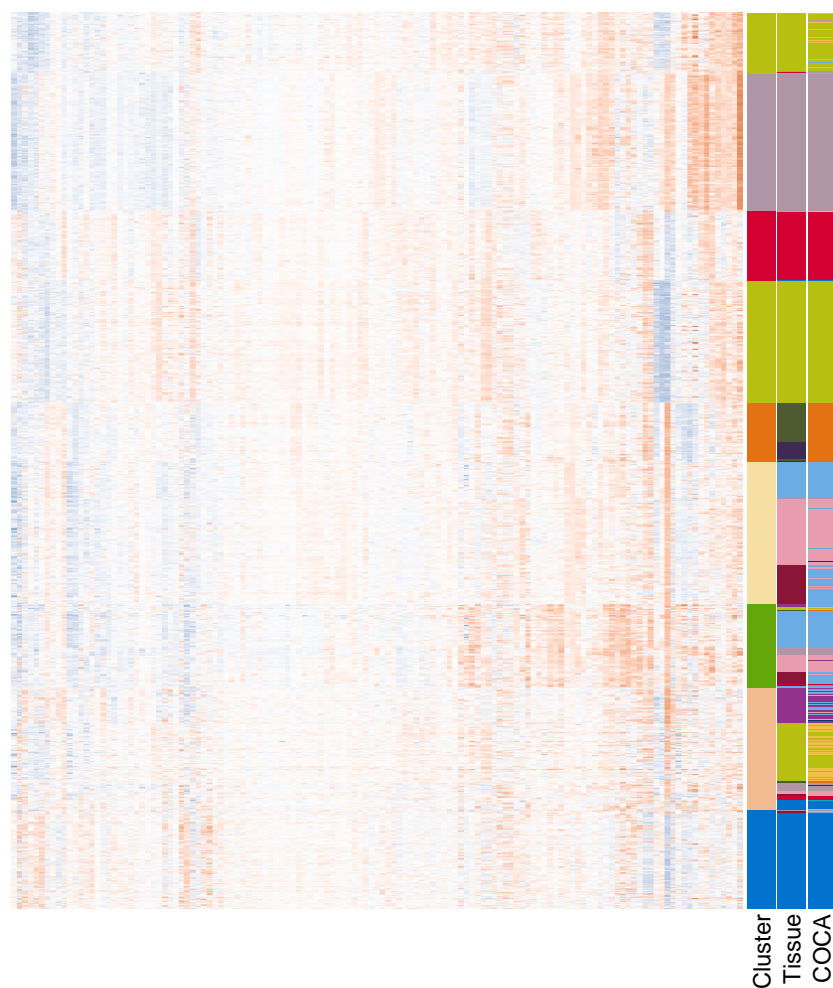
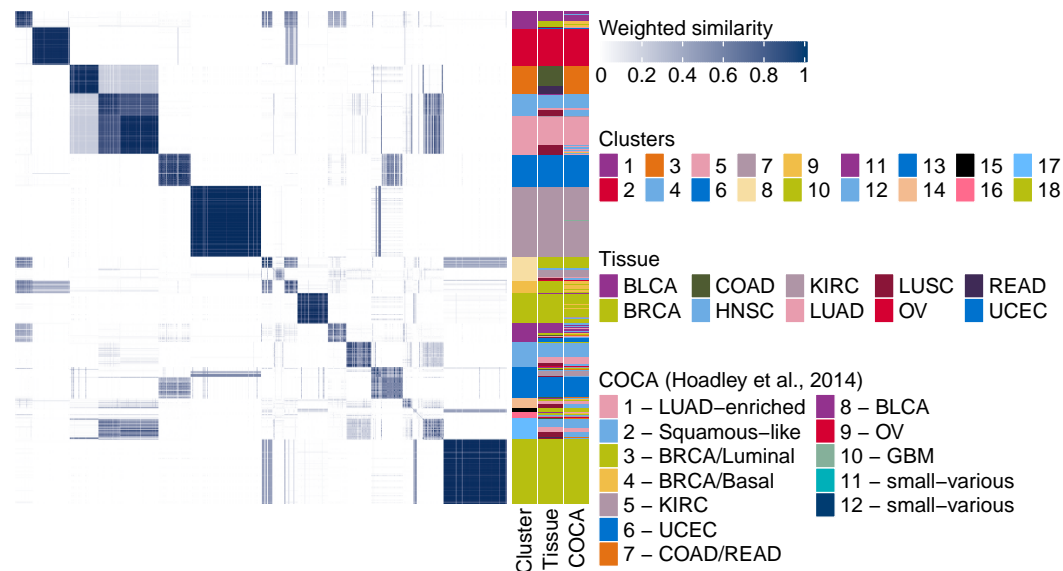


**Figure S36.** Protein expression data and final clusters.

### S2.1.4 Unsupervised integration after variable selection, $\alpha = 0.1$



(a) Weighted kernel and clusters.

**Figure S37.** Unsupervised multiplatform analysis of ten cancer types. Weighted kernel, final clusters, tissues of origin, and COCA clusters.

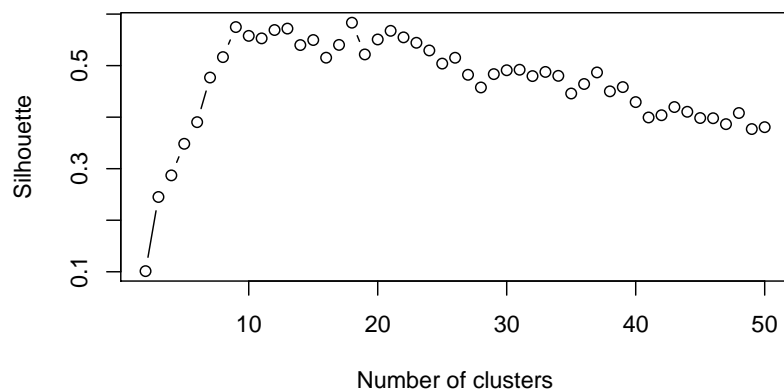
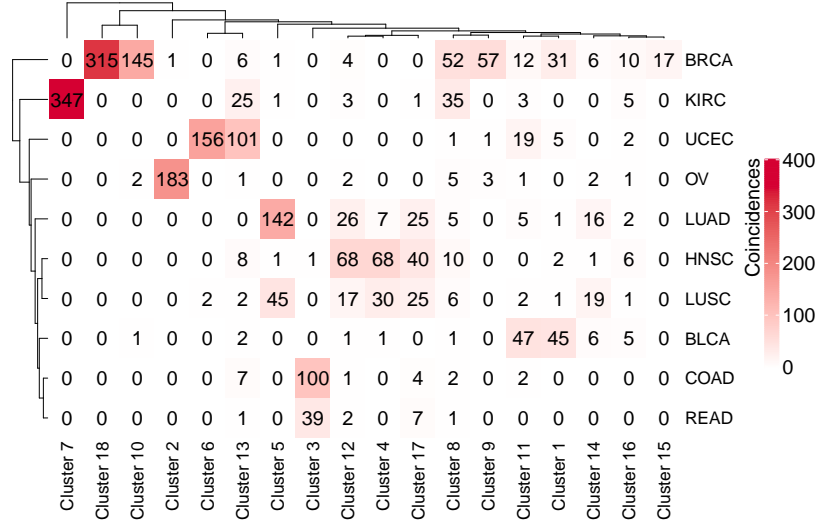
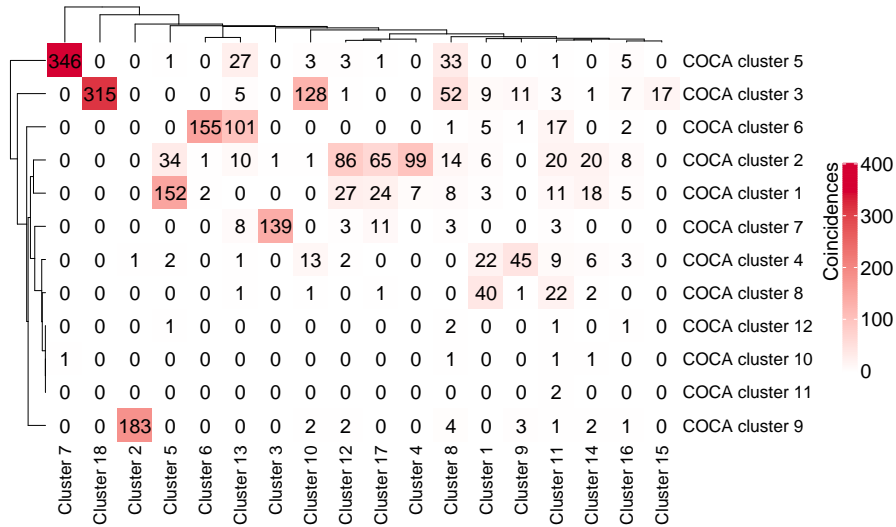


**Figure S39.** Average silhouette.



(a) Comparison to tissue of origin.



(b) Comparison to COCA clusters.

**Figure S38.** Unsupervised multiplatform analysis of ten cancer types. **(a)** Coincidence matrix comparing the tissue of origin of the tumour samples to the new clusters. **(b)** Coincidence matrix comparing the COCA clusters of Hoadley *et al.* to the new clusters.

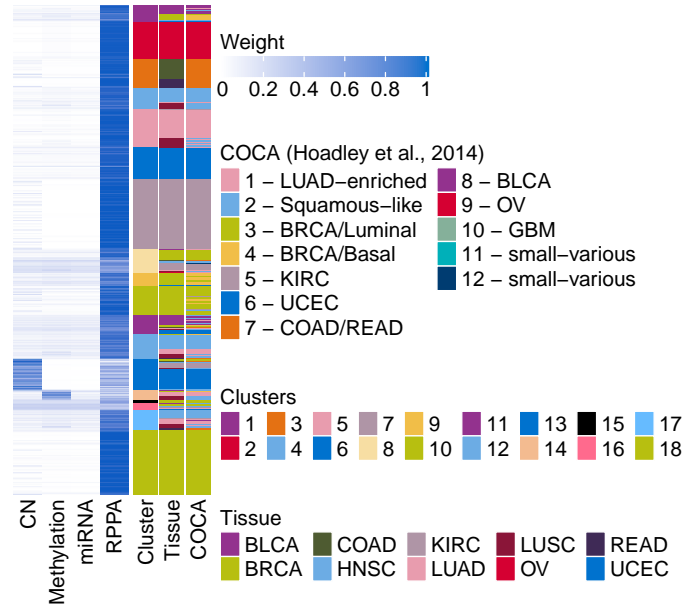
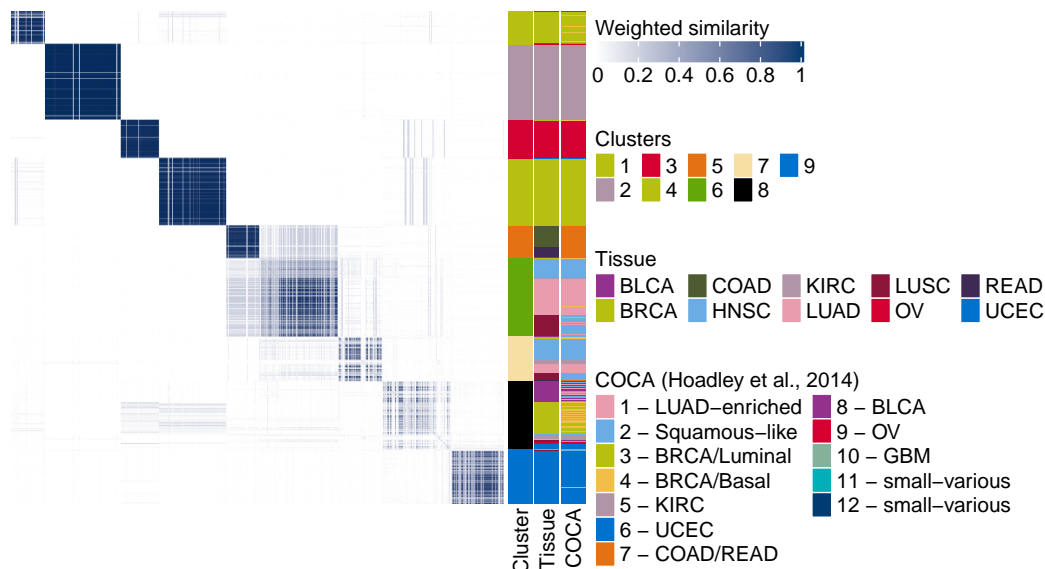
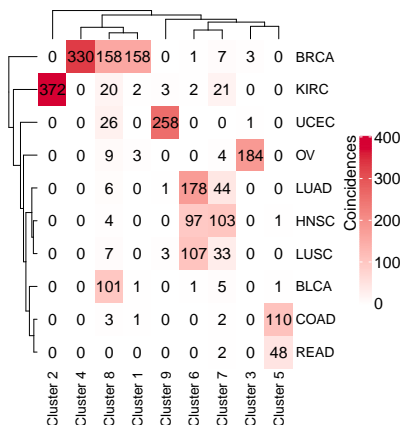


**Figure S40.** Weights assigned by the multiple kernel  $k$ -means algorithm to each observations in each layer, where “CN” stands for copy number and “RPPA” for reverse phase protein array. The weights assigned on average to the tumour samples in each layer are: copy number 7.9%, methylation 4.6%, miRNA 3.2%, protein 84.3%.

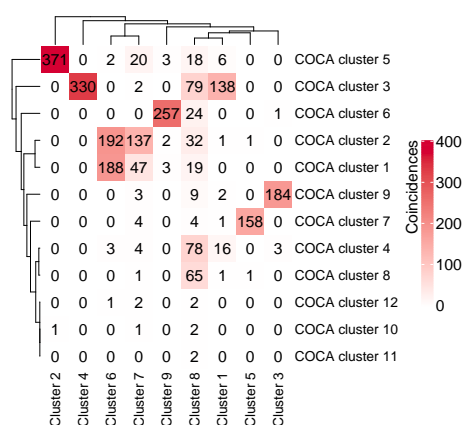
### S2.1.5 Unsupervised integration after variable selection, $\alpha = 0.5$



(a) Weighted kernel and clusters.



(b) Comparison to tissue of origin.



(c) Comparison to COCA clusters.

**Figure S41.** Unsupervised multiplatform analysis of ten cancer types. (a) Weighted kernel, final clusters, tissues of origin, and COCA clusters. (b) Coincidence matrix comparing the tissue of origin of the tumour samples to the new clusters. (c) Coincidence matrix comparing the COCA clusters of Hoadley *et al.* to the new clusters.

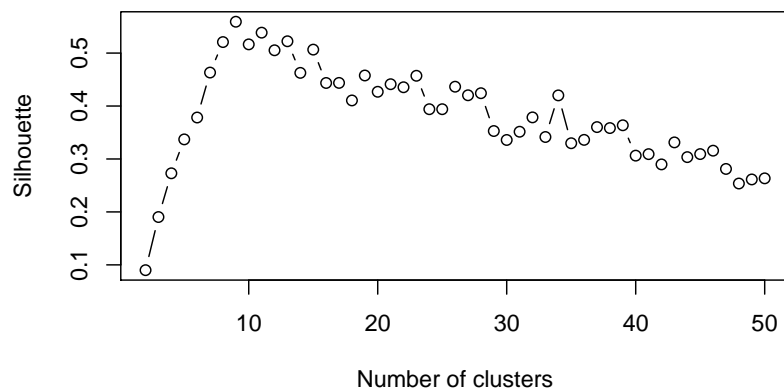


**Figure S42.** Average silhouette.

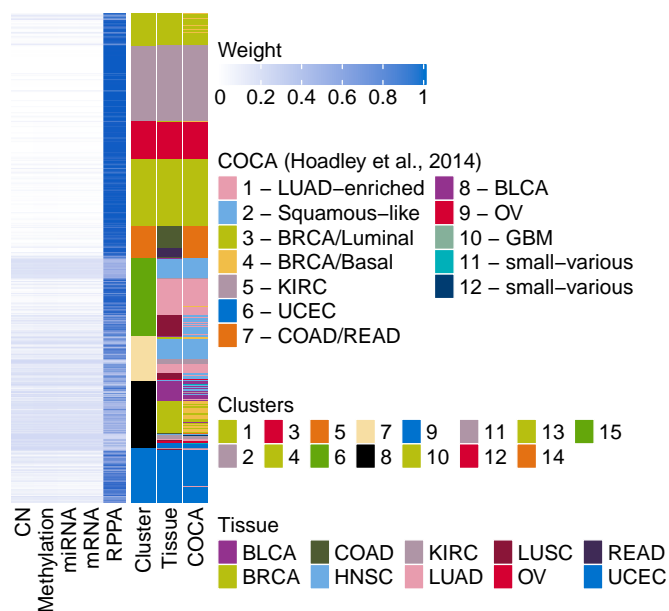


**Figure S43.** Weights assigned by the multiple kernel  $k$ -means algorithm to each observations in each layer, where “CN” stands for copy number and “RPPA” for reverse phase protein array. The weights assigned on average to the tumour samples in each layer are: copy number 5.8%, methylation 6%, microRNA 5.9%, mRNA 5.9%, protein 76.4%.

### S2.1.6 Unsupervised integration after variable selection, $\alpha = 1$

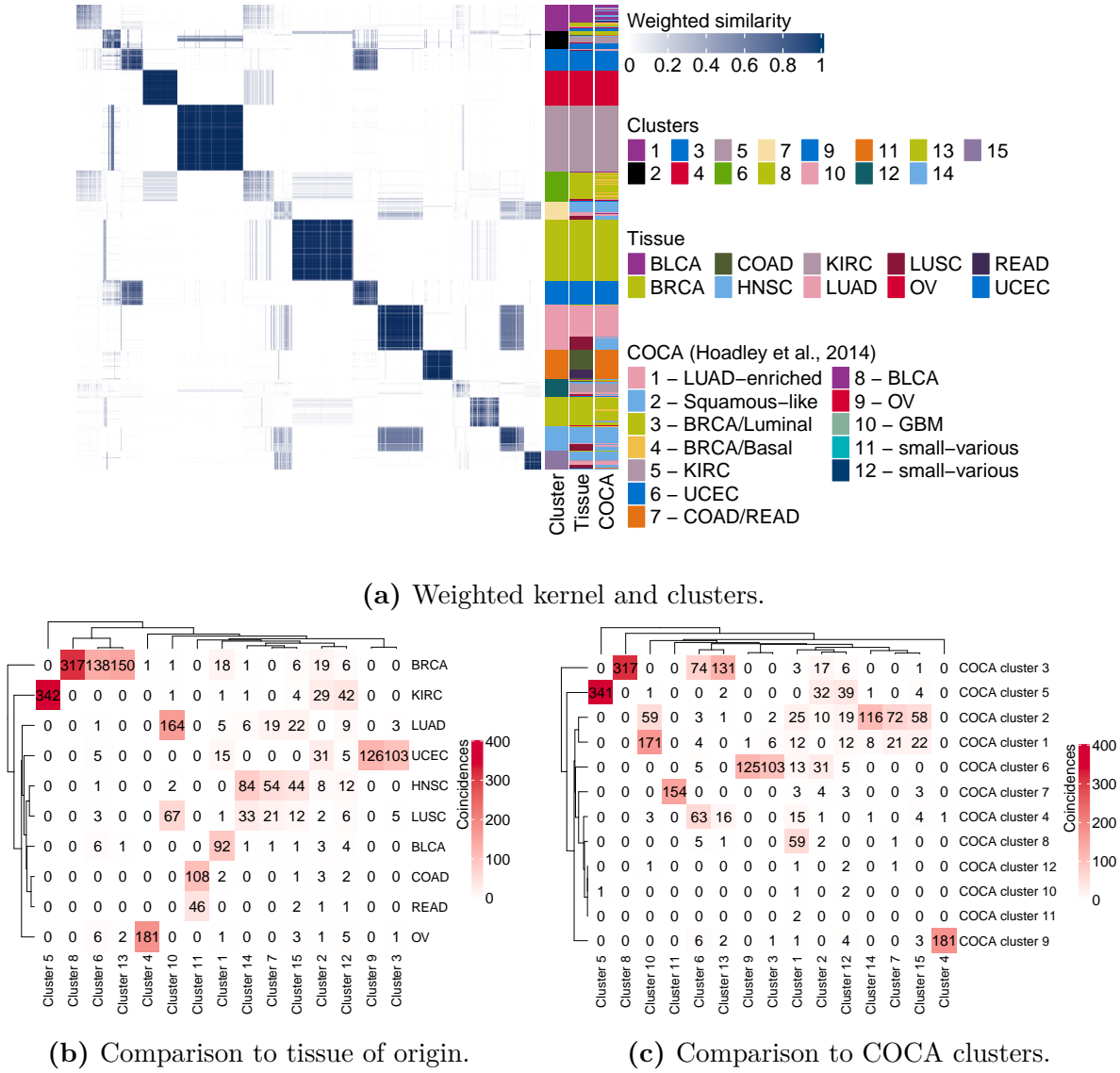


**Figure S44.** Unsupervised multiplatform analysis of ten cancer types. **(a)** Weighted kernel, final clusters, tissues of origin, and COCA clusters. **(b)** Coincidence matrix comparing the tissue of origin of the tumour samples to the new clusters. **(c)** Coincidence matrix comparing the COCA clusters of Hoadley *et al.* to the new clusters.

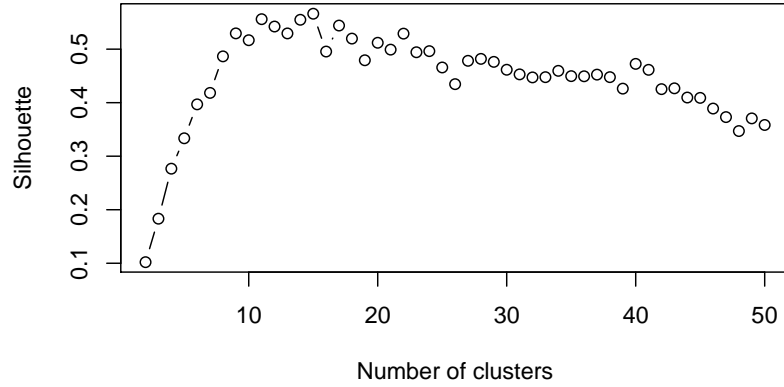


**Figure S45.** Average silhouette.

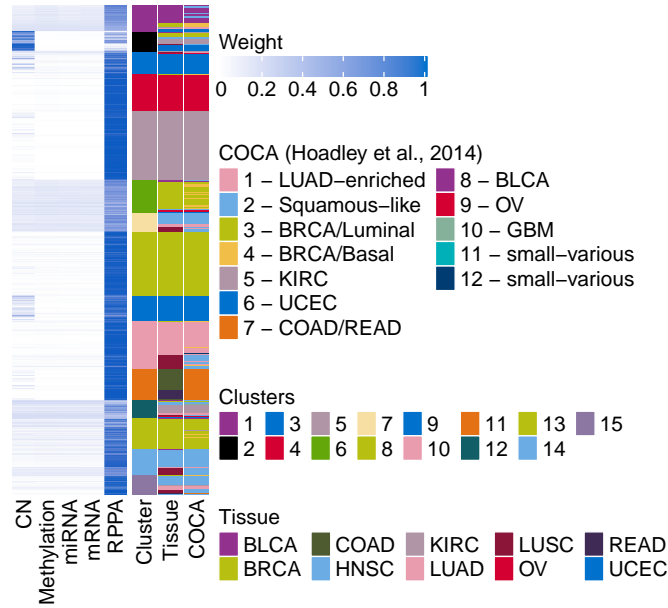


**Figure S46.** Weights assigned by the multiple kernel  $k$ -means algorithm to each observations in each layer, where “CN” stands for copy number and “RPPA” for reverse phase protein array. The weights assigned on average to the tumour samples in each layer are: copy number 8.1%, methylation 3.8%, microRNA 3.6%, mRNA 3.7%, protein 80.8%.



### S2.1.7 Outcome-guided integration: additional figures

**Choice of the number of clusters** In Figure S47 are reported the average values of the silhouette when the number of clusters goes from 2 to 50. The maximum is at  $K = 27$ .

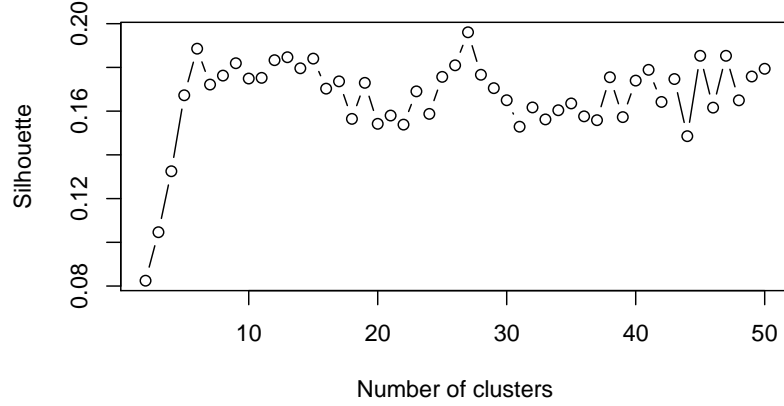


Figure S47. Average silhouette.

**Comparison with the clusters identified by Hoadley et al. (2014)** In Figure S48 are shown the correspondences between the clusters found in the main paper in the outcome-guided case and the clusters identified by Hoadley et al. (2014) using Cluster-Of-Clusters Analysis (COCA).

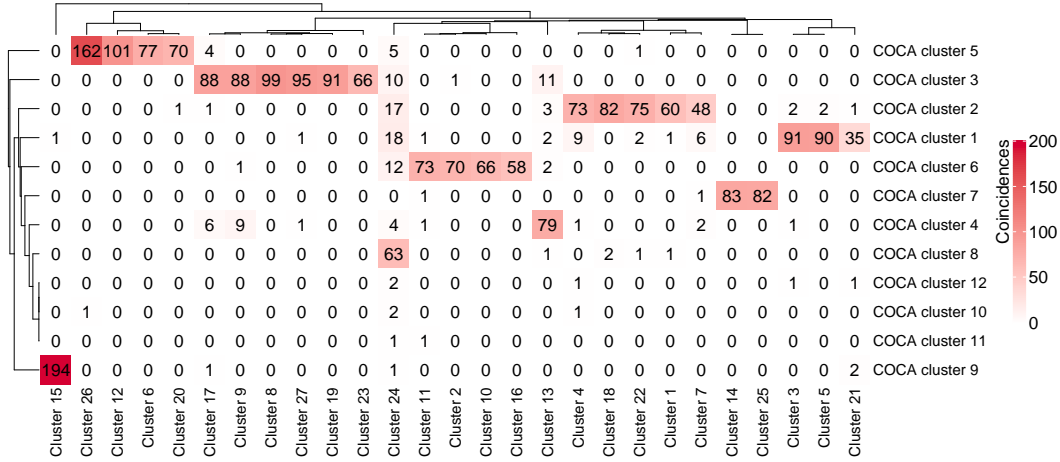
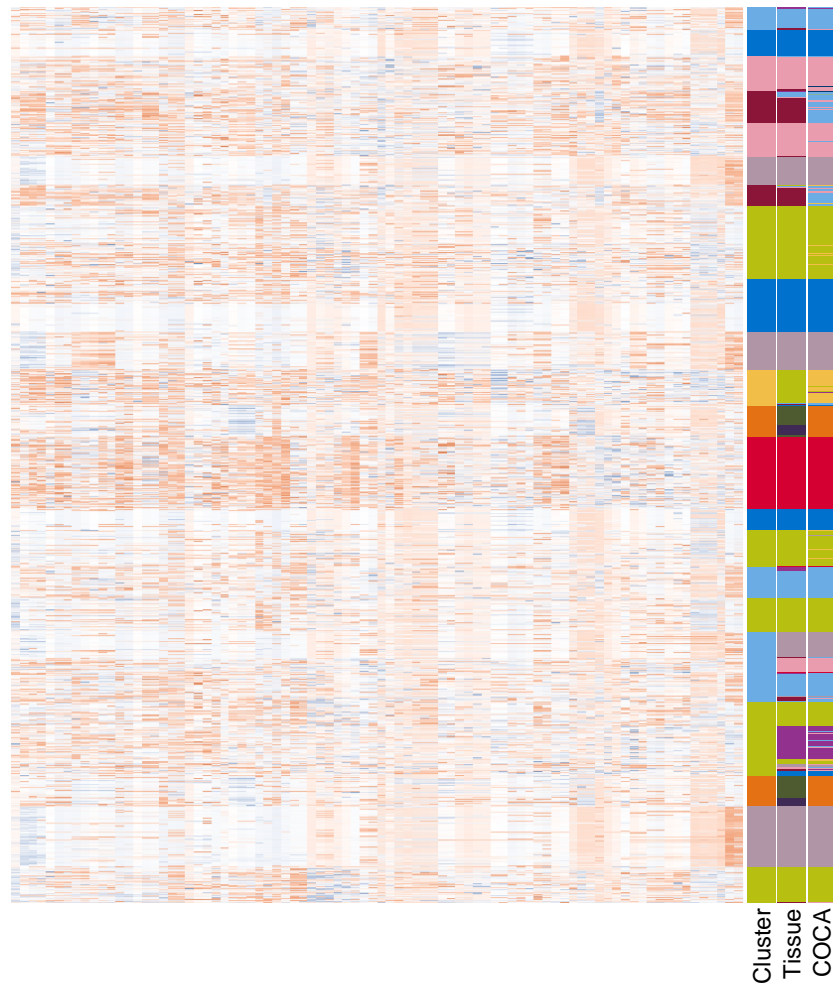
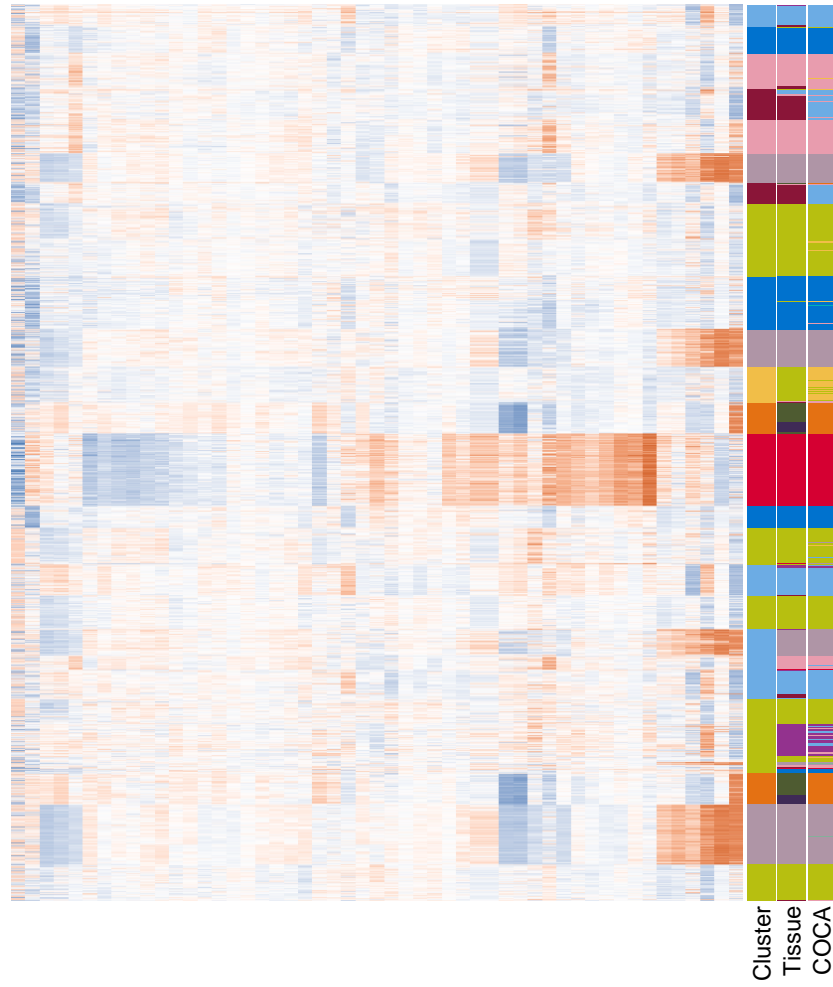


Figure S48. Comparison between the clusters found combining the PSMs of each layer using the outcome-guided approach and those identified by Hoadley et al. (2014) using COCA.

**Clustering structure in the data** Figures S49, S50, S50, and S52 show the four data layers where the rows have been sorted by final cluster.



**Figure S49.** Copy number data and final clusters.



**Figure S50.** microRNA expression data and final clusters.

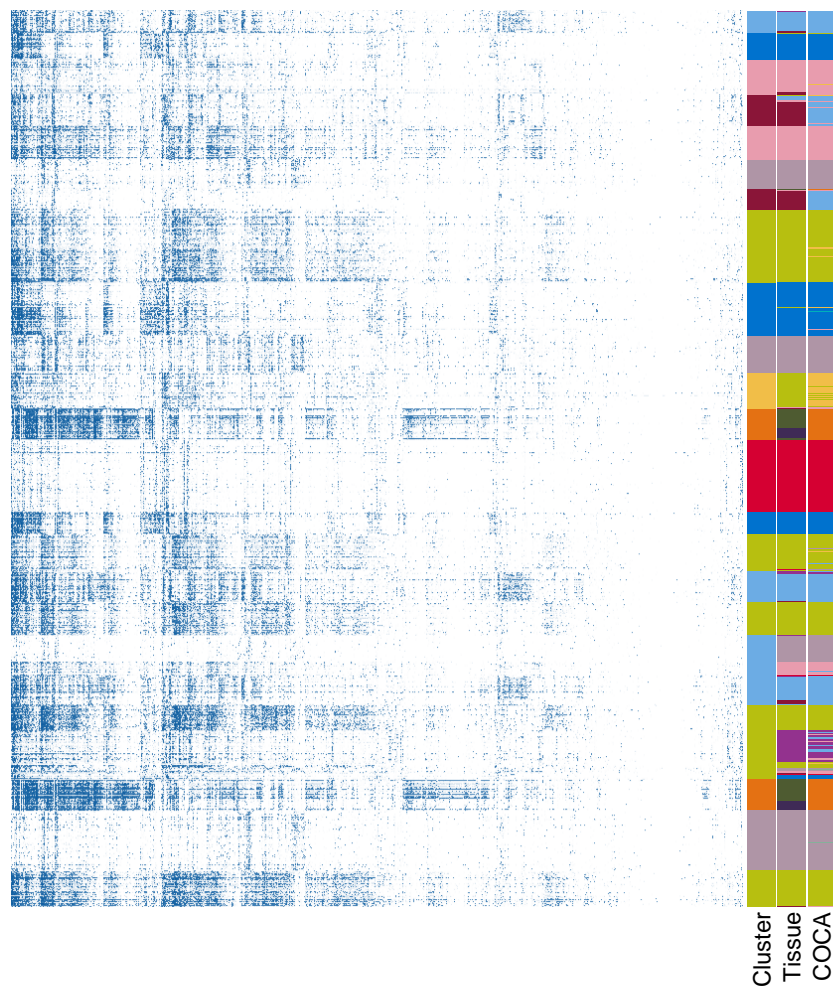


**Figure S51.** Methylation data and final clusters.

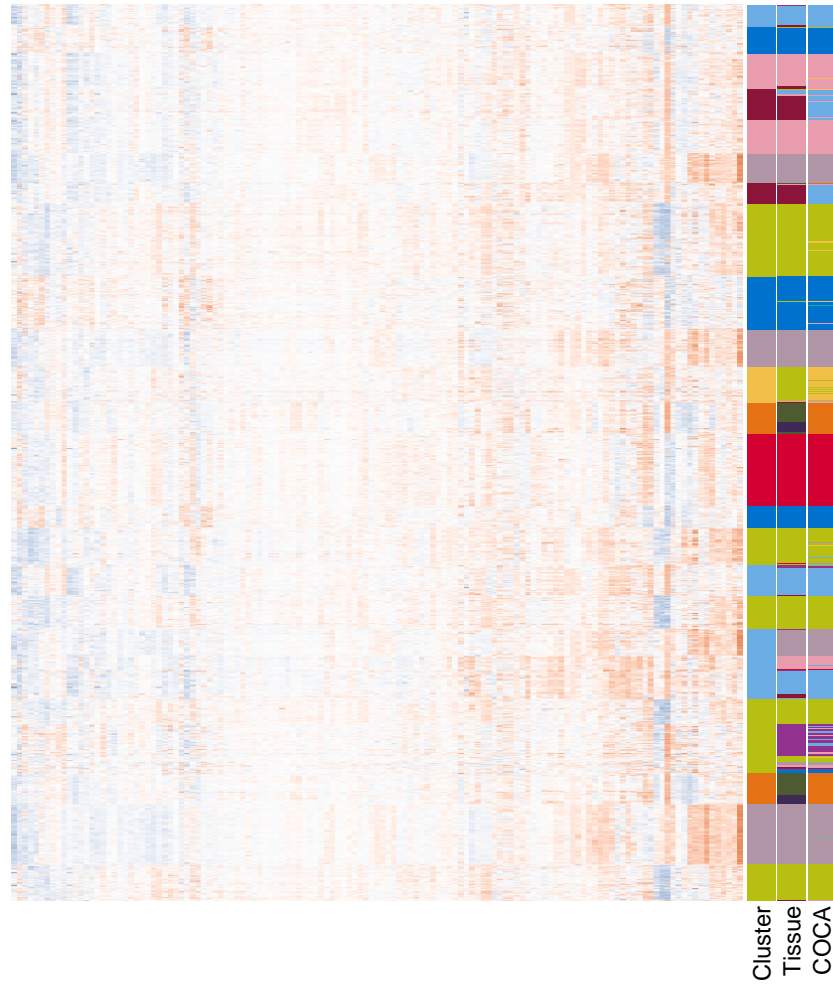
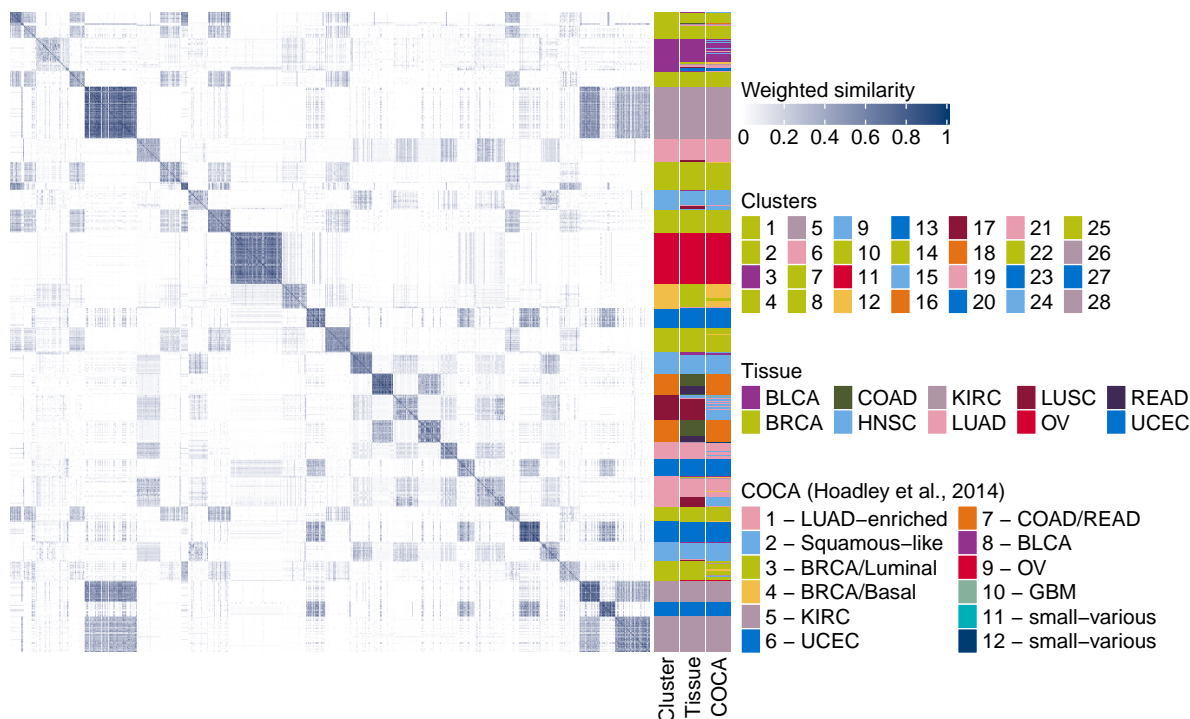


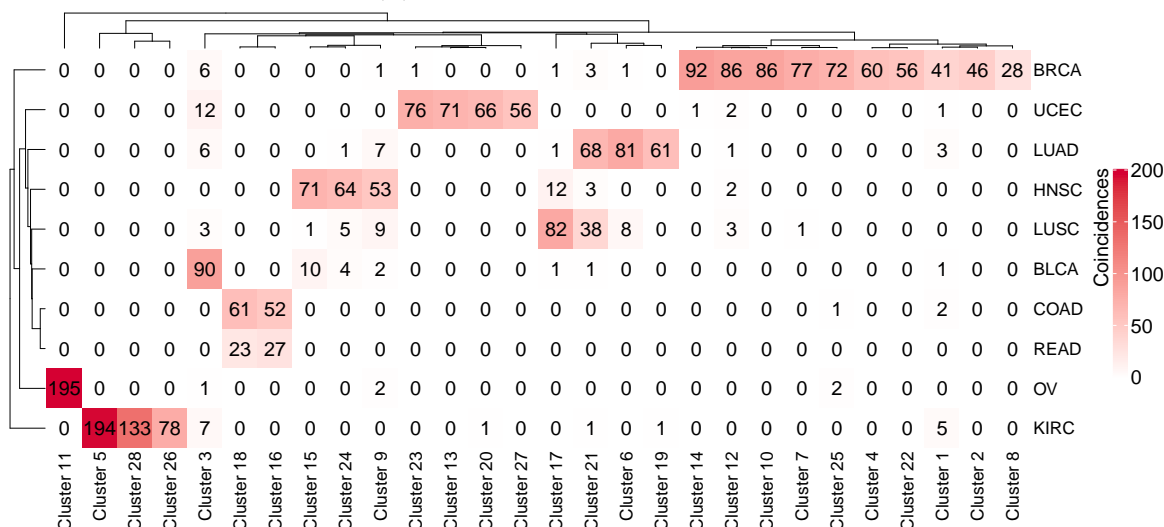
**Figure S52.** Protein expression data and final clusters.

### S2.1.8 Outcome-guided integration after variable selection, $\alpha = 0.1$

The weights assigned on average to the tumour samples in each layer are: copy number 33.1%, methylation 16.3%, microRNA 34.1%, and protein 16.5%.



(a) Clusters and weighted kernel.



(b) Coincidence matrix.

**Figure S53.** Outcome-guided multiplatform analysis of ten cancer types. (a) Weighted kernel, final clusters, tissues of origin, and COCA clusters. (b) Coincidence matrix comparing the tissue of origin of the tumour samples with the clusters.

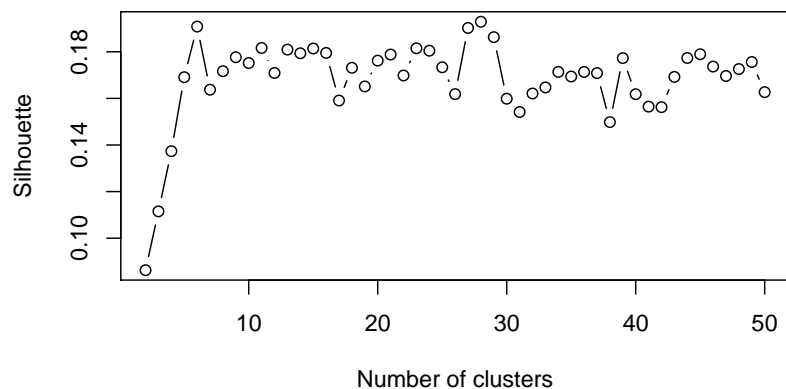


**Figure S54.** Average silhouette.

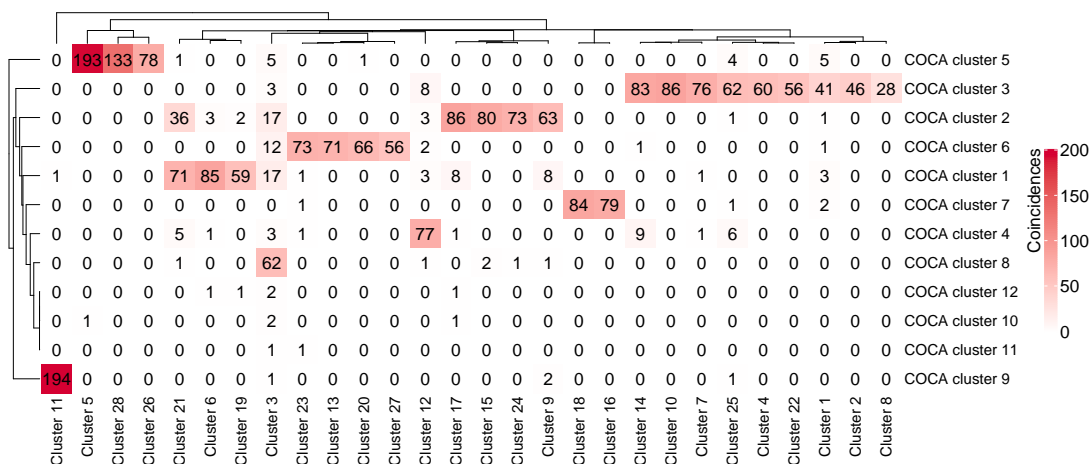
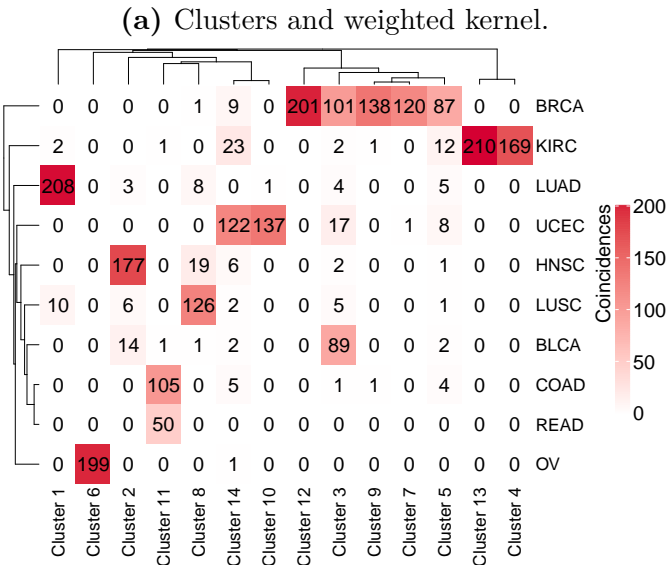
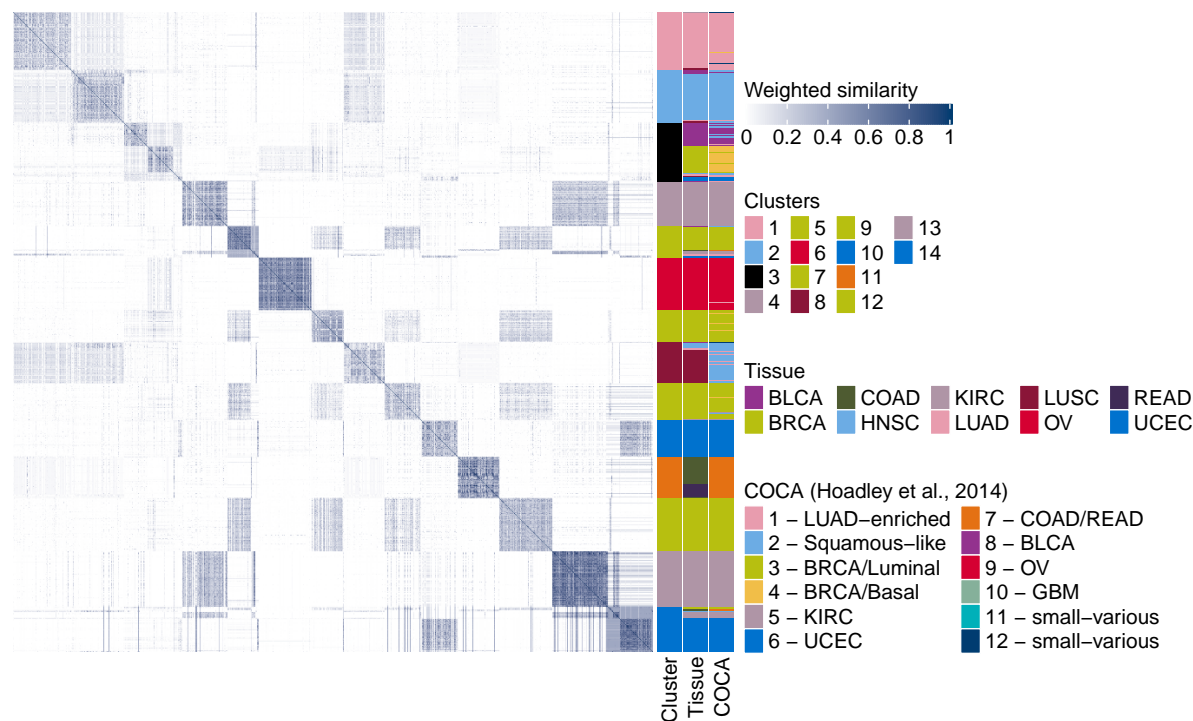


**Figure S55.** Comparison between the clusters found combining the PSMs of each layer using the outcome-guided approach and those identified by Hoadley et al. (2014) using COCA.



S2.1.9 Outcome-guided integration after variable selection,  $\alpha = 0.5$

The weights assigned on average to the tumour samples in each layer are: copy number 34.2%, mRNA 17.7%, methylation 7.2%, miRNA 27.4%, protein 13.5.



(b) Coincidence matrix.

**Figure S56.** Outcome-guided multiplatform analysis of ten cancer types. (a) Weighted kernel, final clusters, tissues of origin, and COCA clusters. (b) Coincidence matrix comparing the tissue of origin of the tumour samples with the clusters.



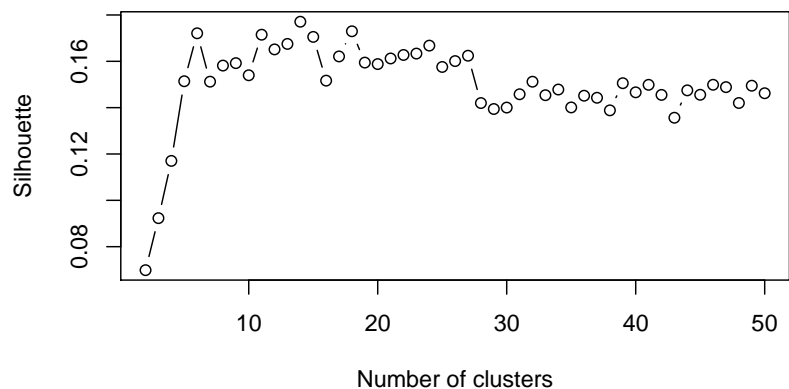


**Figure S57.** Average silhouette.

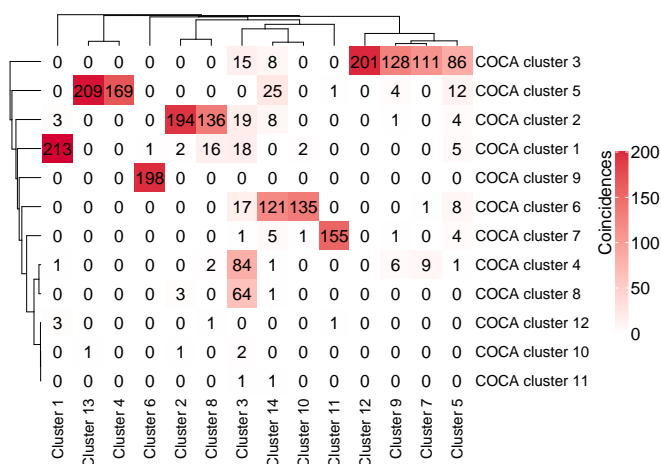
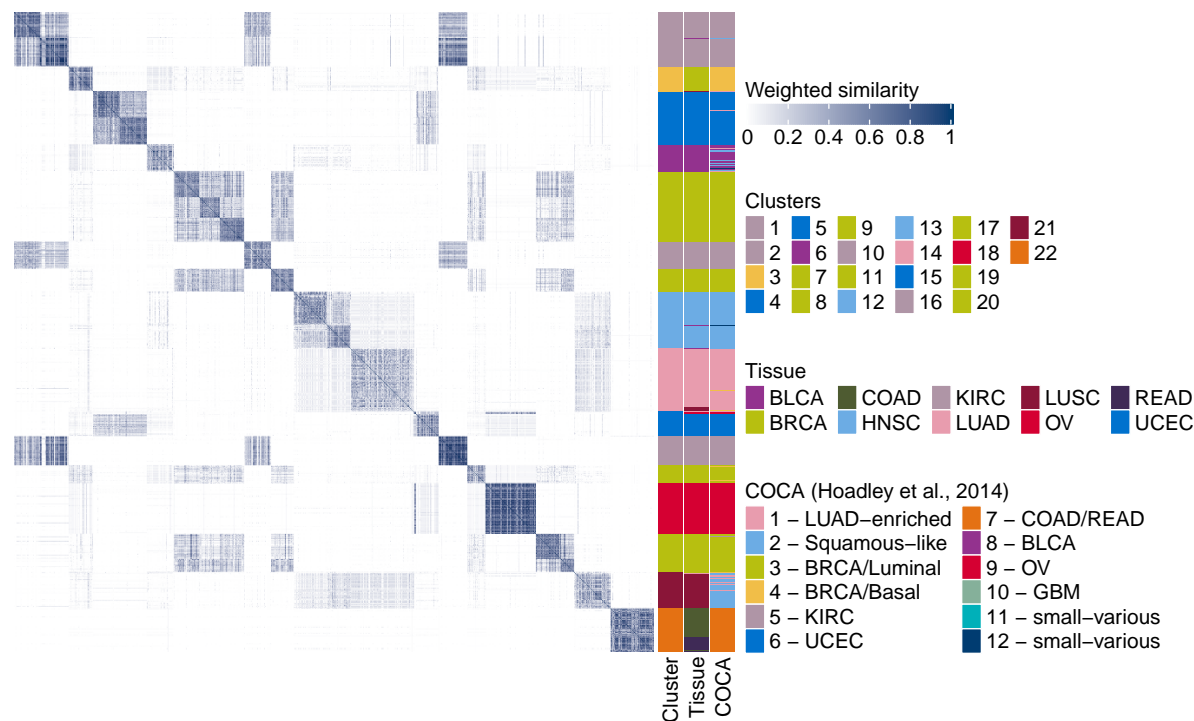


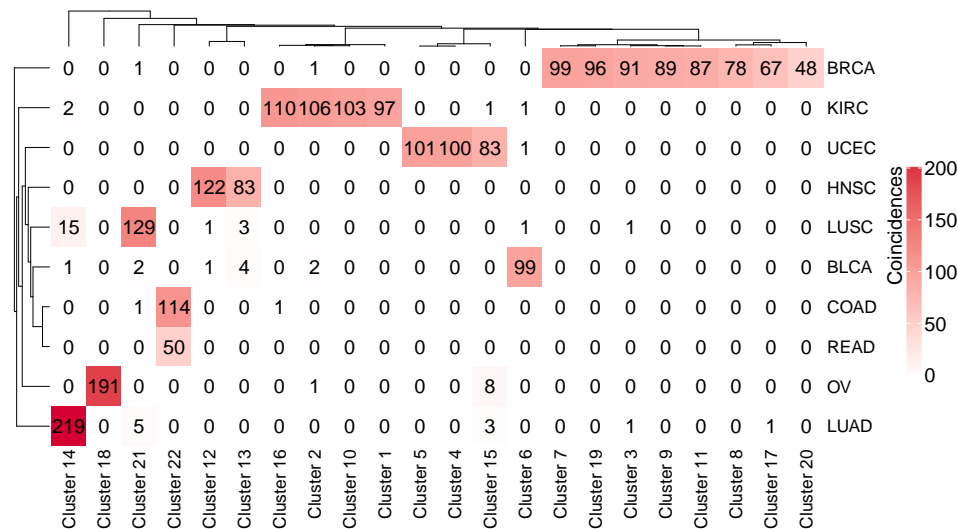
**Figure S58.** Comparison between the clusters found combining the PSMs of each layer using the outcome-guided approach and those identified by [Hoadley et al. \(2014\)](#) using COCA.

S2.1.10 Outcome-guided integration after variable selection,  $\alpha = 1$

The weights assigned on average to the tumour samples in each layer are: copy number 0%, mRNA 37.6%, methylation 25.2%, miRNA 24.5%, protein 12.7%.



(a) Clusters and weighted kernel.



(b) Coincidence matrix.

**Figure S59.** Outcome-guided multiplatform analysis of ten cancer types. (a) Weighted kernel, final clusters, tissues of origin, and COCA clusters. (b) Coincidence matrix comparing the tissue of origin of the tumour samples with the clusters.

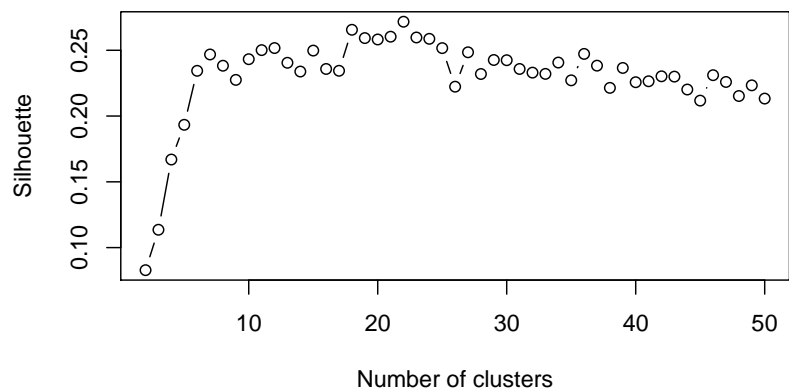


**Figure S60.** Average silhouette.

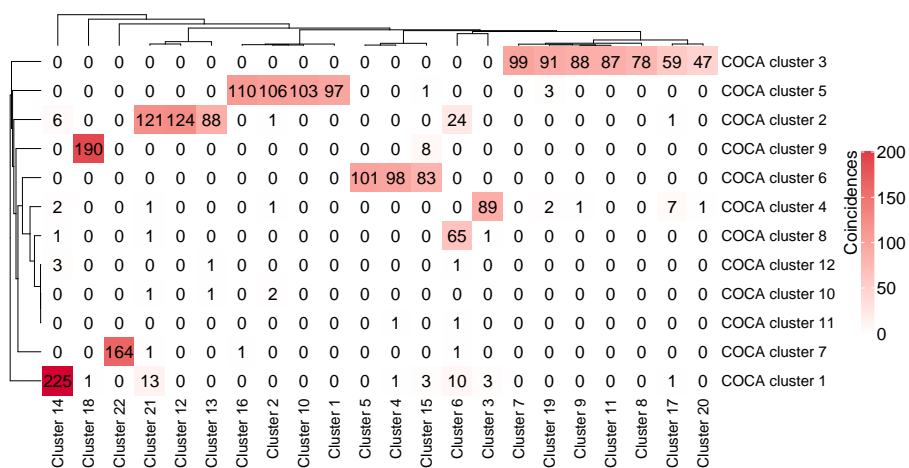


**Figure S61.** Comparison between the clusters found combining the PSMs of each layer using the outcome-guided approach and those identified by [Hoadley et al. \(2014\)](#) using COCA.

## S2.2 Transcriptional module discovery

### S2.2.1 Additional figures

Figures S62 and S63 show the initial data, the clusterings obtained on each dataset individually and the PSMs. The cophenetic correlation coefficients are 0.953685 for the expression data and 0.9841434 for the ChIP data. 3.5% of the weight is assigned on average to the ChIP data, and the remaining 96.5% to the expression data.

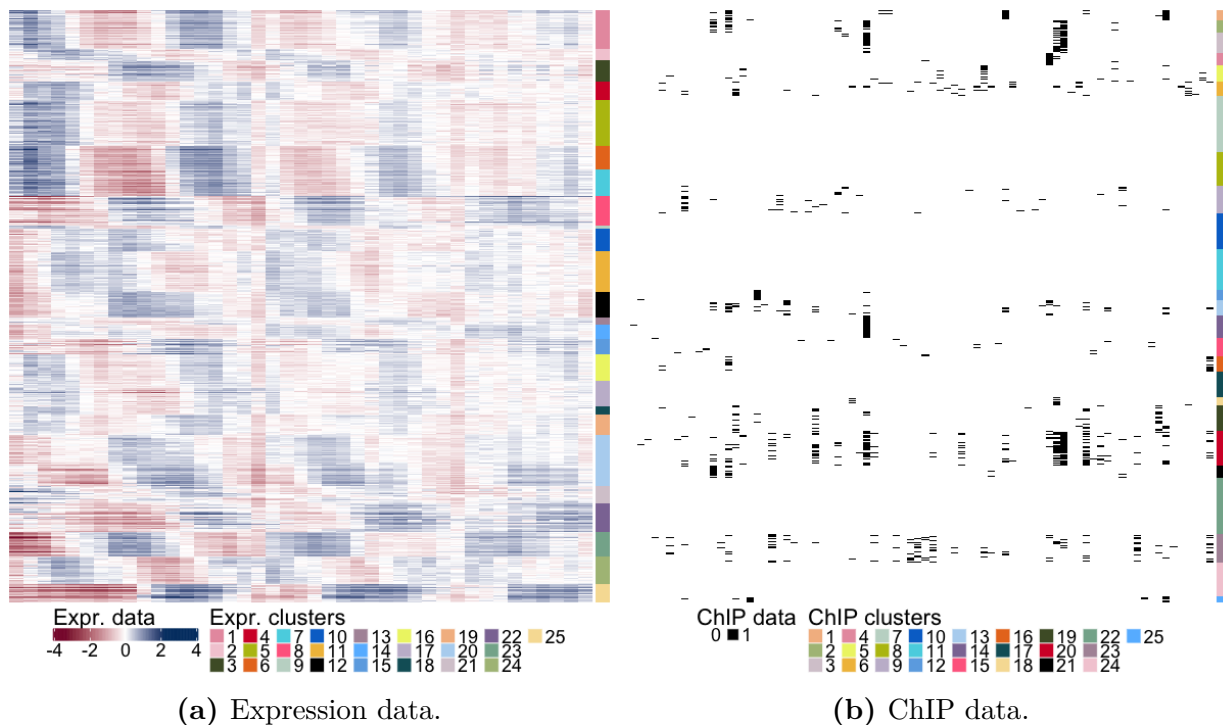


**Figure S62.** Clusters obtained on each dataset separately. The ordering of the rows is different in the two figures.

In Figure S64 are reported the values of the average silhouette for different values of the number of clusters  $K$ . We choose  $K = 25$ , which gives the highest value of the silhouette.

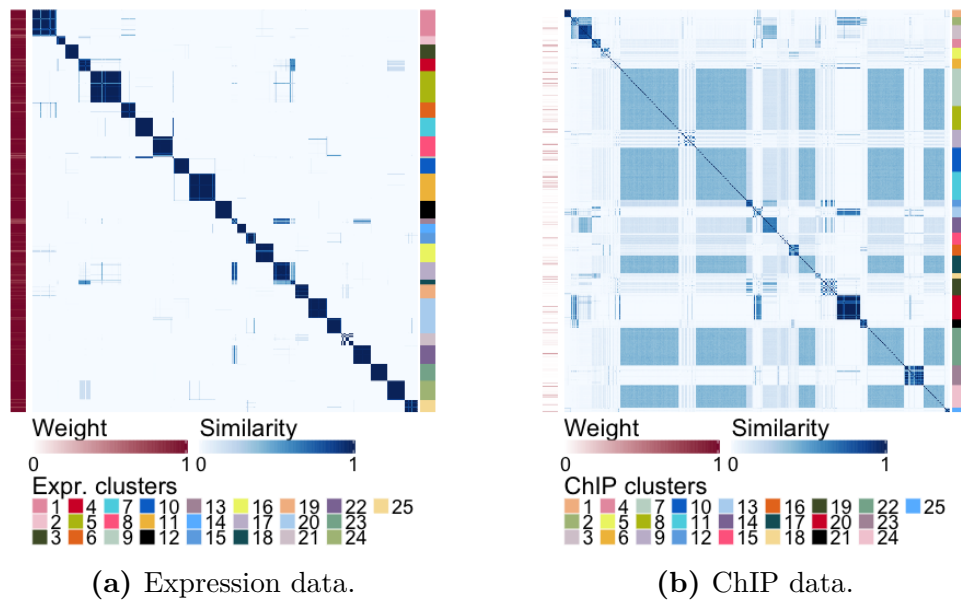


**Figure S63.** Posterior similarity matrices and clusterings obtained via kernel  $k$ -means on each dataset separately. The ordering of the observations is different in the two figures.

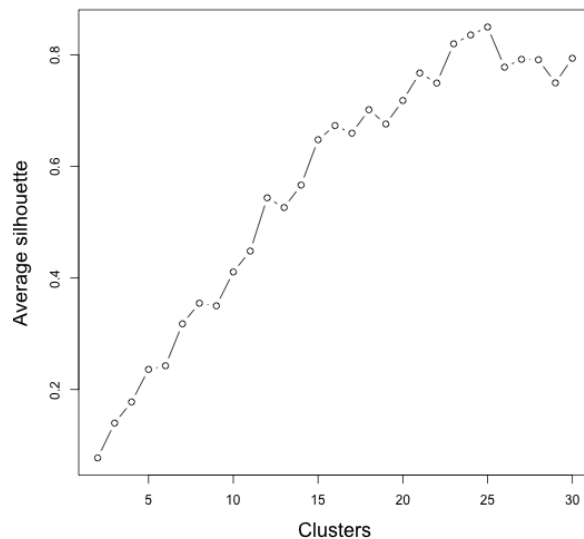


**Figure S64.** Plot of silhouette for different numbers of clusters for the integration of the datasets of Harbison *et al.* and Granovskaia *et al.*. The maximum value is attained at  $K = 25$ .

### S2.2.2 A different set of data

Here we combine the expression dataset of [Ideker et al. \(2001\)](#) with the ChIP-chip dataset of [Harbison et al. \(2004\)](#), which provides binding information for 117 transcriptional regulators. Both datasets are discretised as in [Savage et al. \(2010\)](#) and [Kirk et al. \(2012\)](#). The dataset of [Ideker et al. \(2001\)](#) contains measurements related to 205 genes whose expression patterns reflect four functional categories based on gene ontology annotations.

Figure S66 shows the PSMs obtained for each dataset. In Figure S66, the cophenetic correlation coefficient is 0.9999932 for the ChIP data and 0.9999184 for the PSM of the expression data.

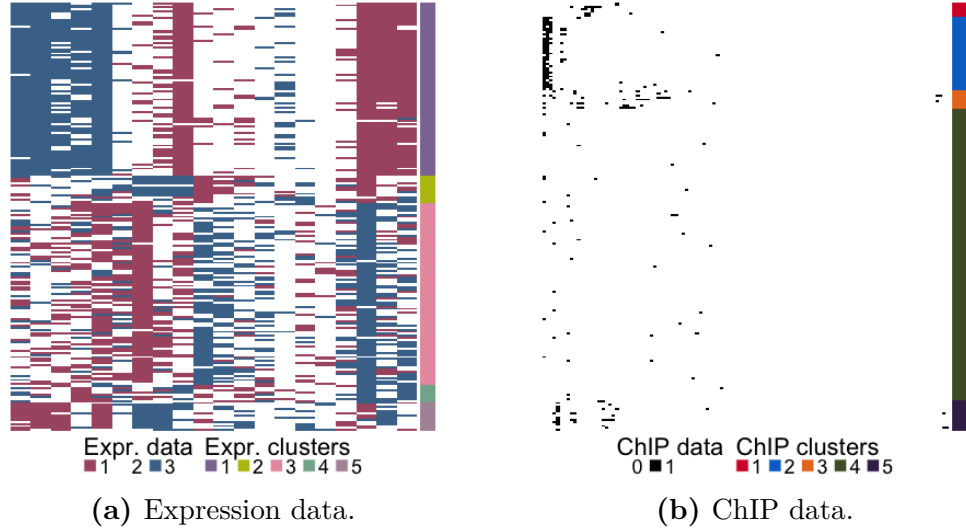


**Figure S65.** Clusters obtained on each dataset separately. The ordering of the observations (i.e. rows) is different in the two figures.

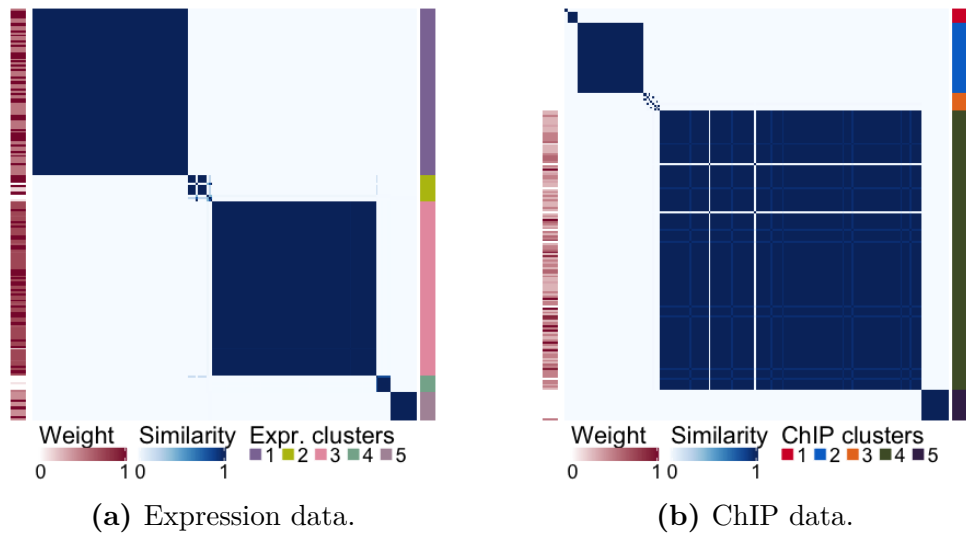


**Figure S66.** Posterior similarity matrices and clusterings obtained via kernel  $k$ -means on each dataset separately. The ordering of the observations (i.e. rows) is different in the two figures.

In Figure S67 are reported the values of the average silhouette for different values of the number of clusters  $K$ . The number of clusters chosen for the data analysis is 5, since it has a similar value of the average silhouette to 2.

The final clusters are shown in Figure S68 next to the initial datasets and combined PSM. 28.7% of the weight is assigned on average to the ChIP data, the remaining 71.3% to the expression data.

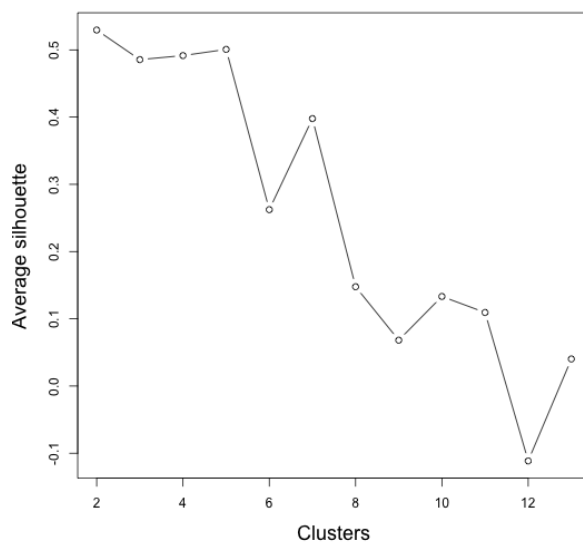


**Figure S67.** Plot of silhouette for different numbers of clusters for the integration of the datasets of Harbison *et al.* and Ideker *et al.*. The maximum value is attained for  $K = 2$ .

Dataset(s)	GOTO BP	GOTO MF	GOTO CC
ChIP (Harbison <i>et al.</i> )	13.36	1.37	12.26
Expr. (Ideker <i>et al.</i> )	<b>17.34</b>	<b>2.52</b>	<b>15.38</b>
Both	16.51	2.15	14.84

**Table S13.** Gene Ontology Term Overlap scores. “BP” stands for Biological Process ontology, “MF” for Molecular Function, and “CC” for Cellular Component. The number of clusters used to combine the datasets of Harbison *et al.* and Ideker *et al.* is 5.

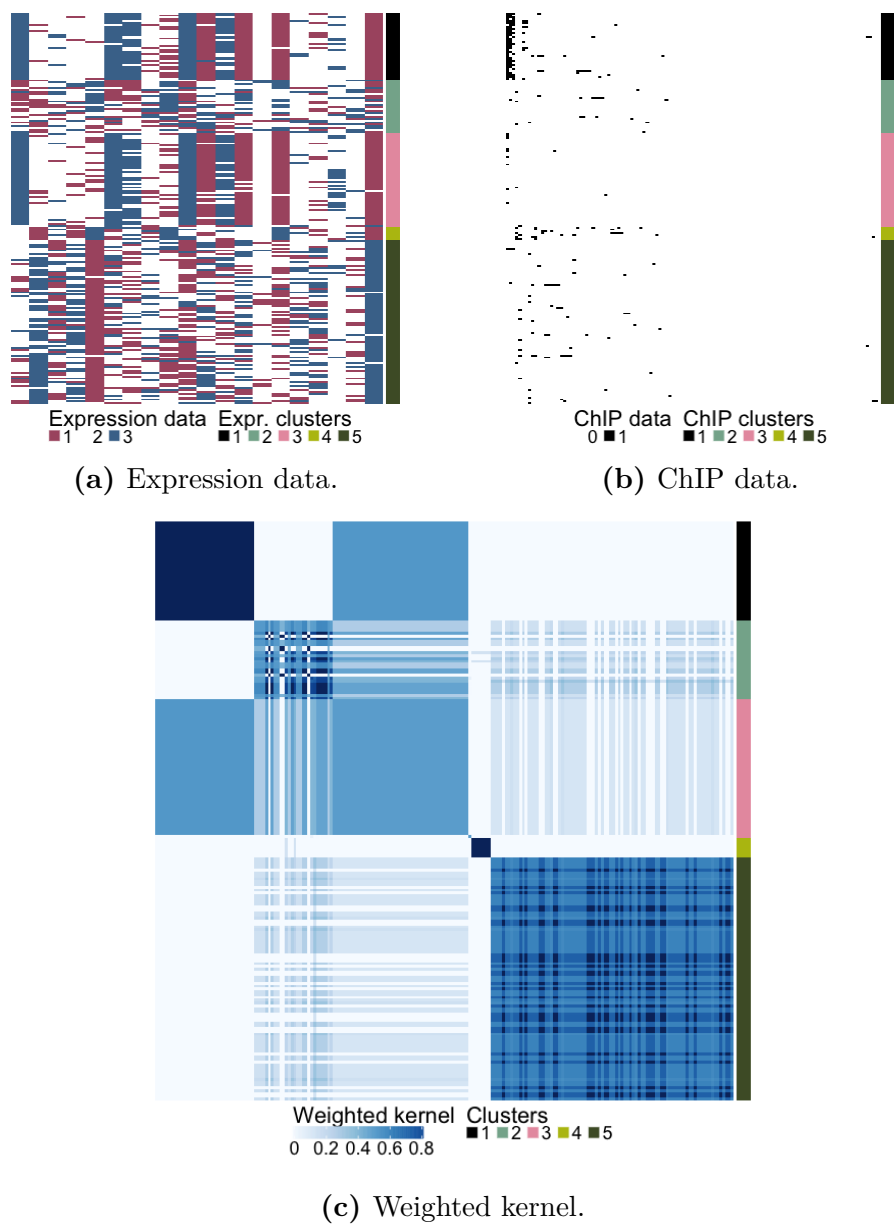


**Figure S68.** Transcriptional module discovery, integration of the Harbison et al. (2004) and Ideker et al. (2001) datasets.



## References

- Cabassi, A., Seyres, D., Frontini, M., and Kirk, P. D. W. (2020). Penalised logistic regression for multi-omic data with an application to cardiometabolic syndrome. *arXiv*. 2008.00235. *Referred to on page S10.*
- Harbison, C. T., Gordon, D. B., Lee, T. I., Rinaldi, N. J., Macisaac, K. D., Danford, T. W., Hannett, N. M., Tagne, J.-B., Reynolds, D. B., Yoo, J., et al. (2004). Transcriptional regulatory code of a eucaryotic genome. *Nature*, 431(7004):99–104. *Referred to on pages S59 and S61.*
- Hoadley, K. A., Yau, C., Wolf, D. M., Cherniack, A. D., Tamborero, D., Ng, S., Leiserson, M. D., Niu, B., McLellan, M. D., Uzunangelov, V., et al. (2014). Multiplatform analysis of 12 cancer types reveals molecular classification within and across tissues of origin. *Cell*, 158(4):929–944. *Referred to on pages S34, S46, S52, S54, and S56.*
- Ideker, T., Thorsson, V., Ranish, J. A., Christmas, R., Buhler, J., Eng, J. K., Bumgarner, R., Goodlett, D. R., Aebersold, R., and Hood, L. (2001). Integrated genomic and proteomic analyses of a systematically perturbed metabolic network. *Science*, 292(5518):929–934. *Referred to on pages S59 and S61.*
- Kirk, P. D., Griffin, J. E., Savage, R. S., Ghahramani, Z., and Wild, D. L. (2012). Bayesian correlated clustering to integrate multiple datasets. *Bioinformatics*, 28(24):3290–3297. *Referred to on page S59.*
- Savage, R. S., Ghahramani, Z., Griffin, J. E., De La Cruz, B. J., and Wild, D. L. (2010). Discovering transcriptional modules by bayesian data integration. *Bioinformatics*, 26(12):i158–i167. *Referred to on page S59.*
- Seyres, D., Cabassi, A., Lambourne, J. J., Burden, F., Farrow, S., McKinney, H., Batista, J., Kempster, C., Pietzner, M., Slingsby, O., et al. (2020). Transcriptional, epigenetic and metabolic signatures in cardiometabolic syndrome defined by extreme phenotypes. *bioRxiv*. 2020.03.06.961805. *Referred to on page S10.*
- Vats, D. and Knudson, C. (2018). Revisiting the Gelman-Rubin diagnostic. *arXiv*. 1812.09384. *Referred to on page S10.*